Title
HIGH ENERGY pp AND pp FORWARD ELASTIC SCATTERING AND TOTAL CROSS SECTIONS

Authors
Block, M.M.
Cahn, R.N.

Publication Date
1984-03-01

LBL-17522
Preprint

Lawrence Berkeley Laboratory
UNIVERSITY OF CALIFORNIA

Physics Division

Submitted for publication

HIGH ENERGY $p\bar{p}$ AND pp FORWARD ELASTIC SCATTERING AND TOTAL CROSS SECTIONS

M.M. Block and R.N. Cahn

March 1984

Prepared for the U.S. Department of Energy under Contract DE-AC03-76SF00098

DISCLAIMER

March 1984 LBL-17522

High Energy $p\bar{p}$ and pp Forward Elastic Scattering and Total Cross Sections *

M.M. Block

Department of Physics, Northwestern University
Evanston, Illinois 60201

R.N. Cahn

Lawrence Berkeley Laboratory, Univ. of California
Berkeley, California 94720

*This work supported by the Director, Office of Energy Research, Office of High Energy and Nuclear Physics, Division of High Energy Physics of the U.S. Department of Energy under contract DE-AC03-76SF00098 and DE-AC02-76-ER-02289 Task B.

ABSTRACT

The present status of elastic pp and $p\bar{p}$ scattering in the high energy domain is reviewed, with emphasis on the forward and near forward regions. The experimental techniques for measuring σ_{tot}, ρ and B are discussed, emphasizing the importance of the Coulomb region. The impact parameter representation is exploited to give simple didactic demonstrations of important rigorous theorems based on analyticity, and to illuminate the significance of the slope parameter, B, and the curvature parameter, C. Models of elastic scattering are discussed and a criterion for the onset of "asymptopia" is given. A critique of dispersion relations is presented. Simple analytic functions are used to fit simultaneously the real and imaginary parts of forward scattering amplitudes for both pp and $p\bar{p}$, obtained from experimental data for σ_{tot} and ρ. It is found that a good fit can be obtained using only 5 parameters (with a cross section rising as $\log^2 s$), over the energy range $5 < \sqrt{s} < 62$ GeV. The possibilities that: a) the cross section rises only as $\log s$, b) the cross section rises only locally as $\log^2 s$, and eventually goes to a constant value, and c) the cross section difference between pp and $p\bar{p}$ does not vanish as $s \to \infty$, are examined critically. The nuclear slope parameters B are also fitted in a model-independent fashion. Examination of the fits reveals a new regularity of the $p\bar{p}$ and pp systems. Predictions of all of the elastic scattering parameters are made at ultra-high energies, and are compared to the available SPS collider measurements.

Table of Contents

I. INTRODUCTION

The advent of $p\bar{p}$ collider physics at the CERN ISR and SPS during the last three years has extended the maximum $p\bar{p}$ center of mass energy from $\sqrt{s} \sim 20$ GeV to $\sqrt{s} = 540$ GeV. Experimental groups at the SPS have measured σ_{tot}, the total cross section, and B, the nuclear slope parameter, at the highest available energy, $\sqrt{s} = 540$ GeV. In the energy range $30 < \sqrt{s} < 62$ GeV, experimental groups at the ISR have made precision measurements of these quantities for both $p\bar{p}$ and pp, with the same apparatus used for comparison of $p\bar{p}$ and pp. Moreover, new ISR measurements of elastic scattering in the Coulomb interference region have made possible accurate determinations of ρ, the ratio of the real to the imaginary portion of the forward nuclear scattering amplitude, for both $p\bar{p}$ and pp. The latter data, taken together with earlier results, enable us to make a critical comparison of $p\bar{p}$ and pp elastic scattering parameters in the high energy domain from $\sqrt{s} = 5$ GeV to $\sqrt{s} = 62$ GeV, and allow theoretical extrapolations to higher energies. As we shall show, the agreement between these predictions and the new SPS results at $\sqrt{s} = 540$ GeV gives some confidence in further extrapolation to the energy regions of $\sqrt{s} = 2$ TeV (the Tevatron collider, scheduled for 1986) and $\sqrt{s} = 40$ TeV (the proposed SSC).

We will deal exclusively with $p\bar{p}$ and pp collisions, reviewing the relevant experimental results for elastic scattering and total cross section measurements for center of mass energies greater than 5 GeV, with emphasis on the new data for $\sqrt{s}$ greater than 30 GeV. In particular, we will concern ourselves with the analysis of elastic scattering in the low $|t|$ region, $-t < 0.02(\text{ GeV}/c)^2$, where t is the 4-momentum transfer squared. A brief description will recall to the reader the experimental techniques

and problems associated with these high energy measurements.

The principles of analyticity and unitarity are truly fundamental to our understanding of particle physics. A requirement of analyticity is that the forward scattering amplitudes for $p\bar{p}$ and pp elastic nuclear scattering come from the same analytic function. Further, unitarity provides a relation — the optical theorem — between the total cross section and the imaginary portion of the forward scattering amplitude. The existence of the new $p\bar{p}$ and pp data now makes possible a critical confrontation of the consequences of analyticity with accurate experimental data over a wide energy range.

We will review the consequences of analyticity for forward elastic scattering amplitudes. The presentation will be didactic in nature, and will only assume a general understanding of elementary scattering theory from non-relativistic quantum mechanics. The appropriate relativisitc generalizations will be made. Rigorous theorems following from analyticity, including the Froissant bound, generalizations of the Pomeranchuk theorem for rising cross sections, the Cornille and Martin bounds and the Fischer theorem, will be discussed. Using the impact parameter representation, these theorems will either be proved heuristically or be illustrated by simple examples. Their applicability and utility will be critically appraised.

Elastic scattering will be discussed in terms of an impact parameter representation. Using this physical picture, we will provide heuristic derivations of many of the important theorems relating to elastic scattering that are based on analyticity and unitarity. We express the slope parameter, B, $(=d/dt(\log(d\sigma_n/dt)))$ and the curvature parameter, C, $(=$

$\frac{1}{2}d^2/dt^2(\log(d\sigma_n/dt)))$ in impact space. Models of elastic scattering are dicussed and it is shown that $C = 0$ is a convenient criterion for the onset of "asymptopia", defined as the energy domain where differential elastic scattering cross section approaches that of a sharp disk.

A *model free* analysis will be made of the experimental quantities σ_{tot}, ρ and B. Traditionally, the requirements of analyticity have been compared with experimental data by means of dispersion relations. We will demonstrate how the same ends can be achieved more transparently and easily through direct use of simple analytic functions. The success of our fits is an experimental confirmation of the principles of analyticity. The comprehensive fit to $p\bar{p}$ and pp scattering reveals an unexpected regularity between the two systems over the full energy domain considered.

II. KINEMATICS AND CONVENTIONS

We consider elastic pp or $p\bar{p}$ scattering with the initial 4-momenta p_1 and p_2 and the final 4-momenta p_3 and p_4. The c.m. energy squared is

$$s = (p_1 + p_2)^2 = 4(k^2 + m^2), \tag{2.1}$$

where m is the proton mass and k is the c.m. momentum. In terms of the lab momentum p and lab energy $E = \sqrt{p^2 + m^2}$, we have

$$s = 2(m^2 + mE). \tag{2.2}$$

The 4-momentum transfer squared is

$$t = (p_1 - p_3)^2 \tag{2.3}$$

$$= -4k^2 \sin^2\theta/2, \tag{2.4}$$

where θ is the c.m. scattering angle. The third Mandelstam variable is

$$u = (p_1 - p_4)^2, \tag{2.5}$$

and we have

$$s + t + u = 4m^2. \tag{2.6}$$

We shall use elastic scattering amplitudes with several different normalizations. For f_{cm}, the c.m. scattering amplitude,

$$\frac{d\sigma}{d\Omega_{cm}} = |f_{cm}|^2, \tag{2.7}$$

$$\frac{d\sigma}{dt} = \frac{\pi}{k^2}|f_{cm}|^2, \tag{2.8}$$

$$\sigma_{tot} = \frac{4\pi}{k} Im\, f_{cm}(\theta = 0). \tag{2.9}$$

The lab scattering amplitude will be denoted simply by f. It satisfies

$$\frac{d\sigma}{d\Omega_{lab}} = |f|^2, \tag{2.10}$$

$$\frac{d\sigma}{dt} = \frac{\pi}{p^2}|f|^2, \tag{2.11}$$

$$\sigma_{tot} = \frac{4\pi}{p} Im f(\theta_L = 0), \tag{2.12}$$

where θ_L is the lab scattering angle. The lab scattering amplitude is related to the usual Lorentz invariant amplitude $\mathcal{M}$ by

$$\begin{aligned}\mathcal{M} &= -8\pi\sqrt{s}\left(\frac{k}{p}\right)f \\ &= -8\pi m f,\end{aligned} \tag{2.13}$$

so

$$\begin{aligned}\sigma_{tot} &= -\frac{1}{2pm} Im\mathcal{M}(t=0) \\ &= -\frac{1}{2k\sqrt{s}} Im\mathcal{M}(t=0).\end{aligned} \tag{2.14}$$

As a final normalization, we introduce F with the properties

$$\frac{d\sigma}{dt} = |F|^2, \tag{2.15}$$

$$\sigma_{tot} = 4\sqrt{\pi} Im\, F(t=0). \tag{2.16}$$

The normalizations for these elastic scattering amplitudes are related by

$$f = \frac{p}{k} f_{cm} = \frac{p}{\sqrt{\pi}} F = -\frac{1}{8\pi m}\mathcal{M}. \tag{2.17}$$

The context will dictate which of these amplitudes is most convenient to use.

III. REVIEW OF EXPERIMENTAL RESULTS FOR σ_{tot}, ρ, and B

Prior to presenting an overview of the experimental $p\bar{p}$ and pp results for σ_{tot}, ρ and B, we review briefly the theory of elastic hadronic scattering in the presence of a Coulomb field. This review will help us put into perspective measurements of elastic scattering made at small $|t|$ and will remind the reader of both the types of experimental measurements and the actual physical quantities which must be measured to extract the parameters σ_{tot}, ρ, and B.

A. Theoretical Formulation of Elastic Hadronic Scattering in the Presence of the Coulomb Field

For the moment, we consider separately the effects of either a Coulombic or a hadronic field, alone. We will later combine these fields to act simultaneously. In the presence of only a Coulomb field, we have the familiar Rutherford scattering cross section for pp ($p\bar{p}$), which is

$$\frac{d\sigma_c}{d\Omega}_{cm} = \left|\frac{-(\pm)\alpha G^2(t)}{2k\sin^2(\theta/2)}\right|^2, \tag{3.1}$$

where α is the fine-structure constant $\approx 1/137$, the upper sign is for pp, the lower sign is for $p\bar{p}$, and $G^2(t)$ is the proton's electromagnetic form factor squared. It is readily shown that

$$\frac{d\sigma}{dt} = \frac{\pi}{k^2}\frac{d\sigma}{d\Omega_{cm}}, \tag{3.2}$$

and we can rewrite Eq. (3.1) as

$$\frac{d\sigma_c}{dt} = \pi\left|-(\pm)G^2(t)\frac{2\alpha}{|t|}\right|^2. \tag{3.3}$$

Experiment has shown that we can adequately parametrize the nuclear (hadronic) elastic scattering cross section in the small $|t|$ region as

$$\frac{d\sigma_n}{dt} = \left(\frac{d\sigma_n}{dt}\right)_{t=0} e^{Bt}, \tag{3.4}$$

i.e., if we plot $\log(d\sigma_n/dt)$ *vs.* t, we get a straight line of slope B, for the small $|t|$ region. Now, we write Eq. (3.4), at $t = 0$, as (see Eq. (2.7))

$$\begin{aligned}\left(\frac{d\sigma_n}{dt}\right)_{t=0} &= \frac{\pi}{k^2}\left(\frac{d\sigma_n}{d\Omega}_{cm}\right)_{\theta=0} \\ &= \frac{\pi}{k^2}|Ref_{cm}(0) + iImf_{cm}(0)|^2.\end{aligned} \tag{3.5}$$

Introducing $\rho = Ref_{cm}(0)/Imf_{cm}(0)$, we rewrite Eq. (3.5) as

$$\begin{aligned}\left(\frac{d\sigma_n}{dt}\right)_{t=0} &= \pi\left|\frac{(\rho+i)Imf_{cm}(0)}{k}\right|^2 \\ &= \pi\left|\frac{(\rho+i)\sigma_{tot}}{4\pi}\right|^2,\end{aligned} \tag{3.6}$$

where the last step used the optical theorem Eq. (2.9). Thus, we can now write the elastic hadronic scattering cross section as a function of t as

$$\frac{d\sigma_n}{dt} = \pi\left|(\rho+i)\frac{\sigma_{tot}}{4\pi}e^{Bt/2}\right|^2. \tag{3.7}$$

It is convenient at this point to introduce the invariant scattering amplitudes of Eqs. (2.15) and (2.16),

$$F_c = -(\pm)\frac{2\alpha G^2(t)\sqrt{\pi}}{|t|}, \tag{3.8a}$$

and

$$F_n = \frac{(\rho+i)\sigma_{tot}e^{Bt/2}}{4\sqrt{\pi}}, \tag{3.8b}$$

so that the invariant differential cross sections are

$$\frac{d\sigma_c}{dt} = |F_c|^2, \tag{3.9a}$$

and

$$\frac{d\sigma_n}{dt} = |F_n|^2. \tag{3.9b}$$

The above results treat the case of only one interaction at a time. However, the simultaneous presence of both the nuclear and the Coulomb fields, although coherent, does not allow us simply to superimpose the amplitudes F_c and F_n. Instead, we must introduce a phase factor $\alpha\phi(t)$ into the Coulomb amplitude, such that the complete elastic differential cross sections is given by

$$\begin{aligned}\frac{d\sigma}{dt} &= \frac{d\sigma_c}{dt} + \frac{d\sigma_{cn}}{dt} + \frac{d\sigma_n}{dt} \\ &= \left|F_c e^{i\alpha\phi(t)} + F_n\right|^2 \\ &= \pi\left|-(\pm)G^2(t)\frac{2\alpha}{|t|}e^{i\alpha\phi(t)} + (\rho+i)\frac{\sigma_{tot}}{4\pi}e^{Bt/2}\right|^2,\end{aligned} \tag{3.10}$$

where we assume tacitly that ρ varies negligibly over the very small t-region of interest. The phase factor $\alpha\phi(t)$ reflects the distortion of the pure amplitudes F_c and F_n due to the simultaneous presence of both hadronic and Coulombic scattering. This is perhaps most simply understood if we use the language of Feynman diagrams, in which F_c corresponds to summing all diagrams in which only photons are present and F_n corresponds to summing all diagrams in which only hadronic exchanges are present. However, when both fields are turned on, there are new diagrams possible which have both photons and hadronic exchanges present in the same diagram, which are not accounted for in F_c and F_n. This gives rise to the phase $\alpha\phi(t)$. This phase was first investigated by Bethe (1958), and later by West and Yennie (1968), using a Q.E.D. calculation of Feynman diagrams. Most recently, the phase was recalculated by Cahn (1982b), using an eikonal approach, with the result

$$\begin{aligned}\phi(t) = -(\pm)\Big[&\gamma + \log\left(\frac{B|t|}{2}\right) + \log\left(1+\frac{8}{B\Lambda^2}\right) \\ &+ \left(\frac{4|t|}{\Lambda^2}\right)\log\left(\frac{4|t|}{\Lambda^2}\right) + \frac{2|t|}{\Lambda^2}\Big],\end{aligned} \tag{3.11}$$

where $\gamma = 0.577\ldots$ is Euler's constant, B is the slope parameter,

Λ^2 ($= 0.71$ (GeV/c)^2) appears in the dipole fit to the proton's electromagnetic form factor, and the upper sign is for pp and the lower sign for p$\bar{\text{p}}$. In the low $|t|$ region of interest, the numerical values given by Cahn agree very closely with those given by West and Yennie. In the t region near the interference maximum of Eq. (3.10), the value of $\phi(t)$ is very slowly varying and is ≈ 2. Thus, $\alpha\phi$ is $\ll 1$, as also is $Bt/2$, while $G^2(t)$ is ≈ 1. We can now simplify the interference (cross) term of $d\sigma/dt$, defined as $d\sigma_{cn}/dt$ in Eq. (3.10), to be

$$\begin{aligned} \frac{d\sigma_{cn}}{dt} &\approx 2(\rho + \alpha\phi)F_cF_n \\ &\approx -(\pm)(\rho + \alpha\phi)\left(\frac{\alpha\sigma_{tot}}{|t|}\right), \end{aligned} \tag{3.12}$$

with the upper sign for pp and the lower sign for p$\bar{\text{p}}$ and where F_n is evaluated at $t = 0$. The importance of this term is clearly maximal when $|F_c| = |F_n|$, *i.e.* when $d\sigma_c/dt = d\sigma_n/dt$. If $\rho + \alpha\phi$ is positive, the interference is destructive for pp and constructive for p$\bar{\text{p}}$. A typical value for $|\alpha\phi|$ in Eq. (3.12) is ≈ 0.02. Thus, the presence of the interference cross section $d\sigma_{cn}/dt$ allows one to measure the quantity $\rho+\alpha\phi$. Assuming that we know σ_{tot}, the interference term allows the evaluation of ρ, the ratio $Ref_{cm}(0)/Imf_{cm}(0)$. Therefore, the Coulomb amplitude serves as a standard against which the phase of the hadronic amplitude is measured. Inspection of Eq. (3.10) indicates that the interference term is of maximum significance when

$$|t|_{int} \approx \frac{8\pi\alpha}{\sigma_{tot}} = \frac{0.071}{\sigma_{tot}(\text{mb})}, \quad \text{for} \quad t \quad \text{in}\,(\text{GeV}/c)^2. \tag{3.13}$$

We note that the differential elastic scattering cross section given by Eq. (3.10) divides up naturally into three distinct t regions. Region 1 is for $|t| \ll |t|_{int}$, where the Coulomb scattering dominates, and $d\sigma/dt$ goes as $1/t^2$. Region 3 is where $|t| \gg |t|_{int}$, where the nuclear scattering predominates, and $d\sigma/dt$ goes as e^{Bt}. Region 2 is where $t \simeq t_{int}$, which is the interference region between the Coulombic and the hadronic amplitudes.

For a colliding beam experiment, where $|t| = (k\theta)^2$, it is useful to define the interference angle θ_{int} as

$$\theta_{int} = \frac{\sqrt{|t|_{int}}}{k}. \tag{3.14}$$

Table 3.1 gives $|t|_{int}$ and θ_{int} for p$\bar{\text{p}}$ as a function of the energy, $\sqrt{s}$, for typical colliding beam accelerators. For example, at the ISR, for $\sqrt{s} =$ 30.7 GeV (corresponding to each beam having $k \approx 15$ GeV/c), we find $|t|_{int} = 0.0017$ (GeV/c)^2, and hence, $\theta_{int} = \sqrt{0.0017}/15 = 2.7$ mrad. However, when we get up to the Tevatron collider energy, $\sqrt{s} = 2$ TeV, where we expect $\sigma_{tot} \approx 100$ mb, we find that $|t|_{int} = 0.00073$ (GeV/c)^2 and that $\theta_{int} = 0.027$ mrad, a very small angle, indeed. At a distance of 100 meters from the interaction region, it corresponds to a transverse displacement of only 3.7 mm. This illustrates the difficulty of penetrating into the Coulomb interference region, let alone the Coulomb region, as we go to higher energy colliders. Clearly, the experimental problems become extremely severe for the proposed SSC collider, at $\sqrt{s} = 40$ TeV, where θ_{int} is only about 0.001 mrad.

B. Measurement of σ_{tot}, ρ, and B from Elastic Scattering

The measured quantity in an experiment is a counting rate, not a cross section. For example, in an elastic scattering differential cross section experiment, the quantity measured is $\Delta N(t)$, the number of counts/sec/Δt in a Δt interval around t, corrected for background and any inefficiencies, such as azimuthal coverage, deadtime, etc. This rate must be normalized to get $d\sigma/dt$, and thus we write

$$\Delta N(t) = L\left(\frac{d\sigma}{dt}\right), \tag{3.15}$$

where L is the normalization factor (for colliding beams, L is the luminosity). If we can get deeply into the Coulomb region, *i.e.*, in Region 1 where $|t| \ll |t|_{int}$, then $d\sigma/dt$ is for all practical purposes given by $d\sigma_c/dt \approx 4\pi(\alpha/t)^2$. Thus, $d\sigma/dt$ is a known cross section, which allows the experimenter to measure L directly from Eq. (3.15). To take a concrete example, if the experiment is carried out at the ISR at $\sqrt{s} = 23.5$ GeV and the experiment is capable of achieving a minimum $|t|$ of 0.00035 (GeV/c)^2, then the value of $d\sigma/dt$ at this t is $\approx$ 96% Coulombic. Thus, the data are easily and accurately normalized, provided that the t scale is well determined. We note the vital role the known Coulomb cross section plays in this type of measurement. If the normalization factor L is known, the total cross section σ_{tot} is determined by plotting the counting rates $\Delta N(t)$ in the nuclear region (Region 3) on a $\log\Delta N(t)$ vs. t plot and fitting a straight line in order to obtain $\Delta N(0)$, the hadronic counting rate at $t = 0$. From Eqs. (3.4), (3.6) and (3.15), knowing the normalization L, we find

$$\begin{aligned}\sigma_{tot}(1+\rho^2)^{1/2} &= 4\sqrt{\pi\left(\frac{d\sigma_n}{dt}\right)_{t=0}} \\ &= 4\sqrt{\pi\left(\frac{\Delta N(0)}{L}\right)}.\end{aligned} \tag{3.16}$$

Thus, this technique, in which L is separately evaluated, measures the quantity $\sigma_{tot}\sqrt{1+\rho^2}$. The ρ value can be evaluated from the Coulomb interference term in Region 2; see Eqs. (3.10), (3.12). Of course, there are alternative ways of measuring the luminosity, without using the Coulomb technique, such as the Van der Meer (1968) method of sweeping beams through each other, etc. In all cases, a direct measurement of L, along with a measurement of $\Delta N(0)$, yields the result in Eq. (3.16), *i.e.*, $\sigma_{tot}\sqrt{1+\rho^2}$.

To demonstrate the power of Coulomb normalization and to illustrate the quality of the available data, we show in Fig. 3.1 an experimental plot of $\log(d\sigma/dt)$ *vs.* $|t|$ for pp elastic scattering at $\sqrt{s} =$ 23.5 GeV, taken in 1982 at the ISR by the Northwestern-Louvain group (Block, 1983b). There are $\approx 10^6$ events used to determine the elastic differential cross section. The minimum $|t|$ obtained in the experiment is $\approx$ 0.00025 (GeV/c)^2, well below the value (see Table 3.1) of $|t|_{int} =$ 0.0017 (GeV/c)^2. Thus, this experiment probed deeply into the Coulomb region (Region 1) and therefore also easily probed Region 2, the interference region. The fitted curve used the parametrization of Eq. (3.10). The ρ value extracted was $\rho = -0.006 \pm 0.010$, using Coulomb normalization. The quality of the fit was quite satisfactory, giving a $\chi^2/d.f. \approx 1.2$ for 93 degrees of freedom. A plot of $\log(d\sigma/dt)$ *vs.* $|t|$ for $p\bar{p}$ elastic scattering at $\sqrt{s} = 52.8$ GeV, taken by the Northwestern-Louvain group

(Amos *et al.*, 1983a ;Block, 1983b) at the ISR in 1982, is shown in Fig. 3.2. This spectrum contains $\approx 10^5$ events. Because of the higher beam momentum, the miminum $|t|$ is $\approx 0.0010\,(\,\mathrm{GeV}/c)^2$, compared to $t_{int} = 0.0016\,(\,\mathrm{GeV}/c)^2$ for this energy, and hence, the Coulomb region is only slightly penetrated. The parametrization of Eq. (3.10) was used to obtain the fitted curve. In this case, the measured quantities were σ_{tot}, ρ and B, with the values $\sigma_{tot} = 43.2 \pm 0.4$ mb, $\rho = 0.13 \pm 0.02$ and $B = 13.0 \pm 0.5\,(\,\mathrm{GeV}/c)^{-2}$. The quality of the fit was good, yielding $\chi^2/d.f. = 0.59$, for 117 degrees of freedom.

Another method for determining the cross section is the so called "luminosity free" method, in which one simultaneously measures N_{tot}, the total counting rate due to any interaction, along with the elastic scattering intercept rate, $\Delta N(0)$. We write

$$N_{tot} = L\sigma_{tot}, \tag{3.17a}$$

and

$$\Delta N(0) = L\left(\frac{d\sigma_n}{dt}\right)_{t=0}. \tag{3.17b}$$

From Eq. (3.16) and (3.17b), we find L and substitute it into Eq. (3.17a) to obtain

$$\sigma_{tot}(1+\rho^2) = \frac{16\pi\Delta N(0)}{N_{tot}}. \tag{3.18}$$

We see from Eq. (3.18) that the measured quantity from the "luminosity

free" technique is $\sigma_{tot}(1+\rho^2)$, in contrast to the direct measurement of L which yields $\sigma_{tot}\sqrt{1+\rho^2}$. In both cases, the measurements require $\Delta N(0)$, the extrapolated hadronic counting rate at $t = 0$, which is found by measurements in Region 3, the pure nuclear region. We note that a knowledge of ρ is needed in both cases in order to extract σ_{tot}. However, these measurements only depend weakly on ρ, since for ρ as large as 0.2, $1+\rho^2$ is only 1.04, a 4% effect in one case and a 2% effect in the other. Thus, even a very inaccurate knowledge of ρ yields a relatively accurate value of σ_{tot}.

The value of the nuclear slope B is found by plotting the unnormalized curve, $\log(\Delta N(t))$ *vs.* t, in the purely hadronic region (Region 3) and extracting the slope of this straight line. Thus the measurement of B does not require a knowledge of the normalization L.

Experiment shows that in the region of $|t| > \approx 0.10\,(\,\mathrm{GeV}/c)^2$, the parametrization (Eq. (3.4)) of an exponential in Bt fails and a "break" in the slope occurs, with the slope getting smaller in the higher $|t|$ region. The experimental elastic differential cross section data can be parametrized over this larger $|t|$ region as

$$\frac{d\sigma_n}{dt} = \left(\frac{d\sigma_n}{dt}\right)_{t=0} \exp(Bt + Ct^2), \tag{3.19}$$

where the curvature C is $\approx 5\,(\,\mathrm{GeV}/c)^{-4}$. Thus if we define a t dependent slope

$$B(t_0) = \left(\frac{d}{dt}\log\frac{d\sigma_n}{dt}\right)_{t=t_0}, \tag{3.20}$$

we obtain $B(t_0) = B - 2C|t_0|$. If the experimental t range is limited to $|t| < 0.02\,(\mathrm{GeV}/c)^2$, we have a mean $|t_0|$ of $\approx 0.01\,(\mathrm{GeV}/c)^2$. Since a typical value of B is $\approx 12\,(\mathrm{GeV}/c)^2$, we get $B(t = 0.01\,(\mathrm{GeV}/c)^{-2}) \approx 0.993\,B$, where $B = B(0)$. Thus, the difference between B and the measured value $B(t_0)$ is negligible below $|t| \approx 0.02\,(\mathrm{GeV}/c)^2$.

The total elastic scattering cross section σ_{el} is defined as $\int_{-\infty}^{0}(d\sigma_n/dt)dt$. With the parametrization used in Eq. (3.4) and the results of Eq. (3.6), it is easily shown that

$$\begin{aligned}\sigma_{el} &= \frac{1}{B}\left(\frac{d\sigma_n}{dt}\right)_{t=0} \\ &= \frac{\sigma_{tot}^2(1+\rho^2)}{16\pi B}.\end{aligned} \tag{3.21}$$

This result will be given a special name. We will define Σ_{el} as

$$\Sigma_{el} = \frac{\sigma_{tot}^2(1+\rho^2)}{16\pi B}. \tag{3.22}$$

If the parametrization (Eq. (3.4)) were valid over the entire t range, then σ_{el} would be Σ_{el}. We note that the value of Σ_{el} is the number often given in the literature as the experimental value of σ_{el}. From Eq. (3.22), we find that the ratio of Σ_{el}/σ_{tot} is

$$\frac{\Sigma_{el}}{\sigma_{tot}} = \frac{\sigma_{tot}(1+\rho^2)}{16\pi B}, \tag{3.23}$$

a result that will be used later.

C. An Overview of Experimental Results

Measurements of elastic scattering have had a rich history at the Brookhaven AGS (Foley *et al.*, 1967), Serpukhov, (Denisov *et al.*, 1971a, 1971b), CERN PS (Belletini *et al.*, 1965), Fermilab (Bartenev *et al.*, 1972, 1973a, 1973b, Carroll *et al.*, 1974, Fajardo *et al.*, 1981), CERN ISR (Amaldi *et al.*, 1971, Barbiellini *et al.*, 1972, Holder *et al.*,1971,Amaldi and Schubert, 1980, Favart *et al.*, 1981, Amos *et al.*, 1983a, 1983b, Carboni *et al.*, 1982a, 1982b) and the CERN SPS (UA4 Collaboration, 1982a, 1982b, UA1 Collaboration, 1983)collider. There is now an approved experiment for the Tevatron collider, to be carried out in 1986. Indeed, plans are currently in progress to try to measure the elastic scattering at the proposed SSC in the 1990's.

The utilization of $\bar{\mathrm{p}}$ beams have made possible accurate comparisons of the $\mathrm{p\bar{p}}$ system with the pp system up to $\sqrt{s} = 62.8$ GeV, using colliding beams. The colliding beam experiments all use "Roman Pots" named by the CERN-Rome (Amaldi *et al.*, 1973a) group which first used them. The Roman Pots are re-entrant bellows in the vacuum chambers used to get the counters (or drift chambers) close to the beams. This is done so that the minimum angle of detection, θ_{min}, is small compared to θ_{int}, the Coulomb interference angle, to maximize Coulomb effects and to measure the interference term proportional to $\rho + \alpha\phi$.

Before the advent of the ISR collider ($\sim$ 1971), the available pp data appeared to have σ(pp) leveling off with increasing energy to a value of $\approx$ 40 mb. The anti-proton cross sections available in this era were higher than the pp cross sections, and $\sigma(\mathrm{p\bar{p}})$ appeared to be falling with increasing energy and approaching σ(pp). Thus, it was assumed at this

time that the two cross sections were approaching a common constant value of $\approx$ 40 mb, as $\sqrt{s} \to \infty$. The nuclear slope parameters $B(p\bar{p})$ were larger than $B(pp)$. The $B(pp)$ were increasing with $\sqrt{s}$ (diffractive shrinkage), whereas the $B(p\bar{p})$ were slightly decreasing with increasing $\sqrt{s}$, and it appeared that both were going to a common value. The values of $B(pp)$ at the top energy were $\approx 12\,(\,\mathrm{GeV}/c)^{-2}$.

When the ISR was turned on in 1971, one of the first experiments done was an elastic scattering measurement of $\sigma(pp)$ for the CERN-Rome group (Amaldi *et al.*, 1971), using the Van der Meer method of luminosity determination and a measurement of $\sigma(pp)$ by the Pisa-Stony Brook group (Amendolia, *et al.*, 1973 a,b) using total counting rate and luminosity. These early measurements showed that the pp cross section was rising with energy, and indeed, had a rise that could be fitted with a $\log^2 s/s_0$ term, where s_0 is a scale constant. These measurements were confirmed later when the Fermilab accelerator and the SPS came into operation. The value for the anti-proton cross section was still dropping at the highest available energy ($\sqrt{s} \approx 10$ GeV). With the introduction of a $\bar{p}$ beam into the ISR, in 1982, experiments on $p\bar{p}$ scattering were done both by the Northwestern-Louvain group (Favart *et al.*, 1982, Amos *et al.*, 1983a, 1983b) using elastic scattering and Coulomb normalization, and by the Pisa-Stony Brook (Carboni, *et al.*, 1982a, 1982b)group, using total counting rate and Van der Meer luminosity. The Northwestern-Louvain group measured σ_{tot}, ρ and B for $p\bar{p}$, while the Pisa-Stony Brook group measured σ_{tot}. These results conclusively showed that the value of $\sigma(p\bar{p})$ at $\sqrt{s} = 52.8$ GeV was rising from its low energy value and that $\sigma(p\bar{p})$ appeared to be approaching $\sigma(pp)$. The ρ values, as well as the slope parameters B also seemed to be approaching one another.

Shown in Fig. 3.3 are the currently available experimental cross section data in the energy interval $5 < \sqrt{s} < 62$ GeV for both pp and $p\bar{p}$. In Fig. 3.4 are shown the ρ data, and Fig. 3.5 shows the B data. We observe that $\sigma(p\bar{p})$ falls from the value of $\approx$ 50 mb at $\sqrt{s} = 5$ GeV to a minimum of $\approx$ 41.5 mb at $\sqrt{s} \approx 20$ GeV and rises to $\approx$ 44 mb at $\sqrt{s} \approx$ 62 GeV. The cross section $\sigma(pp)$ starts at $\approx$ 39.6 mb at $\sqrt{s} = 5$ GeV, goes through a very shallow minimum of $\approx$ 39 mb at $\sqrt{s}$ near 12 GeV and climbs to $\approx$ 43.5 mb at $\sqrt{s} = 62$ GeV. The $\rho(pp)$ values rise from ≈ 0.27 at $\sqrt{s} = 5$ GeV, going through zero at $\sqrt{s} = 23$ GeV, and reach about 0.10 at $\sqrt{s} = 62$ GeV. The $\rho(p\bar{p})$ values are about zero in the energy region $10 < \sqrt{s} < 20$ GeV, and rise to ≈ 0.10 at $\sqrt{s} = 53$ GeV. The slope parameter data show that $B(pp)$ is rising, going from about $9.5\,(\,\mathrm{GeV}/c)^{-2}$ at $\sqrt{s} = 5$ GeV to $12.5\,(\,\mathrm{GeV}/c)^{-2}$ at $\sqrt{s} = 62$ GeV. The values for $B(p\bar{p})$ stay relatively constant at low $\sqrt{s}$, around $12\,(\,\mathrm{GeV}/c)^{-2}$, and rise to about $12.5\,(\,\mathrm{GeV}/c)^{-2}$ at $\sqrt{s} = 53$ GeV.

The ratio of the "total" elastic scattering cross section to the total cross section, $R = \Sigma_{el}/\sigma_{tot}$, is relatively flat in the ISR energy region, being ≈ 0.18. It appears to have fallen slightly from its low energy value. As we will show later, it is expected to rise as high as $\sqrt{s}$.

The dominant experimental problems for the future, at high energy will be:

(1) to see if the current trends of $\Delta\sigma_{tot}$, $\Delta\rho$ and ΔB going to zero (for $\Delta = [(p\bar{p}) - (pp)]$) continue as we go to very high s;

(2) to verify that the cross section σ_{tot}, which currently rises as $\log^2 s/s_0$, continues this rise as we increase s;

(3) to find out if B also increases as $\log^2 s$ as we go up in s;

(4) to determine whether $R = \Sigma_{el}/\sigma_{tot}$ keeps increasing and find out its asymptotic constant value, *i.e.*, to determine whether the $p\bar{p}$ system is a gray disc ($R < 0.5$) or a black disc ($R = 0.5$), or indeed, if $1 > R > 0.5$.

These are important questions. The answers become more difficult at high $\sqrt{s}$, and the required measurements pose a real challenge to tomorrow's experimentalists.

IV. THEORETICAL DISCUSSION

A. Unitarity

In the next two sections, it is convenient to work in the center of mass frame. For elastic scattering, unitarity is embodied in the optical theorem,

$$\sigma_{tot} = \frac{4\pi}{k} Im f_{cm}(t=0). \tag{4.1}$$

Writing an expansion in terms of Legendre polynomials gives the standard partial wave expansion for spinless particles (for our purpose of examining the nearly forward region, we can ignore spin)

$$f_{cm}(s,t) = \frac{1}{k}\sum_{l=0}^{\infty}(2l+1)P_l(\cos\theta)a_l(k), \tag{4.2}$$

where θ is the c.m. scattering angle. Comparing coefficients in

$$\sigma_{tot} = \int dt \frac{d\sigma}{dt} = \int dt \frac{\pi}{k^2}|f_{cm}|^2 = \frac{4\pi}{k} Im f(t=0), \tag{4.3}$$

we find for purely elastic scattering

$$Im\, a_l = Im\, a_l^2 + Re\, a_l^2, \tag{4.4}$$

so the amplitude for each partial wave lies on the Argand circle Fig. (4.1)

$$\left(Ima_l - \frac{1}{2}\right)^2 + Rea_l^2 = \frac{1}{4}. \tag{4.5}$$

If there is inelasticity, the amplitude lies inside the Argand circle (Fig. 4.1). Such an amplitude can be represented as

$$a_l = \frac{e^{2i\delta_l} - 1}{2i}, \tag{4.6}$$

where δ_l is purely real if there is only elastic scattering and $Im\delta_l > 0$ if there is inelasticity.

A more complete formalism is needed to express the full content of unitarity in the inelastic case. For this purpose we employ the conventional Lorentz invariant amplitude M which is related to the S-matrix by

$$S = I - i(2\pi)^4\delta^4(p_1 + p_2 - \textstyle\sum_i p_i')\frac{\langle p_1' p_2' \ldots p_n' | M | p_1 p_2\rangle}{(2E_1)(2E_2)\prod_i (2E_i')}, \tag{4.7}$$

where $p_1(E_1)$ and $p_2(E_2)$ are the initial momenta (energies), the primes indicate final momenta and energies, and I is the unit matrix. The states are normalized with

$$\langle p'|p\rangle = (2\pi)^3\delta^3(p - p'), \tag{4.8}$$

so completeness is expressed by

$$I = \sum_n \prod_{i=1}^n \left(\int \frac{d^3p_i'}{(2\pi)^3}\right) |p_1' p_2' \ldots p_n'\rangle\langle p_1' p_2' \ldots p_n'|, \tag{4.9}$$

or symbolically,

$$I = \sum_n |n><n|. \tag{4.10}$$

Unitarity is the statement

$$S^\dagger S = I. \tag{4.11}$$

Evaluated between two-body states $|p_1 p_2\rangle$ and $|p_3 p_4\rangle$, Eq. (4.11) gives

$$\begin{aligned}\langle p_3 p_4| - iM + iM^\dagger |p_1 p_2\rangle &= 2Im\langle p_3 p_4 | M | p_1 p_2\rangle \\ &= -(2\pi)^4 \sum_n \prod_{i=1}^n \left[\int \frac{d^3p_i'}{(2\pi)^3 2E_i'}\right] \delta^4(p_1 + p_2 - \textstyle\sum_{j=1}^n p_j') \\ &\quad \langle p_3 p_4 | M^\dagger | p_1' p_2' \ldots p_n'\rangle\langle p_1' p_2' \ldots p_n' | M p_1 p_2\rangle.\end{aligned} \tag{4.12}$$

We recognize the usual n-body phase space

$$d\Phi_n = (2\pi)^4 \sum_n \prod_{i=1}^n \left[\int \frac{d^3p_i'}{(2\pi)^3 2E_i'}\right] \delta^4(p_1 + p_2 - \textstyle\sum_{j=1}^n p_j'), \tag{4.13}$$

which relates the cross section to the amplitude squared:

$$d\sigma_n = \frac{1}{2E_1 2E_2 \times \text{flux factor}} |\mathcal{M}|^2 d\Phi_n. \tag{4.14}$$

The flux factor ("the relative velocity of the incoming particles") multiplied by $2E_1 2E_2$ is simply $4k\sqrt{s}$ where k is, as always, the c.m. momentum in the initial state. Thus specializing to forward scattering with $p_1 = p_2$, $p_3 = p_4$, we find with $\mathcal{M}(t=0) = \langle p_1 p_2 | \mathcal{M} | p_1 p_2 \rangle$,

$$2Im\mathcal{M}(t=0) = -4k\sqrt{s}\sum_n \sigma_n = -4k\sqrt{s}\sigma_{tot}, \tag{4.15}$$

or

$$\sigma_{tot} = -\frac{1}{2k\sqrt{s}} Im\mathcal{M}(t=0). \tag{4.16}$$

In this proof of the optical theorem, we see how a sum over physical intermediate states is central to exploiting the formal statement of unitarity, Eq. (4.11).

B. Geometrical Picture

1. Impact Parameter Representation

Elastic pp scattering is described by five amplitudes, but in the very forward direction, which is our concern, it suffices to imagine that there is a single amplitude, just as one has for spinless particles. For this amplitude we will be able to develop a geometrical picture based on impact parameter space, the two dimensional physical space perpendicular to the beam direction. (See Jackson, 1973, for an earlier account of some

of this material.) Throughout, we consider only hadronic scattering and ignore the Coulomb effects which are important only at very small $|t|$. The standard partial wave expansion for the scattering amplitude given in Eq. (4.2) is

$$f_{cm}(s,t) = \frac{1}{k}\sum_{l=0}^{\infty}(2l+1)P_l(\cos\theta)a_l(k),$$

where, as in Eq. (4.6),

$$a_l(k) = \frac{\exp(2i\delta_l) - 1}{2i},$$

and δ_l is the phase shift in the l^{th} partial wave. If the scattering is purely elastic, δ_l is real. If there is inelasticity, $Im\delta_l > 0$. From Eq. (4.1) it follows that the contribution of the l^{th} partial wave to the total cross section is bounded:

$$\sigma_l \leq \frac{4\pi(2l+1)}{k^2}. \tag{4.17}$$

Since the bound is a decreasing function of the energy, it follows that an increasing number of partial waves must contribute to the high energy amplitude. It is thus sensible to convert the discrete sum, Eq. (4.2), into an integral.

A classical description of the scattering would introduce the impact parameter, b, which is related to the angular momentum by $bk = l + \frac{1}{2}$. The extra 1/2 is thrown in for convenience and in recognition of its appearance in the WKB approximation. To convert Eq.(4.2) to an integral, we replace $\sum_l \to \int dl \to \int k\, db$ and $a_l(k) \to a(b,s)$. We need also to express $P_l(\cos\theta)$ in terms of b and q, where $q^2 = -t = 4k^2\sin^2(\theta/2)$.

For large l, we have (Erdélyi,1953)

$$P_l(\cos\theta) \to J_0((2l+1)\sin\theta/2). \tag{4.18}$$

With these replacements, Eq.(4.2) becomes

$$f_{cm}(s,t) = 2k\int_0^\infty bdbJ_0(qb)a(b,s), \tag{4.19}$$

or, using the integral representation of J_0 (Abramowitz and Stegun, 1964, p. 360)

$$J_0(z) = \frac{1}{2\pi}\int_0^{2\pi} d\phi \exp(iz\cos\phi), \tag{4.20}$$

it is simply

$$f_{cm}(s,t) = \frac{k}{\pi}\int d^2b\ \exp(i\mathbf{q}\cdot\mathbf{b})a(b,s), \tag{4.21a}$$

where $d^2b = b\,dbd\phi$. The Fourier transform can be inverted to give

$$a(b,s) = \frac{1}{4\pi k}\int d^2q\exp(-i\mathbf{q}\cdot\mathbf{b})f_{cm}(s,t). \tag{4.21b}$$

With our normalization, we have, using Eq. (4.21a),

$$\sigma_{el} = \frac{\pi}{k^2}\int dt|f_{cm}|^2 = \frac{1}{k^2}\int d^2q|f_{cm}|^2 = 4\int d^2b|a(b,s)|^2, \tag{4.22}$$

and

$$\sigma_{tot} = \frac{4\pi}{k}Imf_{cm}(s,0) = 4\int d^2b\ Im\ a(b,s). \tag{4.23}$$

The amplitude $a(b,s)$ is given in impact parameter space which is perpendicular to the beam direction and thus is the same in the lab and c.m. systems. Its form is still that of Eq. (4.6). Therefore it lies in the usual

Argand plot, shown in Fig. 4.1. Elastic scattering corresponds to δ being real. If there is inelastic scattering as well, then δ has a positive imaginary part and $a(b,s)$ lies inside the Argand circle.

Equation (4.21a) has a simple physical interpretation. The function $a(b,s)$ can be viewed as a distribution of sources of waves which produce an interference pattern. Equivalently, it can be viewed as the distribution of an absorber which produces a diffraction pattern when plane waves are incident on it. There is a clear analogy with diffraction in optics (for an extensive review of this analogy, see Amaldi, Jacob, and Matthiae (1976)). Total absorption corresponds to $Im\,\delta = \infty$ or $a(b,s) = i/2$. Thus a black disk of radius R gives a total cross section (see Eq.(4.23)) $2\pi R^2$ and an elastic cross section (see Eq. (4.22)) πR^2. For a Gaussian shape in impact parameter space, the elastic scattering amplitude is a Gaussian in momentum transfer. In particular, if the scattering amplitude is $f = (ik\sigma_{tot}/4\pi)\exp(-Bq^2/2)$, so that B is the nuclear slope parameter, the impact parameter space representation is $a = (i\sigma_{tot}/8\pi B)\exp(-b^2/2B) = (2i\sigma_{el}/\sigma_{tot})\exp(-b^2/2B)$. Note that $|a(b=0)| = 2\sigma_{el}/\sigma_{tot} = 2\Sigma_{el}/\sigma_{tot}$. The connection between $a(b=0)$ and σ_{el}/σ_{tot} is more general. Suppose that the scattering amplitude is $f = (k/4\pi)(i+\rho)\sigma_{tot}g(q^2/\Lambda^2)$ where ρ is independent of q^2 and g is some function of a single variable, $u = q^2/\Lambda^2$. Then it is easy to show that

$$a(b=0) = \frac{\sigma_{el}}{(1+\rho^2)\sigma_{tot}}\frac{\int_0^\infty dug(u)}{\int_0^\infty dug^2(u)}. \tag{4.24}$$

Thus for scattering amplitudes of this generic form, $a(b=0)$ is given by $\sigma_{el}/(1+\rho^2)\sigma_{tot}$ times a pure number which depends on the shape of g,

but not on the actual value of the parameter, Λ^2.

2. The Slope Parameter B and the Mac Dowell - Martin Bound

Using the impact parameter amplitude, we can obtain a physical picture of the slope parameter,

$$B(s,t) = \frac{d}{dt}\left(\ln \frac{d\sigma}{dt}\right), \tag{4.25a}$$

which we often evaluate at zero momentum transfer

$$B = B(s) = B(s, t = 0). \tag{4.25b}$$

Beginning with

$$f_{cm} \sim \int d^2b \exp(i\mathbf{q}\cdot\mathbf{b})\, a(b,s), \tag{4.26}$$

we expand about $q = 0$ to find

$$f_{cm} \sim \int d^2b a(b,s)[1 + i\mathbf{q}\cdot\mathbf{b} - \frac{1}{2}(\mathbf{q}\cdot\mathbf{b})^2 \ldots]. \tag{4.27}$$

This yields a general expression for B,

$$B = \frac{\mathcal{R}e \int dbba(b,s) \int dbb^3 a^*(b,s)}{2\left|\int dbba(b,s)\right|^2}. \tag{4.28}$$

Thus, if the phase of $a(b,s)$ is independent of b, we have

$$B = \frac{\int db\, b^3 a(b,s)}{2\int db\, ba(b,s)} = \frac{\int d^2b\, b^2 a(b,s)}{2\int d^2b\, a(b,s)}. \tag{4.29}$$

This shows that B measures the size of the proton. More precisely, B is one-half the average value of the impact parameter squared as weighted by a.

Let us suppose that the phase of $a(b,s)$ is independent of b, so that $\mathcal{R}e\, a(b,s)/\mathcal{I}m\, a(b,s) = \rho$. Then we can write

$$a(b,s) = \frac{i+\rho}{\sqrt{1+\rho^2}}|a(b,s)|. \tag{4.30}$$

Combining Eqs. (4.22), (4.23), and (4.29), we find

$$\frac{\sigma_{el}}{\sigma_{tot}} = \sqrt{1+\rho^2}\frac{\int bdb|a(b,s)|^2}{\int bdb|a(b,s)|}, \tag{4.31}$$

$$\frac{\Sigma_{el}}{\sigma_{tot}} = \frac{\sigma_{tot}}{16\pi B} = \frac{1}{\sqrt{1+\rho^2}}\frac{[\int bdb|a(b,s)|]^2}{\int dbb^3|a(b,s)|}. \tag{4.32}$$

As an example, suppose $a(b,s)$ is purely imaginary and constant, with $a = iA/2$, where $0 < A \leq 2$, for $b < R$ and zero for $b > R$. Then $\sigma_{el}/\sigma_{tot} = \Sigma_{el}/\sigma_{tot} = A/2$. A perfectly black disk has $A = 1$. The equality of σ_{el} and Σ_{el} is characteristic. In fact, the Mac Dowell - Martin (Mac Dowell and Martin, 1964) bound states that

$$\frac{\sigma_{el}}{\Sigma_{el}} \geq \frac{8}{9}. \tag{4.33}$$

We can demonstrate this using the impact parameter representation assuming that $a(b)$ is purely imaginary. Then letting $a' = Ima$,

$$\sigma_{tot} = 4\int d^2b a', \tag{4.34a}$$

$$\sigma_{el} = 4\int d^2b\, a'^2, \tag{4.34b}$$

$$\sigma_{tot}B = 2\int d^2b b^2 a', \tag{4.34c}$$

and

$$\frac{\sigma_{el}}{\Sigma_{el}} = 2\pi\frac{\int d^2b\, a'^2 \int d^2b\, b^2 a'}{(\int d^2b\, a')^3}. \tag{4.35}$$

Now to minimize σ_{el}/Σ_{el} we consider varying the form of a' by $\delta a'$. Then at the minimum

$$\begin{aligned}\delta\frac{\sigma_{el}}{\Sigma_{el}} &= 0 \\ &= \Big[\int d^2b\, 2a'\delta a' \int d^2b\, b^2 a' \int d^2b\, a' + \int d^2b\, a'^2 \int d^2b\, b^2\delta a' \int d^2b\, a' \\ &\quad -3\int d^2b\, a'^2 \int d^2b\, b^2 a' \int d^2b\, \delta a'\Big](\int d^2b\, a')^{-4}.\end{aligned} \tag{4.36}$$

Since this is true for arbitrary $\delta a'$, the coefficient of $\int d^2b\, \delta a'$ must vanish and

$$2a'\int d^2b b^2 a' \int d^2b a' + b^2 \int d^2b a'^2 \int d^2b a' - 3\int d^2b a'^2 \int d^2b b^2 a' = 0. \tag{4.37}$$

Thus a' is of the form

$$a' = C_1 - C_2 b^2, \tag{4.38}$$

where C_1 and C_2 are positive constants, as seen in Eq. (4.37). Now a' cannot be negative, since $Ima \geq 0$, so a' vanishes outside some radius R and we write

$$a' = A[1 - (b/R)^2], \qquad b \leq R \tag{4.39a}$$

$$a' = 0, \qquad b > 0. \tag{4.39b}$$

This gives

$$\sigma_{tot} = 2\pi AR^2, \tag{4.40a}$$

$$\sigma_{el} = \frac{4\pi}{3}A^2R^2, \tag{4.40b}$$

$$B = \frac{1}{6}R^2, \tag{4.40c}$$

$$\Sigma_{el} = \frac{3\pi}{2}A^2R^2, \tag{4.40d}$$

and

$$\frac{\sigma_{el}}{\Sigma_{el}} = \frac{8}{9}. \tag{4.41}$$

Our success in deriving the proper result, while using the approximation of the impact parameter representation rather than the fully correct discrete partial wave series, is easy to understand. Since the minimum is achieved with a form which in fact requires many partial waves, there is no loss in treating the partial wave sum as an integral.

For most reasonable shapes of a, the ratio σ_{el}/Σ_{el} is actually quite near unity. Thus it is difficult to distinguish between models on the basis of this ratio. For example, if $a \sim 1 - (b/b_0)^n$ and vanishes for $b \overset{>}{)} b_0$, we find for the ratio values between 8/9 for $n = 2$ and 0.91 for $n = 5$. For the form $a \sim [1 - (b/b_0)]^n$ the minimum value is about 0.89 (just slightly greater than 8/9) when $n = 0.6 - 0.7$ and the ratio increases so that for $n = 4$, it is 1.07. Putting a Gaussian form in Eqs.(4.32) gives a ratio of exactly 1, just as the black disk gave.

The relationship between the impact parameter amplitude, a, and the differential cross section can be illustrated with some simple examples. For definiteness, we shall fix the parameters in each model so that they produce $\sigma_{tot} = 43$mb and $B = 13$ GeV/c^{-2}. These are characteristic of the values found at the ISR.

The simplest model has a constant value for a inside some radius R, and zero outside it. Since the forward elastic scattering amplitude at high energies is mostly imaginary, we take

$$a = \frac{1}{2} iA, \tag{4.42}$$

with A real. Thus $A = 1$ correponds to a purely black disk. From Eqs. (4.22) and (4.23) we find,

$$\sigma_{tot} = 2\pi R^2 A, \tag{4.43}$$

$$\sigma_{el} = \pi R^2 A^2, \tag{4.44}$$

and from Eq. (4.22) and (4.19) or (4.21),

$$\begin{aligned} \frac{d\sigma}{dt} &= \pi A^2 \left| \int_0^R b\, db J_0(qb) \right|^2 \\ &= \pi A^2 R^4 \left| \frac{J_1(qR)}{qR} \right|^2 . \end{aligned} \tag{4.45}$$

3. The Curvature Parameter, C

As discussed in Section III, the t-dependence of the elastic differential cross section is described at small t by

$$\begin{aligned} \frac{d\sigma_n}{dt} &= \left(\frac{d\sigma_n}{dt}\right)_{t=0} \exp(Bt + Ct^2 \cdots) \\ &= \left(\frac{d\sigma_n}{dt}\right)_{t=0} [1 + Bt + (\frac{B^2}{2} + C)t^2 \cdots]. \end{aligned} \tag{4.46}$$

If we take a to be purely imaginary, we can easily compute C from

$$f_{cm} \sim \int d^2b \, \exp(i\mathbf{q}\cdot\mathbf{b})a(b)$$
$$\sim \int d^2b \, (1 - \frac{1}{4}q^2b^2 + \frac{1}{64}q^4b^4\cdots)a(b). \qquad (4.47)$$

By noting that

$$\frac{d\sigma_n}{dt} \sim (\int d^2b\, a)^2 + \frac{1}{2}\int d^2b\, b^2a \int d^2b\, a$$
$$+\frac{1}{16}t^2(\int d^2b\, b^2a)^2 + \frac{1}{32}t^2 \int d^2b\, a \int d^2b\, b^4a + \cdots , \qquad (4.48)$$

we find that

$$C = \frac{1}{32}\frac{\int d^2b\, b^4a}{\int d^2b\, a} - \frac{1}{16}\left(\frac{\int d^2b\, b^2a}{\int d^2b\, a}\right)^2. \qquad (4.49)$$

Thus B is certainly positive, while C may be positive, negative or zero.

4. Models of Elastic Scattering

In Fig. 4.2, the profile for the disk and several shapes to be considered subsequently are shown. The corresponding differential cross sections are shown in Fig. 4.3 for the values of the parameters which give $\sigma_{tot} = 43\text{mb}$ and $B = 13(\text{GeV}/c)^{-2}$. For the sharp disk, $R = 1.42f$ and $A = 0.34$. It is easy to verify that for the sharp disk we have $\sigma_{el}/\sigma_{tot} = A/2 = \sigma_{tot}/16\pi B$, that is, $\Sigma_{el} = \sigma_{el}$. The value of C is negative: $C = -R^4/192$.

Ball and Zachariasen (1972) developed a model by solving the multiperipheral equation for diffractive scattering. The result was an elastic scattering amplitude

$$f_{cm}(s,t) = i\kappa R_0^2 p \frac{J_1(qR_0 \ln s/s_0)}{qR_0}. \qquad (4.50)$$

By comparison with the amplitude used in Eq. (4.45) we see that this model corresponds to a uniformily gray disk of growing radius $R = R_0 \ln(s/s_0)$ and amplitude $A = \kappa[\ln(s/s_0)]^{-1}$. The total cross section grows as $\ln s$, the elastic cross section is constant and B increases as $\ln^2(s/s_0)$.

A softer profile is given by

$$a = iA[1 - (b/R)^2], \qquad b \le R \qquad (4.51a)$$
$$a = 0, \qquad b > R. \qquad (4.51b)$$

This is the shape that saturates the MacDowell-Martin bound, $\sigma_{el}/\Sigma_{el} = 8/9$. For our chosen total cross section and slope, the appropriate parameters are $R = 1.74\,\text{f}$, and $A = 0.226$. The differential cross section,

$$\frac{d\sigma}{dt} = 4\pi A^2R^4\left|\frac{4J_1(qR)}{q^3R^3} - \frac{2J_0(qR)}{q^2R^2}\right|^2 \qquad (4.52)$$

is shown in Fig.4.3.

As a further example, consider a Gaussian profile,

$$a = \frac{1}{2} iA \exp(-(b/R)^2) \tag{4.53}$$

which gives $\sigma_{tot} = 2\pi AR^2$, $\sigma_{el} = \pi A^2 R^2/2$, and $B = R^2/2$. Thus, as for the sharp disk, $\Sigma_{el} = \sigma_{el}$. Of course, $C = 0$ for the Gaussian form. The appropriate parameters are $R = 1.00$ f, and $A = 0.68$. The differential cross section is compared to that for the previous examples in Fig. 4.3.

More realistic examples of the impact parameter amplitude, $a(b, s)$ can be found among the models which have been proposed for elastic scattering. The Chou-Yang (Chou and Yang, 1968, 1983; Durand and Lipes, 1968) model postulates that the elastic scattering is the shadow of the absorption resulting from the passage of one hadronic mass distribution through another. The transverse distribution of the matter is assumed to have the same shape as the charge distribution as measured by the electromagnetic form factor. This assumption leaves only the strength of the absorption to be fixed, and this can be done by requiring that the total cross section as calculated in the model agree with experiment. Thus the only energy dependence is that which comes implicitly through the energy dependence of the total cross section. If the absorption at an impact parameter b is $\Omega(b)$, then one writes

$$a(b, s) = \frac{1}{2i}(e^{2i\delta} - 1) \equiv \frac{i}{2}(1 - e^{-\Omega}). \tag{4.54}$$

If a dipole electromagnetic form factor is used,

$$G(q^2) = \left(\frac{\Lambda^2}{\Lambda^2 + q^2}\right)^2, \tag{4.55}$$

then Ω is a function of $x = \Lambda b$:

$$\Omega = A\frac{1}{8}x^3 K_3(x). \tag{4.56}$$

Here K_3 is a modified Bessel function and the constant A is selected so that the amplitude, Eq. (4.54), yields the correct value for the total cross section. The normalization in Eq. (4.56) is chosen so that as $x \to 0, \Omega \to A$. For large x, $\Omega \to cx^{5/2}e^{-x}$ where c is a constant. In Fig. 4.2 the profile, a/i, is displayed as a function of impact parameter, with $A = 1.35$ and $\Lambda = 0.845$GeV/c, which give the same total cross section and slope parameter as before. The value of Λ obtained in the fit is in remarkably good agreement with the value $\Lambda^2 = 0.71(\text{GeV/c})^2$ deduced from the electromagnetic form factor. The resulting differential cross section in shown in Fig. 4.3.

The model of Cheng, Walker and Wu (Cheng, Walker, and Wu, 1973; Bourrely, Soffer and Wu, 1983) is based on field theoretic studies which showed that at high energies, the dominant exchanges give amplitudes varying as $s^{1+\epsilon}$. Multiple exchanges produce an eikonalized amplitude. As a phenomenological form, Cheng, Walker, and Wu used in Eq. (4.54)

$$\Omega = f(Ee^{-i\pi/2})^c \exp\left(-\lambda\sqrt{b^2 + b_0^2}\right), \tag{4.57}$$

where f, c, λ, and b_0 are parameters. The phase associated with the energy dependence will be discussed later. The constant c is small and plays the role of ϵ.

The sign of the curvature, C,for the four displayed models is

apparent in Fig. 4.3. The Gaussian form with $C = 0$ is a straight line on the semi-log plot. The sharp disk and the parabolic form which saturates the MacDowell-Martin bound both fall below the Gaussian, and thus have negative values of C. The Chou-Yang has a positive values of C for the given parameters. The measured value of C is ≈ 4 (GeV/c)$^{-4}$. Roughly speaking, a positive value of C requires a broader tail than the Gaussian distribution has.

From Eq. (4.49) we see that the condition that C be positive is

$$\langle b^4 \rangle > 2\langle b^2 \rangle^2, \tag{4.58}$$

where

$$\langle b^n \rangle = \frac{\int d^2b\, b^n a}{\int d^2b\, a}. \tag{4.59}$$

It is easy to see that $a \sim [1-(b/R)^p]$ gives a negative C for every $p > 0$, while $a \sim [1-(b/R)]^p$ gives a positive C for $p > 4$. If we consider shapes of the form $a \sim \exp[-(b/R)^p]$ then, if $p > 2$, the curvature C is positive, while if $p < 2$, C is negative. In Fig. 4.3 we see that among the curves with diffraction minima, those with negative C tend to have the minima at smaller values of t, since the differential cross section turns down sooner than for curves with positive C.

C. Energy Dependence of Cross Sections and Slopes in Models, and the Approach to "Asymptopia"

While our primary concern is with model independent analysis, it is worthwhile to consider what the simple models discussed above have

to say about the energy dependence of the total cross section, elastic cross section, and slope of the elastic peak.

First we consider the geometric model. The fundamental assumption of the model is that the only dimensionful parameter is the total cross section. It follows that σ_{el}/σ_{tot} and Σ_{el}/σ_{tot} must be energy independent. While this model is successful in treating the ISR data, it cannot contend with the energy dependence of these quantities observed in going from the ISR to the SPS Collider.

Next we consider a generic Chou-Yang model with

$$a(b,s) = \frac{1}{2}i(1-\exp(-A\Omega(b))), \tag{4.60}$$

where Ω is some generalization of the specific form of Chou and Yang. Then A measures the strength of the hadronic interaction and Ω measures the hadronic overlap density at a separation b. We take Ω to be independent of the energy. The parameter A must be chosen to reproduce the total cross section. Now if the cross section increases indefinitely, so does A. The cross section is roughly $2\pi R^2$, where R is the value of b at which $\Omega(b) \approx 1/A$. If Ω falls exponentially with b, $R \sim \ln A$. Thus we obtain a cross section growing as $\ln^2 s$ if A varies as a power of s. The amplitude is, for large A, nearly $i/2$ for $b < R$, and nearly zero for $b > R$. We see, then, that for this class of models, asymptotically the profile approximates a black disk with growing radius.

The ratio of σ_{el}/σ_{tot}, which asymptotically will be 1/2 in these models, is only 0.22 at the SPS Collider, so we are not yet at the asymptotic state of the black disk. The ratios

$$X = \sigma_{el}/\sigma_{tot} \qquad (4.61a)$$

and

$$Y = \Sigma_{el}/\sigma_{tot} \qquad (4.61b)$$

are shown as functions of the total cross section in Fig. 4.4, where we have fixed the Chou-Yang model to have $\Lambda = 0.845$ GeV and varied the remaining parameter, A. The behavior is not too different from the observed changes between the ISR and the SPS Collider.

For models which become gray or black disks asymptotically, the curvature parameter, C, must eventually become negative, as it is for the sharp disk. In Fig. 4.5 we show the behavior of C in the Chou-Yang model as a function of the total cross section. We note that C which is positive at the ISR is indeed positive in the model at the appropriate cross section of about 40 mb. However, in the model, C becomes negative when the cross section reaches about 100 mb. Thus we expect that the value of C will change sign around the energy region of the Tevatron Collider. For this reason, it is important for experimenters to measure directly the energy dependence of C in going from the ISR to the Tevatron. The prediction that it will change sign is more general than the Chou-Yang model. It is the consequence of the nucleon-nucleon profile becoming more and more that of a disk.

In Fig. 4.4, we see that the curves for X and Y cross when $\sigma_{tot} \approx 85$mb. A Gaussian shape has $C = 0$ and $X = Y$. Not surprisingly, we find in Figs. 4.4 and 4.5 that $X = Y$ near $C = 0$. Of course,

asymptotically, the model becomes that of a black disk and X eventually becomes equal to Y again.

While we are concerned primarily with very low momentum transfer, it is instructive to use the Chou-Yang model to make some predictions at larger momentum transfer (Block and Cahn, 1984). As stressed above, the Chou-Yang model has no intrinsic energy dependence. It acquires energy dependence through the variable A of Eq.(4.56) which is adjusted at a given energy to reproduce the correct total cross section. Once A is determined, there are no remaining free parameters. In the next Section we shall make predictions for the total cross section as a function of the center of mass energy. Anticipating these results, we can use the cross section at each of several energies to fix the model and thus predict the differential cross section. We show in Fig. 4.6 the impact parameter amplitude at several energies, and for comparison, a gray disk with the same total cross section. The cross section is taken from the the fits of Section V. The slope parameter, B, is then determined in the Chou-Yang model. The gray disk has been chosen to reproduce the same values of σ_{tot} and B. In Fig. 4.7 we display the differential cross sections generated by these impact parameter distributions. If the amplitudes are taken to be purely imaginary, there are sharp diffraction minima, in fact, zeroes. To obtain more realistic results, we have incorporated small imaginary parts by the prescription of Martin (1973). If f is the purely imaginary amplitude and we wish to give it a real part so that a particular value of ρ is achieved, we use

$$\frac{d\sigma_n}{dt} = \left(\frac{\pi}{k^2}\right)\left(|f|^2 + \rho^2\left|\frac{d(tf)}{dt}\right|^2\right). \qquad (4.62a)$$

For the sharp gray disk with $a = iA/2$ inside a radius R, this yields

$$\frac{d\sigma_n}{dt} = \pi A^2 R^4 \left[\left(\frac{J_1(qR)}{qR} \right)^2 + \frac{\rho^2}{4} (J_0(qR))^2 \right]. \qquad (4.62b)$$

Figure 4.7 shows that at the SSC (40 TeV), the differential cross section for elastic scattering is likely to be indistinguishable from that of a black disc. The location of the first minimum moves in rapidly for the Chou-Yang model until it is nearly as close in as in the gray disk model. The general arguments above demonstrate that this must happen eventually. Hence we define "asymptopia" as the energy domain where the elastic differential cross section is essentially indistinguishable from that of a sharp disk. What the numerical study reveals is that the coalescence of the models with the sharp disk will take place with the SSC machine presently being designed.

At the ISR and SPS Collider, the observed values of C are positive. Figure 4.7 shows that C should be negative at the SSC, according to the Chou-Yang model. A quantitative indicator of the onset of "asymptopia" is the energy at which $C = 0$ and our fits indicate that this occurs very close to the energy of the Tevatron Collider. This progression can be viewed in Fig. 4.6, where the profile of nucleon-nucleon system is seen to develop a characteristic "flat-top", starting at the Tevatron Collider energy.

We shall find in Section VI, that when our fit to the experimental values of the slope is extrapolated to very high energies, the values of B thus obtained are in substantial agreement with those calculated from the Chou-Yang model, using Eq. (4.62a). In conclusion, we have used a

model-free analysis of $t = 0$ and very small $|t|$ data at lower energies to predict the parameters needed to fix differential elastic scattering cross sections at very large $\sqrt{s}$ and at large $-t$. We consider this much more reliable than using the dip structure at large $-t$ of $d\sigma_n/dt$ (at low $\sqrt{s}$) to determine the energy dependences of the total cross section and the ρ values, which are either undefined or ill-defined in most models of elastic scattering cross sections.

D. Analyticity

The physical amplitude for elastic scattering, f, is defined for $s \geq 4m^2$ and $-4m^2 \leq t \leq 0$. It is possible to show that $f(s,t)$ is really the limit of a more general function in which s and t may take on complex values. (See Eden (1967) for a comprehensive introduction and Martin and Cheung (1970) for a thorough treatment. See also, Jackson (1960,1973).) In particular, if we fix $t = 0$, then $f(s, t = 0)$ is the limit of an analytic function $\mathcal{F}$ according to

$$f_{\rm pp}(s, t = 0) = \lim_{\epsilon \to 0} \mathcal{F}(s + i\epsilon, t = 0), \qquad (4.63)$$

where $\epsilon \to 0$ from positive values. Not only is the pp amplitude a limit of an analytic function, the $\rm p\bar{p}$ forward amplitude is another limit of the same analytic function. The principle of crossing states that to go from the pp amplitude to the $\rm p\bar{p}$ amplitude we merely replace p_2 by $-p_4$ and *vice versa*. This is equivalent to interchanging u and s. The $\rm p\bar{p}$ amplitude is obtained from $\mathcal{F}$ by

$$f_{p\bar{p}}(s, t=0) = \lim_{\epsilon \to 0} \mathcal{F}(-s + 4m^2 - i\epsilon, t=0), \qquad (4.64)$$

again with $\epsilon > 0$. Now, for $t = 0$, $u = -s + 4m^2$ so we see that the $p\bar{p}$ amplitude is found by evaluating $\mathcal{F}$ using u as the variable, rather than s. This symmetry is clearer if we use as a variable

$$E = (s - u)/4m. \qquad (4.65)$$

For $t = 0$, E is the lab energy for pp scattering. The pp to $p\bar{p}$ interchange reverses the sign of E. More precisely, the physical amplitude, f_{cm}, at $t = 0$, is the limit of an analytic function, $\mathcal{F}$, of a complex variable E, with cuts on the real axis. The physical amplitude for pp scattering, $f_{cm}(E, t = 0)$. is the limit of $\mathcal{F}(E + i\epsilon, t = 0)$ as $\epsilon \to 0$ from positive values. The $p\bar{p}$ amplitude at $t = 0$ is obtained as the limit of $\mathcal{F}(-E - i\epsilon, t = 0)$, again as $\epsilon \to 0$ from positive values (i.e., from below). See Fig. 4.8.

Unitarity relates the imaginary part of the elastic scattering amplitude to a sum over all physical states with the same energy, E. See Eq. (4.12). It is possible to show that when we continue the elastic amplitude in the complex variable E, the imaginary part of the elastic amplitude for E next to the real axis vanishes if there is no physical state with energy E which communicates hadronically with pp or $p\bar{p}$. Since $p\bar{p}$ communicates with the $\pi\,\pi$ channel (and the channel with a single π) there is an "unphysical region" on the real axis where $Im\mathcal{F} \neq 0$, even though there is no physical elastic scattering at this energy. (Actually, this region can be probed slightly by studying $p\bar{p}$ atoms whose binding energy reduces the mass below $2m$.)

From these considerations we conclude that the cut structure of

the forward elastic scattering amplitude is as follows. The right hand cut begins at threshold, $E = m$. The single pion pole occurs when $u = m_\pi^2$, that is, when $E = m - m_\pi^2/(2m)$. The two pion cut begins when $u = 4m_\pi^2$, that is, when $E = m - 2m_\pi^2/m$. Between the left hand cut and the right hand cut, except at the pion pole, the amplitude is real on the real axis.

A function like $\mathcal{F}$ which is real on a segment of the real axis is called real analytic. The Schwarz reflection principle states (Titchmarsh, 1939, p. 155) that if $\mathcal{F}$ is real analytic, then $\mathcal{F}(z^*) = \mathcal{F}^*(z)$. Thus if $\mathcal{F}$ has a cut on the real axis, its imaginary part changes sign in going from one side of the cut to the other, but the real part is the same on both sides. In other words, the discontinuity across the cut is imaginary.

The Schwarz reflection principle is quite easy to prove. Suppose $\mathcal{F}(z)$ is analytic in some region and that this region includes a finite segment (however small) of the real axis. Now define a function $\mathcal{G}(z)$ by $\mathcal{G}(z) = \mathcal{F}^*(z^*)$. We can show that $\mathcal{G}$ is in fact an analytic function of z: $\mathcal{F}$ has a power series expansion $\mathcal{F}(z) = a_0 + a_1 z + a_2 z^2 + \cdots$ so $\mathcal{G}(z) = a_0^* + a_1^* z + a_2^* z^2 + \cdots$. Clearly the two series have the same radius of convergence, so $\mathcal{G}$ is analytic. Moreover, by construction $\mathcal{F}$ and $\mathcal{G}$ coincide for values of z on the real axis. However, by the principle of analytic continuation, the function is uniquely determined by its values on a segment so $\mathcal{G}$ and $\mathcal{F}$ are the same. Thus $\mathcal{G}^*(z) = \mathcal{F}^*(z)$ and $\mathcal{G}^*(z) = \mathcal{F}(z^*)$, so $\mathcal{F}^*(z) = \mathcal{F}(z^*)$, as we wished to show.

In practice, we shall use real analytic functions which have a simple cut structure. The left hand cut will begin at $E = -m$, just as the right hand cut begins at $E = m$. Ignoring the unphysical region of

the pion pole and the two pion cut is permissible, since we are interested in the high energy region, which is far from these singularities.

It is very useful to define two amplitudes which are combinations of the pp and $p\bar{p}$ elastic amplitudes:

$$f_{\pm} = \frac{1}{2}(f_{p\bar{p}} \pm f_{pp}). \tag{4.66}$$

The amplitude f_+ is even under $E \to -E$, while f_- is odd.

Consider, as an example, a prototypical function possessing the analyticity properties of scattering amplitude,

$$g_-(E) = (m+E)^{\alpha} - (m-E)^{\alpha}. \tag{4.67}$$

This function has branch points at $\pm m$. We can take the branch cuts to extend from m to infinity and from $-m$ to negative infinity along the real axis. We define the function so that it is real along the real axis between $-m$ and m. This is the behavior appropriate to a forward scattering amplitude. See Fig.4.8.

Just above the right hand cut,

$$g_-(E) = (E+m)^{\alpha} - (E-m)^{\alpha}\exp(-i\pi\alpha), \tag{4.68}$$

and for $E \gg m$,

$$g_-(E) \approx 2i\sin(\pi\alpha/2)|E|^{\alpha}\exp(-i\pi\alpha/2), \tag{4.69}$$

while just below the left hand cut

$$g_-(E) = (-E-m)^{\alpha}\exp(-i\pi\alpha) - (-E+m)^{\alpha}, \tag{4.70}$$

and for $-E \gg m$,

$$g_-(E) = -2i\sin(\pi\alpha/2)|E|^{\alpha}\exp(-i\pi\alpha/2). \tag{4.71}$$

The phases are explained in Fig. 4.9. If g_- were the continuation of the pp amplitude, Eqs. (4.68) and (4.69) would give the pp amplitude and Eqs. (4.70) and (4.71) would give the $p\bar{p}$ amplitude. Clearly the amplitude is odd. It has all the properties we want for odd part of the forward scattering amplitude. Just below threshold, it is purely real. The thresholds are in the correct place if we ignore the unphysical cuts (as we shall do henceforth). From this example, we infer that odd amplitudes which behave asymptotically as E^{α} have the phase $i\exp(-i\pi\alpha/2)$. This inference is made rigorous by the Phragmèn-Lindelöf theorem (Titchmarsh, 1939). The corresponding analysis for even amplitudes shows that their phase is $\exp(-i\pi\alpha)/2)$, if their power behavior is E^{α}.

Of course, not all amplitudes need have power law behavior. An example of an even function of a different sort is

$$g_+(E) = \frac{1}{2}[\ln((m+E)/E_0) + \ln((m-E)/E_0)], \tag{4.72}$$

which has the same cut structure as before and which we can define so that it is real on the real axis between the two branch points. We then find that above the right hand cut (and below the left hand cut), for $E \gg m$,

$$\mathcal{G}_+(E) = \ln(p/E_0) - \frac{i\pi}{2}, \tag{4.73}$$

where p is the laboratory momentum.

Another useful even function is

$$\mathcal{G}_+ = \sqrt{(m+E)(m-E)}. \tag{4.74}$$

Above the right hand cut, we define this function so it is precisely $-ip$. Asymptotically, this is just $-iE$, in agreement with our general result for even functions with power law behavior.

We conclude this section with an illustrative list of simple analytic functions together with their asymptotic behavior. It is from these forms that we shall eventually build our scattering amplitude.

General Form	High Energy Form above Right Hand Cut
$\mathcal{G}_+ = (m+E)^\alpha + (m-E)^\alpha$	$E^\alpha \exp(-i\pi\alpha/2) 2\cos(\pi\alpha/2)$
$\mathcal{G}_+ = \sqrt{(m+E)(m-E)}$	$-iE$
$\mathcal{G}_+ = \frac{1}{2}[\log((m-E)/E_0) + \log((m+E)/E_0)]$	$\log E/m - i\pi/2$
$\mathcal{G}_- = (m+E)^\alpha - (m-E)^\alpha$	$iE^\alpha \exp(-i\pi\alpha/2) 2\sin(\pi\alpha/2)$

From this table we can recognize the traditional forms for Regge behavior. A forward amplitude varying as E^α contributes to the total cross section as $E^{\alpha-1}$. If the amplitude is even (the pomeron, f, A_2), the phase of the amplitude is $\exp(-i\pi\alpha/2)$. Thus for the usual pomeron with $\alpha \approx 1$, the phase is $-i$. For odd amplitudes (ρ, ω), the phase is $i\exp(-i\pi\alpha/2)$.

E. Integral Dispersion Relations

The traditional means of testing analyticity of the scattering amplitude to is use Cauchy's theorem to obtain a dispersion relation, that is, a relation between the real and imaginary parts of the amplitude. (See Jackson, 1960, and Eden, 1967, for a more complete discussion) Let $\mathcal{F}(E)$

be the analytic continuation of $f(E, t=0)$, so $\mathcal{F}$ is analytic in the cut E plane. Then we can write

$$\mathcal{F}(E) = \frac{1}{2\pi i} \oint dE' \frac{\mathcal{F}(E')}{E' - E} \ , \tag{4.75}$$

where the counterclockwise contour does not cross the cuts or encircle any poles. (As explained above we ignore "unphysical singularities" like the single pion pole and two pion cut. Because we are only interested in high energies, these have little influence on our answers.) We choose a contour which passes just above and just below the cuts on the real axis, as shown in Fig. 4.8. If the contribution from the semicircular contours at ∞ vanish, we have

$$\mathcal{F}(E) = \frac{1}{2\pi i}\left[\int_m^\infty dE' \frac{\mathcal{F}(E'+i\epsilon) - \mathcal{F}(E'-i\epsilon)}{E'-E} + \int_{-\infty}^{-m} dE' \frac{\mathcal{F}(E'+i\epsilon) - \mathcal{F}(E'-i\epsilon)}{E'-E}\right]. \tag{4.76}$$

If $\mathcal{F} = \mathcal{F}_+$ is even, so $\mathcal{F}(E'+i\epsilon) = \mathcal{F}(-E'-i\epsilon)$,

$$\mathcal{F}_+(E) = \frac{1}{\pi}\int_m^\infty dE' \, Im\mathcal{F}_+(E'+i\epsilon)\left[\frac{1}{E'-E} + \frac{1}{E'+E}\right], \tag{4.77}$$

while if $\mathcal{F} = \mathcal{F}_-$ is odd,

$$\mathcal{F}_-(E) = \frac{1}{\pi}\int_m^\infty dE' \, Im\mathcal{F}_-(E'+i\epsilon)\left[\frac{1}{E'-E} - \frac{1}{E'+E}\right]. \tag{4.78}$$

The integrands have singularities at $E' = \pm E$ which just produce the identity $Im\mathcal{F} = Im\mathcal{F}$. The real part of $\mathcal{F}$ is found as a principal value integral. Thus

$$Ref_+(E) = P\frac{1}{\pi}\int_m^\infty dE'\left[\frac{2E'}{E'^2 - E^2}\right] Imf_+(E'), \tag{4.79}$$

$$Ref_-(E) = P\frac{1}{\pi}\int_m^\infty dE'\left[\frac{2E}{E'^2 - E^2}\right] Imf_-(E'). \tag{4.80}$$

If the integrals (4.79) or (4.80) do not converge because of the behavior of f as $E \to \infty$, or because of the contributions from the semicircles at infinity, we must modify the approach slightly. Consider the odd function $\mathcal{G}_- = \mathcal{F}_+/E$. If we insert this in Eq. (4.78) and take notice of the pole at $E = 0$, we find

$$Ref_+(E) = Ref_+(0) + P\frac{1}{\pi}\int_m^\infty dE' \frac{2E^2}{E'(E'^2 - E^2)} Imf_+(E'). \tag{4.81}$$

(Here the amplitude at $f_+(0)$ really is the analytic continuation, $\mathcal{F}_+(0)$, of the physical amplitude.) This is called a singly subtracted dispersion relation, and the first term on the right hand side is called a subtraction constant. Clearly the subtracted dispersion relation has better convergence properties than the unsubtracted relation. On the other hand, there is an additional constant to be determined. If we try the same trick for the odd amplitude $\mathcal{G}_+ = \mathcal{F}_-/E$, we find that we just reproduce the unsubtracted relation (4.80). Instead we must use $\mathcal{G}_- = \mathcal{F}_-/E^2$. With care exercised at the pole at $E = 0$, we find the doubly subtracted dispersion relation for the odd amplitude

$$\mathcal{R}ef_-(E) = E\mathcal{R}ef'_-(0) + \frac{1}{\pi}\int_m^\infty dE' \frac{2E^3}{E'^2(E'^2 - E^2)} \mathcal{I}mf_-(E'), \quad (4.82)$$

where $f'_-(0)$ denotes $d\mathcal{T}_-/dE$, the analytic continuation, at $E = 0$. We see that here the subtraction results in a term linear in E. If the odd amplitude grows as fast as E, it is this doubly subtracted dispersion relation which must be used.

The importance of these dispersion relations is that both $\mathcal{R}ef$ and $\mathcal{I}mf$ can be measured for the forward direction. The latter is measured through the optical theorem . The former is obtained by measuring the interference between the hadronic and Coulombic amplitudes at very small $|t|$, which yields ρ, the ratio of the real to the imaginary part of the forward amplitude.

The dispersion relations above may be combined to give relations for the real part of the pp and $\mathrm{p\overline{p}}$ amplitudes in terms of the measured cross sections. We expect the total cross sections not to grow faster than a power of $\log s$, so the even dispersion relation requires a single subtraction. If the difference of the cross sections falls as a power of s, the odd dispersion relation needs no subtraction. We then combine Eqs. (4.80) and (4.81) and the optical theorem to find (note that $f_{\mathrm{pp}}(0) = f_{\mathrm{p\overline{p}}}(0)$)

$$\mathcal{R}ef_{\mathrm{pp}}(E) = \mathcal{R}ef_{\mathrm{pp}}(0) + P\frac{E}{4\pi^2}\int_m^\infty \frac{dE'}{E'} p'\left[\frac{\sigma_{pp}(E')}{E' - E} - \frac{\sigma_{p\overline{p}}(E')}{E' + E}\right], \quad (4.83)$$

$$\mathcal{R}ef_{\mathrm{p\overline{p}}}(E) = \mathcal{R}ef_{\mathrm{p\overline{p}}}(0) + P\frac{E}{4\pi^2}\int_m^\infty \frac{dE'}{E'} p'\left[\frac{\sigma_{p\overline{p}}(E')}{E' - E} - \frac{\sigma_{pp}(E')}{E' + E}\right]. \quad (4.84)$$

If the difference of the cross sections does not decrease to zero at large E, we must use the twice subtracted odd dispersion relation, Eq.(4.82). The result is

$$\mathcal{R}ef_{\mathrm{pp}}(E) = \mathcal{R}ef_{\mathrm{pp}}(0) + E\frac{d\mathcal{R}ef_{\mathrm{pp}}}{dE}(0) + P\frac{1}{4\pi^2}\int_m^\infty \frac{dE'E^2}{E'^2} p'\left[\frac{1}{E' - E}\sigma_{p\overline{p}} + \frac{1}{E' + E}\sigma_{pp}\right], \quad (4.85)$$

$$\mathcal{R}ef_{\mathrm{p\overline{p}}}(E) = \mathcal{R}ef_{\mathrm{p\overline{p}}}(0) + E\frac{d\mathcal{R}ef_{\mathrm{p\overline{p}}}}{dE}(0) + P\frac{1}{4\pi^2}\int_m^\infty \frac{dE'E^2}{E'^2} p'\left[\frac{1}{E' - E}\sigma_{pp} + \frac{1}{E' + E}\sigma_{p\overline{p}}\right]. \quad (4.86)$$

Note that $df_{\mathrm{pp}}(0)/dE = -df_{\mathrm{p\overline{p}}}(0)/dE$, where more properly we should write $d\mathcal{T}/dE$, and that $f_{\mathrm{p\overline{p}}}(0) = f_{\mathrm{pp}}(0)$.

On occasion, some care must be taken with the contours at infinity which we casually ignored above. Consider for example the analytic function E itself. This is manifestly odd and has no imaginary part. The dispersion integral along the real axis, even unsubtracted, certainly converges, since it is identically zero. The unsubtracted dispersion relation , Eq. (4.80), would then say $E = 0$. The problem is that the contribution from the contour at infinity cannot be ignored. The twice subtracted dispersion relation, Eq. (4.82), correctly gives the identity $E = E$.

We review briefly some applications of dispersion relations to pp and $\mathrm{p\overline{p}}$ scattering. The first use of a dispersion relation for analyzing pp

and $p\bar{p}$ elastic scattering was made by P. Söding (1964). He introduced a singly-subtracted dispersion relation, taking into account the unphysical region by a sum over poles. Experimental cross sections were inserted into the relation for $\sqrt{s} < 4.7$ GeV, and asymptotic power laws were used to parametrize the data for higher energies. He calculated ρ values for both pp and $p\bar{p}$ scattering. At that time, experimental data only for $\sqrt{s} \leq 6$ GeV were available.

The next use of dispersion relations, by Amaldi *et al.* (1977), occured after the ISR data had shown that the pp cross sections were rising. The data then available included pp cross sections and ρ values up to $\sqrt{s} < 62$ GeV and $p\bar{p}$ cross sections up to $\sqrt{s} \sim 15$ GeV. They used the singly-subtracted relations Eqs (4.83), (4.84). Contributions from pole terms and the unphyscal region were neglected. The authors did not use experimental cross sections directly, but rather chose to parametrize them by

$$\sigma_{pp} = B_1 + C_1 E^{-\nu_1} + B_2 \ln^\gamma s - C_2 E^{-\nu_2}, \qquad (4.87)$$

and

$$\sigma_{p\bar{p}} = B_1 + C_1 E^{-\nu_1} + B_2 \ln^\gamma s + C_2 E^{-\nu_2}, \qquad (4.88)$$

where E is in Gev and s is in GeV^2. These forms were then inserted into the dispersion relations.

From a χ^2 fit made simultaneously to the data for σ_{pp}, $\sigma_{p\bar{p}}$, and ρpp, for the high energy region $5 < \sqrt{s} < 62$GeV, the parameters B_1, C_1,

ν_1, B_2, γ, C_2 and ν_2, as well as the subtraction constant, were extracted. However, there were several other parameters fitted that considerably smoothed their results (and incidentally lowered the χ^2 per degree of freedom substantially), by allowing the normalizations of various data sets, including the ρ values, to be varied within the range allowed by the systematic errors. In addition, in the forms (4.87) and (4.88) they arbitrarily chose as a scale for s the value 1 GeV^2. A more proper procedure would be to use the form $\log^\gamma(s/s_0)$ and fit both γ and s_0. That the fit found by Amaldi *et al.* is successful is probably fortuitous. The authors also did not fit the $\rho(p\bar{p})$ data that then existed. Since the time this work was published, precise experimental measurements of σ and ρ for the $p\bar{p}$ system have been made at high $\sqrt{s}$. These new measurements now allow one to pin down accurately the choice of parameters.

Dispersion relations were applied to the pp and $p\bar{p}$ system by Del Prete (1983) who considered the possibility that the difference of the cross sections grew asymptotically as $\ln s$. As demonstrated above, in such an instance the twice subtracted dispersion relations are required, since the integrals in Eqs. (4.83) and (4.84) are divergent. Del Prete claimed to have used the singly subtracted dispersion relations of Söding, which do *not* converge for growing cross section differences. Presumably, the reported finite results quoted are artifacts of the numerical integration scheme employed.

F. Differential Dispersion Relations

The integral dispersion relations require extensive numerical work for their evaluation. At low energies where the cross sections are rapidly varying near resonances, this is an unavoidable problem. At higher energies, the cross sections are smooth and this can be exploited by assuming that the cross sections are well described by a simple function. This was the approach of Bronzan and co-workers (Bronzan, 1973; Bronzan, Kane and Sukhatme, 1974; Jackson, 1973) who obtained and utilized "differential dispersion relations". Before we can derive these approximate relations, we need a different sort of integral dispersion relation, one which gives the imaginary part as an integral over the real part. These relations were first employed by W. Gilbert (1957). These "reverse" dispersion relation can be obtained by exploiting the even function

$$\mathcal{G}_+(E) = (m^2 - E^2)^{-1/2}, \tag{4.89}$$

where $\mathcal{G}_+$ is defined to be real on the real axis for $-m < E < m$. This is just the reciprocal of the function given in Eq. (4.74). Thus above the right hand cut, $\mathcal{G}_+ = -i|E^2 - m^2|^{-1/2}$. Now if $\mathcal{F}_+$ is the analytic continuation an even amplitude, f_+, we can construct the even function

$$\mathcal{H}_+(E) = \mathcal{G}_+(E)\mathcal{F}_+(E). \tag{4.90}$$

Ignoring the possible need for subtractions, we have the usual dispersion relation

$$Re\mathcal{H}_+(E) = \frac{P}{\pi}\int_m^\infty dE' \frac{2E' Im\mathcal{H}_+(E' + i\epsilon)}{E'^2 - E^2}, \tag{4.91}$$

or, for E just above the right hand cut,

$$Imf_+(E) = -\frac{P}{\pi}\int_m^\infty dE' \frac{2E' Ref_+(E')}{E'^2 - E^2}\sqrt{\frac{E^2 - m^2}{E'^2 - m^2}}. \tag{4.92}$$

For $E \gg m$, this gives the approximate relation

$$Imf_+(E) = -\frac{P}{\pi}\int_m^\infty dE' \frac{2E Ref_+(E')}{E'^2 - E^2}. \tag{4.93}$$

This looks like the dispersion relation for $\mathcal{F}_-$, except that the real and imaginary parts are interchanged and a minus sign is introduced.

From Eqs. (4.80) and (4.93), we can derive the differential dispersion relations. These are approximate relations which are much easier to employ than true dispersion relations, since they involve only derivatives. The differential dispersion relations can be obtained from the odd dispersion relation:

$$Ref_-(E) = \frac{P}{\pi}\int_m^\infty dE' \frac{2E' Imf_-(E')}{E'^2 - E^2}. \tag{4.94}$$

Now let $E' = m\exp(\varsigma + \eta)$, $E = m\exp(\varsigma)$, and expand

$$Imf_-(\varsigma + \eta) = \sum_n \frac{1}{n!}\eta^n Imf_-^{(n)}(\varsigma). \tag{4.95}$$

Now of course we cannot really do this because there are singularities along the real axis, but we ignore these niceties and assume $E \gg m$, to write

$$\mathcal{R}ef_{-}(\varsigma) = \frac{1}{\pi}\int_{-\infty}^{\infty} d\eta \frac{2\exp(2\varsigma+\eta)}{\exp(2\varsigma+2\eta)-\exp(2\varsigma)} \sum_n \frac{1}{n!}\eta^n \mathcal{I}mf_{\pm}^{(n)}(\varsigma). \tag{4.96}$$

Only the odd terms contribute. Let X be the operator $\partial/\partial\varsigma$.

Formally,

$$\mathcal{R}ef_{-}(\varsigma) = \frac{1}{\pi}\int_{-\infty}^{\infty} d\eta \frac{\sinh \eta X}{\sinh \eta}\mathcal{I}mf_{-}(\varsigma). \tag{4.97}$$

We treat the definite integral as if X were a real number $|X| < 1$, so that the integral above converges, and we find (Gradshteyn and Ryzhik, 1965, p.344)

$$\mathcal{R}ef_{-}(\varsigma) = (\tan\frac{\pi X}{2})\mathcal{I}mf_{-}(\varsigma), \tag{4.98}$$

or

$$\mathcal{R}ef_{-}(\varsigma) = (\tan\frac{\pi\partial}{2\partial\varsigma})\mathcal{I}mf_{-}(\varsigma). \tag{4.99}$$

A similar treatment of the Gilbert dispersion relation, Eq. (4.90), gives

$$\mathcal{I}mf_{+}(\varsigma) = -(\tan\frac{\pi\partial}{2\partial\varsigma})\mathcal{R}ef_{+}(\varsigma). \tag{4.100}$$

The above relations are tractable only when we make a fit to the data using a simple function. For example, if $f = aE^{\alpha}$, the relations can be evaluated exactly. For the odd amplitude we find

$$\mathcal{R}eA = \tan\frac{\pi\alpha}{2}\mathcal{I}mA, \tag{4.101}$$

i.e. $A = -i\exp(-i\pi\alpha/2)|A|$, as already established in the table in Section C above. Similar results are obtained for an even function behaving as a power and for a logarithmic function. So far nothing new has been achieved. If more complicated functions are used, it is hard to evaluate the power series in the differential operator, and the series must be truncated to give an approximation. This prompts the question, why not just use the simple analytic forms themselves and by-pass the differential dispersion relations?

G. Use of Simple Analytic Functions to Fit the Forward Amplitude

We shall circumvent all the difficulties of dispersion relations and differential dispersion relations by the direct use of analytic functions to fit the forward pp and $p\bar{p}$ scattering amplitude. This technique was first employed by Bourrely and Fischer (1973). Since that time, the quality and extent of the of the data have improved enormously, especially for $p\bar{p}$. Thus, significantly better results can now be obtained.

1. Even Amplitudes

The form we have chosen for the even amplitude is

$$4\pi f_+ = -ip\left[A + \frac{\beta(\ln 2mp/s_0 - i\pi/2)^2}{1 + a(\ln 2mp/s_0 - i\pi/2)^2}\right] + C' + \text{Regge term}, \tag{4.102}$$

where the Regge term [shown in Eq.(5.2a) with coefficient C] gives a decreasing contribution to the cross section at high energies and where, as usual, $p = \sqrt{E^2 - m^2}$. For $a = 0$, the form is quite simple at high energies, where $s \approx 2mE$, and gives (neglecting the falling Regge term)

$$\sigma_+ = A + \beta(\log^2 s/s_0 - \pi^2/4), \tag{4.103}$$

which saturates the form of the Froissart bound discussed in the next section. The form is similar to that used by Amaldi, *et al.* (1977) except that s_0 is left properly as a free parameter. Permitting the parameter a to take on small positive values allows for a deviation from this form. Indeed, asymptotically the form gives a constant cross section, $\sigma_+(\infty) = A + \beta/a$. The constant C' is permitted by the requirements of analyticity for the even amplitude and corresponds to a portion of the subtraction constant in the usual dispersion relation treatment. The parameter C' is unimportant in the region of interest since it lacks the factor of p present in the dominant terms. We shall also see that very fine fits are obtained with $a = 0$. In fact, adequate fits are obtained even without the Regge term. This is possible since the $\log^2 s/s_0$ simulates the falling Regge piece for $s < s_0$. Thus we find just three parameters, A (in mb), β (in mb), and s_0(in GeV^2), are needed to parameterize the even amplitude . The parameter a is useful, however, for it will provide a means of estimating how nearly the data conforms to an idealized behavior with Froissart bound form.

2. Conventional Odd Amplitudes

The odd amplitude is known to be dominated by a piece with the approximate behaviour $s^{1/2}$ (that is, $\sigma_{p\bar{p}} - \sigma_{pp} \sim s^{-1/2}$). We write in the high energy limit

$$4\pi f_- = Ds^\alpha \exp[i\pi(1 - \alpha)/2], \tag{4.104}$$

where the power, α, and the magnitude, D, of the amplitude are taken as parameters.

3. Unconventional Odd Amplitudes - The Odderons

While the forms given above are quite adequate to describe all the high energy data, we shall want to consider some less conventional forms for the odd amplitude. If $\sigma_{tot} \sim \log^2 s$, the fastest growth allowed by the Froissart bound, then $\Delta\sigma$ may grow as fast as log$s$ (see next section). We consider three prototypical odd amplitudes:

$$f_-^{(0)} = \epsilon^{(0)} E, \tag{4.105a}$$

$$f_-^{(1)} = \epsilon^{(1)} E(\log 2mp/s_0 - i\pi/2), \tag{4.105b}$$

$$f_-^{(2)} = \epsilon^{(2)} E(\log 2mp/s_0 - i\pi/2)^2, \tag{4.105c}$$

where the ϵ's are real constants. We shall refer to the amplitudes in Eqs.(4.105) as odderon-0, odderon-1 and odderon-2, respectively (Lukaszuk and Nicolescu, 1973; Kang and Nicolescu, 1975;Joynson *et al.*, 1975). The full odd amplitude is given by the sum of f_- from Eq.(4.104) and one of

the terms from Eq. (4.105). Odderon-0 affects the ρ values but not the cross sections, being entirely real. Odderon-1 gives a constant cross section difference, while odderon-2 gives a cross section difference growing as log$s$. In a later section, we analyze the existing data to determine to what extent an odd amplitudes of the above type can be excluded.

H. Asymptotic Behavior: "Pomeranchuk Theorems" and the Froissart Bound

1. The Original Pomeranchuk Theorem

When the highest energy data available came from Serpukhov, it seemed that the pp total cross section was becoming constant. In such circumstances, the original Pomeranchuk theorem would apply (Pomeranchuk, 1958). This theorem states that if pp and p$\bar{\text{p}}$ (or more generally, ab and $a\bar{b}$) cross sections become constant asymptotically and if the ratio of the real to the imaginary part of the forward scattering amplitude increases less rapidly than log$s$, the two cross sections become equal asymptotically.

It is easy to understand this result by considering a class of examples. If pp and p$\bar{\text{p}}$ cross sections become constant, then $f_+ \sim -iE$. If f_- grows slower than this, then surely the difference cross section falls with E. Suppose then that f_- grows asymptotically as $E(\log(s/s_0) - i\pi/2)^\beta$. Certainly β cannot be greater than one. If $\beta = 1$, the difference cross section is asymptotically a non-zero constant, but the ratio of the real to the imaginary part grows as log$s$, violating the conditions of the theorem. If $\beta < 1$, the real part over the imaginary part grows as $(\log s)^\beta$, that is, less rapidly than log$s$, but then the cross section difference goes as $(\log s)^{\beta-1}$, that is, it falls to zero. Thus, we see that the Pomeranchuk

theorem holds for amplitudes of this class.

2. The Froissart Bound

Since the early operation of the ISR it has been known that the pp total cross section starts rising after attaining a minimum of about 38 mb. The rate of the rise was found to be about as $\log^2 s$. The fundamental result of Froissart (refined by Martin) states that this is the fastest rate which is permissible asymptotically. We present here a derivation of the Froissart bound based on two fundamental results which we take as given (Martin and Cheung, 1970 and references therein):

i. The scattering amplitude f grows no faster than s^2.

ii. For fixed s (i.e. k^2), the amplitude is analytic in the region $|q|^2 < 4m_\pi^2$.

We use (ii) and evaluate f at $q = 2im_\pi$ using Eq.(4.21). Thus,

$$\begin{aligned} f &= \frac{p}{\pi}\int d^2b \exp(i\mathbf{q}\cdot\mathbf{b})\, a(b,s) \\ &= \frac{p}{\pi}\int bdb\, d\phi \exp(2m_\pi b\cos\phi)\, a(b,s) \\ &= 2p\int bdb I_0(2m_\pi b)\, a(b,s) \qquad < Cs^2. \end{aligned} \tag{4.106}$$

We seek to maximize the cross section, subject to this constraint. Clearly it is best to make $a(b,s)$ purely imaginary. Since the Bessel function $I_0(z)$ is an increasing function of z, it is best to keep all the contributions at the lowest possible value of b in order to minimize the above integral. For these reasons, we take $a(b,s) = i$ for $b < b_c$ and $a(b,s) = 0$ for $b > b_c$. Thus we have

$$f = 2pi \int_0^{b_c} db\, bI_0(2m_\pi b)$$
$$= \frac{ipb_c}{2m_\pi^2} I_1(2m_\pi b_c) \qquad < Cs^2. \tag{4.107}$$

Now using the asymptotic expression $I_n(z) \to \exp(z)/\sqrt{2\pi z}$ for large z, we see that

$$(2m_\pi b_c)^{1/2} \exp(2m_\pi b_c) < \text{constant} \times s. \tag{4.108a}$$

Thus since $2m_\pi b_c \gg 1$,

$$b_c \approx \frac{1}{2m_\pi}[\log(s/s_0) - \text{loglog}(s/s_0)], \tag{4.108b}$$

where s_0 is an unknown scale.

Now using Eq.(4.23), we find, neglecting the slowly varying term $\text{loglog}(s/s_0)$,

$$\sigma_{tot} = 4 \int d^2b Im\, a(b,s) = 4\pi b_c^2$$
$$= \frac{\pi}{m_\pi^2}(\log(s/s_0))^2 \quad \approx 60\text{mb}\,(\log(s/s_0))^2. \tag{4.109}$$

It should be noted that the form for $a(b,s)$ which saturates the bound is a peculiar one. First, a cuts off sharply. We shall see that this is a rather general feature of all profiles which lead to $\log^2 s$ growth of the total cross section. In addition, where a is non-zero, it is equal to i.

Thus the scattering is purely elastic. It is more common in models to find a totally black disc, with $a = i/2$. In addition, the a chosen above extends as far in impact parameter space as allowed by analyticity. If it extended a distance growing as $\log s$ but with a lesser coefficient, a smaller cross section proportional to the square of this coefficient would result. In particular, a black disk with radius approximately $b_c/7$ would give a cross section growing as 0.6 mb $\log^2 s$, the value we shall find from the data analysis of the next Section.

3. The Revised Pomeranchuk Theorem

Now that cross sections are seen to rise with increasing energy, we need a revised Pomeranchuk theorem. Suppose the pp and $p\bar{p}$ cross sections grow as $(\log s)^\gamma$. Then we can show that the difference of the cross sections cannot grow faster than $(\log s)^{(\gamma/2)}$ (Eden, 1966; Kinoshita, 1966).

The proof goes as follows. Referring to Fig.1a, we see that since the amplitude $a(b)$ must lie in the Argand circle (we drop the indication of the energy at which the amplitude is evaluated),

$$|Re\, a(b)|^2 \leq Im\, a(b). \tag{4.110}$$

As we saw in the demonstration of the Froissart bound, the impact parameters that contribute significantly to scattering must lie within some value b_c which grows as $\log s$. Thus we can approximate the scattering amplitude, Eq. (4.21) as

$$f(q=0) = \frac{p}{\pi} \int d^2b\, a(b) \approx 2p \int_0^{b_c} bdb\, a(b). \tag{4.111}$$

It follows that

$$|Ref(0)| \approx 2p\left|\int_0^{b_c} bdb\, Re\, a(b)\right|$$
$$\leq 2p\int_0^{b_c} bdb|Re\, a(b)|$$
$$\leq 2p\int_0^{b_c} bdb[Im\, a(b)]^{1/2}. \qquad (4.112)$$

Next we apply the Cauchy-Schwartz inequality to (4.112) to obtain

$$|Ref(0)| \leq 2p\left[\int_0^{b_c} bdb\, Im\, a(b)\right]^{1/2}\left[\int_0^{b_c} bdb\right]^{1/2}$$
$$\leq 2p\left(\frac{\sigma_{tot}}{8\pi}\right)^{1/2}\left(\frac{1}{2}b_c^2\right)^{1/2}$$
$$\leq \text{constant}\cdot s\cdot(\log s/s_0)^{\gamma/2}(\log s/s_0). \qquad (4.113)$$

Now the generic form for the odd amplitude is

$$f_- \sim s(\log s/s_0 - i\pi/2)^{\gamma'}. \qquad (4.114)$$

Comparing Eqs. (4.113) and (4.114), we find that

$$\gamma' \leq \gamma/2 + 1. \qquad (4.115)$$

Thus the difference of the cross sections goes as

$$\Delta\sigma \sim (\log s/s_0)^{\gamma'-1} \leq \text{constant} \times (\log s/s_0)^{\gamma/2}, \qquad (4.116)$$

as we wished to show.

4. The Fischer Theorem

We see that growing cross section differences are allowed. Is there any way other than just looking at the existing data for cross section differences to infer whether the cross sections are going to approach each other eventually? There is a theorem, due to Fischer and co-workers (Fischer *et al.*, 1978; Fischer, 1981), which states, in part, that if above some energy, the signs of Imf_-^{tot} and Ref_-^{tot} remain the same, then the difference of the cross sections tends to zero. (However, if the difference of the cross sections tends to zero, no conclusion can be drawn about the relative sign.) Clearly this theorem is satisfied by the amplitude f_- of Eq. (4.104), for $0 < \alpha < 1$. The addition of an odderon-1 or an odderon-2 amplitude leads to opposite signs for Imf_-^{tot} and Ref_-^{tot} in the limit of high s. This is, of course, in accord with the Fischer theorem, since these terms lead to non-vanishing cross section differences.

It seems then, that by looking at high energy data for signs of the real and imaginary parts of the odd amplitude, we might predict whether or not the cross section difference will ultimately go to zero. The problem is that at any finite energy, the contribution of one of the odderon terms might still be too small to have changed the sign of one or the other part of the amplitude. That change could occur farther out in energy. We shall see an example of this among our fits where the cross-over point occurs near $\sqrt{s} = 100\text{GeV}$, while the data extend only to $\sqrt{s} = 62\text{GeV}$.

5. The Cornille-Martin Theorem and a New Corollary

We have seen that as $s \to \infty$, $\sigma_{p\bar{p}}/\sigma_{pp} \to 1$, whether or not $\sigma_{p\bar{p}} - \sigma_{pp} \to 0$. Similarly, Cornille and Martin (1972a, b, c; 1974) have proved that inside the forward diffraction peak (suitably defined),

$$\frac{d\sigma_{p\bar{p}}}{dt}(s,t) \Big/ \frac{d\sigma_{pp}}{dt}(s,t) \to 1, \tag{4.117}$$

even though the difference of the cross sections at fixed t may not go to zero. We will illustrate this theorem by an example. Suppose the cross section goes as $\log^2 s$ and that there is an odderon-2. Then both f_+/p and f_-/p go as $(\log s/s_0 - i\pi/2)^2$ at $t = 0$. We can imagine that the behavior is similar for $t \neq 0$. The odd and even amplitudes, however, are out of phase by $\pi/2$. The result is that

$$\frac{|f_+ + f_-|^2}{|f_+ - f_-|^2} \to 1, \tag{4.118}$$

so the differential cross section ratio goes to unity as required by the Cornille-Martin theorem, although the difference of the differential cross sections grows as $\log^2 s$. A particular consequence of this theorem is that the ratio of the slope parameters goes to unity, *i.e.*

$$B_{\mathrm{pp}}/B_{\mathrm{p\bar{p}}} \to 1. \tag{4.119}$$

It is *not* the case that the ratio of the ρ parameters goes to unity. Using the relation between the differential cross section in the forward direction and the total cross section, we derive a new corollary: the ratio of the *squares* of the ρ values goes to unity, i.e.,

$$(\rho_{\mathrm{pp}}/\rho_{\mathrm{p\bar{p}}})^2 \to 1. \tag{4.120}$$

Indeed, for odderon-2, the two ρ values go to non-zero numbers which are negatives of each other.

6. If the Total Cross Section Grows as $\log^2 s$

For the cross section to grow as $\log^2 s$, there must be contributions to $Ima(b,s)$ for values of b with a range varying as $\log s$. Let us define

$$b_c = \frac{1}{2m_\pi}\log(s/s_0), \tag{4.121}$$

$$\bar{a}(x,s) = a(b = xb_c, s), \tag{4.122}$$

where s_0 is fixed. Now from Eq.(4.103)

$$\int_0^\infty dx s^x \bar{a}(x,s) < Cs. \tag{4.123}$$

This means that for $x > 1$, $\bar{a}(x,s)$ must fall to zero with increasing s. However, there must be some region $x < 1$ where $\bar{a}$ remains finite so that the cross section will truly grow as $\log^2 s$, giving a contribution (see Eq. (4.23))

$$\bar{\sigma} = 4\pi b_c^2 \int_0^\infty x\, dx\, Im\bar{a}(x,s). \tag{4.124}$$

Thus the piece of $a(b,s)$ which gives rise to the $\log^2 s$ cross section is most simply obtained by an $\bar{a}$ which is independent of s and which vanishes for $x > 1$. This excludes, for example, a Gaussian shape in impact parameter space

$$a(b,s) = A\exp(-cb^2/b_c^2), \tag{4.125}$$

which has an infinitely long tail. If there is a piece of the impact parameter distribution which has a Gaussian distribution, it cannot contribute a piece to the total cross section which grows as $\log^2 s$. From the ansatz that $\bar{a}(x,s)$ is independent of s, we can obtain a heuristic proof of the theorem of Auberson, Kinoshita, and Martin (1971) that if the cross section grows as $\log^2 s$, then the amplitude is of the form

$$f \sim is\log^2 sF(t\log^2 s), \tag{4.126}$$

where F is an entire function (of its argument $t\log^2 s$) of order one-half. (That is, $F(z)$ is analytic everywhere in the finite plane and as $|z| \to \infty$, $|F|$ is bounded by $c\exp(c'|z|^{1/2}$ with c and c' positive constants). Now Eq. (4.19) becomes a finite integral:

$$f \sim sb_c^2 \int_0^1 x\, dx\bar{a}(x,s)J_0(qb_c x). \tag{4.127}$$

The theorem follows from the observation that the integral is over a finite range and that the Bessel function is an entire function. Asymptotically, for complex argument, the Bessel function $J_0(z)$ is bounded by an exponential , $\exp|z|$. Thus the integral is bounded by $\exp(c'qb_c) \sim \exp(c'\sqrt{-t\log^2 s})$.

From the representation of Eq. (87), we can derive results for the slope parameter at $t = 0$. It is clear from the MacDowell-Martin bound that if the total cross section grows as fast as $\log^2 s$, so must B, since the elastic cross section cannot grow faster than $\log^2 s$. The same result can be obtained by expanding Eq. (4.126) in powers of $t\log^2 s$

$$f \sim is\log^2 s[a + bt\log^2 s + \cdots], \tag{4.128}$$

so that

$$B(s,0) \sim \log^2 s, \tag{4.129}$$

in agreement with our expectations. If instead of taking $t = 0$, we fix $t \neq 0$ and let $\log s$ increase, we have the exponential bound referred to above. From the definition, Eq. (4.24) we find

$$\begin{aligned} B(s,t) &< \frac{d}{dt} 2c'|t|^{1/2}\log s \\ &< c''\log s, \end{aligned} \tag{4.130}$$

where $c'' = c't^{-1/2}$ at fixed t. Thus c'' becomes very large for very small t.

This non-uniform behavior was discovered by Martin (Martin, 1982). As a practical matter, it still seems reasonable to use the form for $B(s,0)$ even at non-zero values of t since the other form, Eq. (4.130) is derived on the assumption that $|t|\log^2 s$, or equivalently $|t|\sigma_{tot}$, is large. In particular, if the differential cross section had diffraction minima, the limit with t fixed would correspond to measuring the slope *outside* the diffraction minimum.

While the form of the amplitude given by Auberson, Kinoshita, and Martin is a powerful means of examining high energy behavior when the cross section grows as $\log^2 s$, it should be noted that the assumption of this particular energy dependence is critical. If the cross section grows as $\log^{1.9} s$, the proof fails. We are unaware of any weaker form of the theorem which pertains to such circumstances.

V. ANALYSIS OF t=0 AMPLITUDES

A. Conventional Amplitudes

We define $\mathcal{F}$ as the analytic continuation of the forward scattering amplitude into the complex E plane, where E is the complex energy (E is the pp laboratory energy if E is real and $\geq m$, the nucleon mass). The $\mathcal{F}$'s are real analytic functions having cuts on the real axis from $+m$ to ∞ and from $-m$ to $-\infty$. We choose the normalizations such, for fits without odderons,

$$4\pi\mathcal{F}_+ = -\sqrt{(m+E)(m-E)}$$
$$\left\{A+\beta\frac{\{[\log(2m(m+E)/s_0)+\log(2m(m-E)/s_0)]/2\}^2}{1+a\{[\log(2m(m+E)/s_0)+\log(2m(m-E)/s_0)]/2\}^2}\right.$$
$$\left.+\frac{C}{2\sin(\pi\mu/2)}\left[[2m(m+E)]^{\mu-1}+[2m(m-E)]^{\mu-1}\right]\right\}, \tag{5.1a}$$

and

$$4\pi\mathcal{F}_- = -\sqrt{(m+E)(m-E)}$$
$$\times\frac{D}{2\cos(\pi\alpha/2)}\left[[2m(m+E)]^{\alpha-1}-[2m(m-E)]^{\alpha-1}\right], \tag{5.1b}$$

where A, β, s_0, a, C, μ, D, and α are real constants to be fitted by the data. Clearly, $\mathcal{F}_+(E)=\mathcal{F}_+(-E)$ and $\mathcal{F}_-(E)=-\mathcal{F}_-(-E)$, i.e ., $\mathcal{F}_+$ is an even amplitude and $\mathcal{F}_-$ is an odd amplitude. To find the scattering amplitudes for pp scattering, f_+ and f_-, we evaluate $\mathcal{F}_+(E+i\epsilon)$ and

$\mathcal{F}_-(E+i\epsilon)$, in the limit of real E and $\epsilon \to 0$ (for the $p\bar{p}$ amplitudes, we could evaluate the $\mathcal{F}$'s at $-E-i\epsilon$, or, correspondingly, use the appropriate symmetry properties of the $\mathcal{F}$'s). We obtain,

$$\frac{4\pi}{p} f_+ = i\{A + \frac{\beta[\log(2mp/s_0) - i\pi/2]^2}{1 + a[\log(2mp/s_0) - i\pi/2]^2} + C\Big[((2m)(E-m))^{\mu-1} e^{i\pi(1-\mu)/2} + \frac{\left(((2m)(E+m))^{\mu-1} - ((2m)(E-m))^{\mu-1}\right)}{2\sin\pi\mu/2}\Big]\Big\}, \tag{5.2a}$$

and

$$\frac{4\pi}{p} f_- = D\Big\{((2m)(E-m))^{\alpha-1} e^{i\pi(1-\alpha)/2} + i\frac{((2m)(E+m))^{\alpha-1} - ((2m)(E-m))^{\alpha-1}}{2\cos\pi\alpha/2}\Big\}. \tag{5.2b}$$

The optical theorem relates the cross sections σ^+ and σ^- to the above by

$$\sigma^+ = \frac{4\pi}{p} Im f_+ \tag{5.3a}$$

and

$$\sigma^- = \frac{4\pi}{p} Im f_-, \tag{5.3b}$$

where p is the laboratory momentum. Hence, the imaginary portions of (5.2a) and (5.2b) give the appropriate cross sections σ^+ and σ^-, from which we form

$$\sigma(p\bar{p}) = \frac{(\sigma^+ + \sigma^-)}{2} \tag{5.4a}$$

and

$$\sigma(pp) = \frac{(\sigma^+ - \sigma^-)}{2}. \tag{5.4b}$$

The formulae (5.2a) and (5.2b) simplify greatly in the limit of $E \gg m$, where s is given by $s \approx 2mE \approx 2mp$. Using the notation $\bar{f}$ for the limit of f as $E \to \infty$, we obtain

$$\frac{4\pi}{p} \bar{f}_+ = i\left\{A + \beta \frac{\log[(s/so) - i\pi/2]^2}{1 + a[\log(s/so) - i\pi/2]^2} + C s^{\mu-1} e^{i\pi(1-\mu)/2}\right\} \tag{5.5a}$$

and

$$\frac{4\pi}{p} \bar{f}_- = D\left\{s^{\alpha-1} e^{i\pi(1-\alpha)/2}\right\}, \tag{5.5b}$$

forms discussed in Section IV.F. If we put $a = 0$ in (5.5a), we find by inspection of the real and imaginary parts of (5.5a) and (5.5b), the very simple and useful formulae,

$$\sigma(\mathrm{pp}) = A + \beta\left[\log^2 s/s_0 - \frac{\pi^2}{4}\right] + C\sin\left(\frac{\pi\mu}{2}\right)s^{\mu-1} + D\cos\left(\frac{\pi\alpha}{2}\right)s^{\alpha-1}, \tag{5.6a}$$

$$\sigma(\mathrm{p\bar{p}}) = A + \beta\left[\log^2 s/s_0 - \frac{\pi^2}{4}\right] + C\sin\left(\frac{\pi\mu}{2}\right)s^{\mu-1} - D\cos\left(\frac{\pi\alpha}{2}\right)s^{\alpha-1}, \tag{5.6b}$$

$$\rho(\mathrm{pp}) = \frac{\beta\pi\log s/s_0 - C\cos(\pi\mu/2)s^{\mu-1} + D\sin(\pi\alpha/2)}{\sigma(\mathrm{pp})}, \tag{5.6c}$$

$$\rho(\mathrm{p\bar{p}}) = \frac{\beta\pi\log s/s_0 - C\cos(\pi\mu/2)s^{\mu-1} - D\sin(\pi\alpha/2)}{\sigma(\mathrm{p\bar{p}})}. \tag{5.6d}$$

We have essentially used the forms (5.6a-d) in our earlier work (Block and Cahn, 1982a) where we introduced only the coefficients A, β, s_0, D, α and a. We interpret the even amplitude $Cs^{\mu-1}$ as an even Regge exchange term, with the odd amplitude $Ds^{\alpha-1}$ as an odd Regge exchange term. The term in β gives the $\log^2 s$ rising cross section, and A corresponds to a constant cross section. It will turn out that the coefficients using (5.5a-b), i.e., using (5.6a-d), are nearly identical to those obtained using the kinematically correct equations (5.2a-b). The only important difference is that (5.2a-b) give an improved χ^2 for the fit. This is because the low energy kinematics (the cut structure in E) is treated correctly in (5.2a-b) for $\sqrt{s} \sim 5$ GeV, where they are of importance. For $\sqrt{s} > 10$ GeV, the

results using either (5.2a-b) or (5.5a-b) are numerically indistinguishable. However, the introduction of an even Regge amplitude as an alternate description of the date is a departure from our earlier treatment. The $\log^2 s/s_0$ term in the even amplitude, for $s < s_0$, simulates this term in the cross section. We have fixed the power μ to be 0.5, since we expect it to be about the same as α, which turns out to be ~ 0.5.

Clearly, setting $a = 0$ in (5.2a) gives rise to a cross section which continues to rise indefinitely as $\log^2 s/s_0$. The introduction of a non-zero a in (5.2a) gives us a functional form which will have the cross section rise locally as $\log^2 s/s_0$ (in the energy region $5 < \sqrt{s} < 62$ GeV), if $a \ll 1$. However, as $s \to \infty$, i.e., at a very high energy, the cross section will flatten out and tend to a constant value, $A + (\beta/a)$, for positive a. Thus, we model the case where the Froissart bound is not truly saturated (it rises as $\log^2 s/s_0$ only locally), and eventually, the cross section rise stops, going to a constant cross section at ∞. We consider this extreme case a measure of the possible error due to extrapolation beyond the region of the fit, $5 < \sqrt{s} < 62$ GeV.

The fits were made using seven different types of experimental quantities $\sigma(\mathrm{pp})$, $\sigma(\mathrm{p\bar{p}})$, $\Delta\rho$, $\Delta\sigma$, ρ_{av}, $\rho(\mathrm{pp})$ and $\rho(\mathrm{p\bar{p}})$, along with their associated experimental errors (we define $\Delta\sigma = \sigma(\mathrm{p\bar{p}}) - \sigma(\mathrm{pp})$, $\Delta\rho = \rho(\mathrm{\bar{p}p}) - \rho(\mathrm{pp})$ and $\rho_{av} = [\rho(\mathrm{p\bar{p}}) + \rho(\mathrm{pp})]/2$). The χ^2 was minimized using the seven quantities and their quoted errors. No attempt was made to adjust any of the data systematically. (For some related fits, see Gauron and Nicolescu, 1983). The sources of the data used in the fits are given in Table 5.1.

In our earlier work, we had included in f_+ a real constant term

(which of course does not contribute to σ). Since its effect on the ρ value is through the real portion of f_+, its contribution is proportional to the constant term divided by p, and its contribution is vanishingly small in our energy region of interest. Thus, its influence is negligible and we have neglected it in our present work.

The results of our various fits are summarized in Table 5.2. For the cases where $C = a = 0$ (Fit #1), we get an excellent reproduction of the data using 5 parameters, A, β, s_0, D and α, with a $\chi^2/d.f.$ (χ^2/degree of freedom) of 1.17 for 76 degrees of freedom. We obtain $A = 41.74 \pm 0.04$, $\beta = 0.66 \pm 0.01$, $s_0 = 338 \pm 8$, $D = -39.4 \pm 1.6$ and $\alpha = 0.48 \pm 0.01$. If we introduce the even Reggeon (the term in C), we get, for $a = 0$, Fit #2, which has a $\chi^2/d.f. = 1.15$ for 75 degrees of freedom. We find $A = 41.30 \pm 0.28$, $\beta = 0.62 \pm 0.03$, $s_0 = 294 \pm 28$, $D = -40.5 \pm 1.8$, $\alpha = 0.47 \pm 0.01$ and $C = 8.3 \pm 5.1$, using $\mu = 0.5$. Again, this fit is in excellent agreement with the data. The units are such that σ is in mb if E, m, p and $\sqrt{s}$ are in GeV. The introduction of $a \neq 0$ results in Fits #3 and #4. The $\chi^2/d.f.$ is not changed significantly, and we find very small positive values of a, which are between 2 and 2.5 standard deviations from zero. Clearly, had we found negative a and $|a| \ll 1$, we could not have used the fit for extrapolation, since $\sigma \to A + (\beta/a)$ as $s \to \infty$. We find $\sigma \to 156$ mb for Fit #3 and $\sigma \to 113$ mb for Fit #4. All of the above fits are plotted in Figs. 5.1(a) and 5.1(b) for $C = 0$, and in Figs. 5.2(a) and 5.2(b) for $C \neq 0$ (the even Regge term). It is clear that these fits reproduce the observed data in the energy region $5 < \sqrt{s} < 62$ GeV. Also appended to the cross section curves is the recent experimental value for $\sigma(\bar{p}p)$ at the SPS collider at $\sqrt{s} = 540$ GeV (UA4-Collaboration, 1982b, UA1-Collaboration, 1983), which we have corrected for a ρ value of 0.20.

Our predictions are in very good agreement with this measurement. We remark parenthetically that for $a = 0$, the curves are essentially the same for $\sqrt{s} > 10$ GeV, if we use the simple formulae Eqs. (5.6a) - (5.6d).

We find (Figs. 5.1(a) and 5.2(a); also see Table 7.1) that if the cross sections keep rising as $\log^2 s/s_0$, at the Tevatron Collider ($\sqrt{s} = 2$ TeV), $\sigma_1 = 98.3 \pm 1.2$ mb and $\sigma_2 = 95.9 \pm 1.9$ mb, where the subscripts refer to the fit number and the errors are those generated by the fit (#1 without an even Regge term, #2 with an even Regge term, with both having $a = 0$). At the proposed SSC Collider ($\sqrt{s} = 40$ TeV), we predict $\sigma_1 = 196.4 \pm 3.1$ mb and $\sigma_2 = 188.8 \pm 5.6$ mb. The ρ values predicted at the Tevatron Collider are $\rho_1 = 0.198 \pm 0.002$ and $\rho_2 = 0.193 \pm 0.004$, whereas at the SSC, they are $\rho_1 = 0.163 \pm 0.001$, and $\rho_2 = 0.160 \pm 0.002$. Again the errors represent the uncertainties in the fit given the functional forms assumed.

For the fits with $a \neq 0$, the predictions at $\sqrt{s} = 540$ GeV are $\sigma_3 = 65.1 \pm 2.4$ mb and $\sigma_4 = 61.6 \pm 2.4$ mb, and $\rho_3 = 0.14 \pm 0.03$ and $\rho_4 = 0.11 \pm 0.02$. The cross section predictions at this energy for $a \neq 0$ are too close to the values predicted by the $a = 0$ fits for the present $\sim 10\%$ cross section measurement to distinguish. At $\sqrt{s} = 2$ TeV, the situation is more favorable and we predict the ($a \neq 0$) values $\sigma_3 = 80.0 \pm 6.8$ mb and $\sigma_4 = 72.2 \pm 5.4$ mb , with the corresponding values $\rho_3 = 0.11 \pm 0.03$ and $\rho_4 = 0.08 \pm 0.02$. Thus, measurements of σ and ρ for $p\bar{p}$ at the Tevatron collider should easily distinguish between the cases of $a \neq 0$ and $a = 0$, i.e., whether or not the cross section keeps rising as $\log^2 s$. At $\sqrt{s} = 40$ TeV (the SSC), the $a \neq 0$ predictions are $\sigma_3 = 107.8 \pm 20.1$ mb and $\sigma_4 = 89.0 \pm 12.8$ mb, along with $\rho_3 = 0.05 \pm 0.02$ and $\rho_4 = 0.04 \pm 0.01$.

At the present time, the measurements of $\sigma(p\bar{p})$ at the SPS Collider are not sufficiently accurate to distinguish between the cases of $a = 0$ and $a \neq 0$. The only evidence bearing on whether the cross sections continue to rise as $\log^2 s/s_0$ is preliminary cosmic ray data, where the cross sections for p-air collisions are reduced to a lower limit on the pp cross section at a mean energy of 10 TeV. The lower limit is shown in Figs. 5.1(a) and 5.2(a), and is evidence in favor of the cross sections continuing to rise logarithmically. In this regard, the value of the $\log^2 s/s_0$ coefficient is $\beta \sim$ 0.6 mb. This is to be contrasted with the Froissart-Martin bound which says that σ must rise less rapidly than $(\pi/m_\pi^2)\log^2 s/s_0 \sim 60 \log^2 s/s_0$ mb, where m_π is the pion mass. Thus, our value of β is only $\sim 1\%$ of the saturation coefficient. Hence, it is not appropriate to say that we have "saturated the Froissart-Martin bound", in spite of the fact that the cross section seems to rise as $\log^2 s/s_0$.

B. Can a log$s$ Rise Fit the Data?

To verify the form of the rise, we have tested the fit using an even amplitude that would cause the cross section to rise *only* as $\log s/s_0$, i.e., we introduce the amplitude f_+, via

$$\frac{4\pi}{p} f_+ = \left\{ A + \beta[\log 2mp/s_0 - i\pi/2] + C\left[(2m(E-m))^{\mu-1} e^{i\pi(1-\mu)/2} + \frac{(2m(E+m))^{\mu-1} - (2m(E-m))^{\mu-1}}{2\sin\pi\mu/2} \right] \right\}, \tag{5.7}$$

with $\mu = 0.5$ and $4\pi f_-/p$ being given by Eq. (5.2b). This was a test to see how well the data could be reproduced utilizing a $\log s/s_0$ term,

as contrasted to a $\log^2 s/s_0$ term. The fit was very poor, giving rise to a $\chi^2/d.f. = 7.2$ for 76 degrees of freedom. The predicted σ at the SPS collider was much too low. Even if we employed $\mu = 0.6$, the $\chi^2/d.f.$ was 4.1, equally unsatisfactory. Fundamentally, one could not use a $\log s/s_0$ term and simultaneously reproduce both the cross sections and the ρ values in the energy region $5 < \sqrt{s} < 62$ GeV. Thus, we conclude that fitting all available data in this energy domain *requires* the presence of a term varying essentially as $\log^2 s/s_0$, and that just a $\log s/s_0$ term (or, indeed, any lower power) is ruled out.

C. Odderon Amplitudes

Up to this point, we have concerned ourselves with fitting the data using the odd amplitude f_- given by Eq. (5.2b). This amplitude, in the limit of $s \to \infty$, has $\Delta\sigma \to 0$ and $\Delta\rho \to 0$. The form of Eq. (5.2b) is suggested by an odd Regge exchange term. However, the requirements of analyticity are compatible with odd amplitudes (the "odderons") which give $\Delta\sigma \to$ non-zero constant or even $\Delta\sigma \to \log s/s_0$, as $s \to \infty$. (Lukaszuk and Nicolescu, 1973; Kang and Nicolescu, 1975;Joynson et al., 1975) See Section IV.H. To test for the presence of these odderon terms, we introduce three types of odderon amplitudes $f_-^{(j)}$, where $j = 0$, 1, or 2, via

$$4\pi f_-^{(0)} = -\epsilon^{(0)} E, \tag{5.8a}$$

$$4\pi f_-^{(1)} = -\epsilon^{(1)} E\left[\log\left(\frac{2mp}{s_0}\right) - \frac{i\pi}{2} \right], \tag{5.8b}$$

$$4\pi f_-^{(2)} = -\epsilon^{(2)} E\left[\log\left(\frac{2mp}{s_0}\right) - \frac{i\pi}{2} \right]^2. \tag{5.8c}$$

where the ϵ's are real constants. We form a new odd amplitude $f^{new,(j)} = f^{old} + f^{(j)}$, where the old odd amplitude is given by Eq. (5.2b). The results of these fits are summarized in Table 5.3. All fits with odderons used $a = 0$. Fits #5 and #6 used odderon 0 ($j = 0$), #7 and #8 used odderon 1 ($j = 1$) and #9 and #10 used odderon 2 ($j = 2$), for the cases of $C = 0$ and $C \neq 0$, respectively. We note from Eqs. (5.8a) - (5.8c) that odderon 0 gives $\Delta\sigma \to 0$, odderon 1 gives $\Delta\sigma \to \epsilon\pi/2$ and odderon 2 gives $\Delta\sigma \to \epsilon \log s/s_0$, as $s \to \infty$. All of the odderon fits give a satisfactory χ^2, with the $\chi^2/d.f.$ ranging between 1.08 and 1.11. The coefficients $\epsilon^{(j)}$ are all small and negative, being about 2 to 2.5 standard deviations from zero. For Fits #5, 7 and 9, which correspond to $C = 0$, we find $\epsilon^{(0)} = -0.29 \pm 0.12$ mb, $\epsilon^{(1)} = -0.12 \pm 0.04$ mb and $\epsilon^{(2)} = -0.04 \pm 0.02$ mb. The results for odderon 2 (with $C = 0$) from Fit #9 are plotted in Figs. 5.3(a) and 5.3(b). We see the crossover of $\Delta\sigma$ from positive to negative values at $\sqrt{s} \sim 80$ GeV in Fig. 5.3(a). The most striking feature of this fit is the separation $\Delta\rho$. The ρ value for $p\bar{p}$ rises to about 0.23, whereas the pp value only goes to 0.15.

It is very difficult to rule out the presence of the odderon terms given only the existing data. Although the odderon amplitudes are very small (in comparison with the constant amplitude A, they are $< 1\%$), they of course dominate the odd amplitude as $s \to \infty$. The data *do not require* adding the presence of odderons, but they also *do not rule out* the presence of these terms at a 2 standard deviation level. If the odderons are as large as in our fits, comparisons of $\sigma(p\bar{p})$ and $\sigma(pp)$ at $\sqrt{s} > 500$ GeV would easily confirm this. Very precise ρ comparisons would be required to rule out odderon 0. The curves for fits #5 (odderon 0, $C = 0$) and #7 (odderon 1, $C = 1$) are shown in Figs. 5.4(a) and 5.4(b), and Figs. 5.5(a)

and 5.5(b), respectively.

The results of the odderon fits illustrate that the Fischer theorem must be applied with care. In the region in which data now exist, Ref^{new} and Imf^{new} have the same sign. For the fits with odderon 1 or 2, at high energies the imaginary part changes sign, since the term in ϵ is negative and dominates the odd amplitude, causing $\Delta\sigma$ to change sign and become negative. Thus, for sufficiently high energy (just beyond the range of existing data), both the real and the imaginary portions of f^{new} have opposite signs, as required by the Fischer theorem, since $\Delta\sigma$ does not go to zero as $s \to \infty$. However, a premature application of the Fischer theorem at existing energies leads one to the false conclusion that the cross sections become asymptotically equal, since at these energies, both the real and imaginary portions of the odd amplitude have the same sign.

D. Summary of Amplitude Analysis

We summarize this section with the following conclusions:

(1) All of the cross sections and ρ values for $p\bar{p}$ and pp above $\sqrt{s} = 5$ GeV can be simply and very satisfactorily parametrized with 6 (or even 5) coefficients, using Eqs. (5.2a) - (5.2b) or using Eqs. (5.1a) - (5.1b). Above $\sqrt{s} = 10$ GeV, the simple formulae Eqs. (5.6a) - (5.6d) are sufficient.

(2) Measurements of σ_{tot} and ρ for $p\bar{p}$ at the Tevatron collider ($\sqrt{s} = 2$ TeV) are necessary to decide whether the cross section continues to rise as $\log^2 s/s_0$, i.e., $a = 0$, or whether the cross section flattens out. If the cross section continues to rise, we predict cross sections of about 100 mb at $\sqrt{s} = 2$ TeV and 200 mb at $\sqrt{s} = 40$ TeV. On the other hand, in

the fit with $a \neq 0$, they are predicted to be only 70 mb and 90 mb, respectively (for fit #4), a very large experimentally accessible difference. Further, the ρ value is 0.20 for $a = 0$ whereas ρ is 0.08 for $a \neq 0$ (fit #4) at $\sqrt{s} = 2$ TeV, again a very large effect.

(3) The measured coefficient β of the $\log^2 s/s_0$ term for the rising cross section is only 1 % of the Froissart-Martin bound of $\approx$ 60 mb for the coefficient.

(4) The existing ρ and σ_{tot} data for $p\bar{p}$ and pp in the energy region $5 < \sqrt{s} < 62$ GeV require a $\log^2 s/s_0$ term. A term only varying as $\log s/s_0$ (or a lower power) is not sufficient.

(5) The odderon amplitudes are within 2 to 2.5 standard deviations of zero, i.e., they are compatible with zero, and are at most about 1 % as strong as the constant even amplitude.

VI. SLOPE ANALYSIS OF NEARLY-FORWARD ELASTIC SCATTERING DATA

The near-forward hadronic amplitude for $p\bar{p}$ and pp elastic scattering is reflected in three experimentally determined parameters, the total cross section σ_{tot}, the ρ value and the nuclear slope parameter B, defined as

$$B(s) = \frac{d}{dt}\log\left(\frac{d\sigma_n}{dt}\right) \quad \text{at} \quad t = 0. \tag{6.1}$$

In the preceding section, we analyzed $t = 0$ data in the energy domain $5 < \sqrt{s} < 62$ GeV, in order to extract forward hadronic elastic scattering amplitudes f_+ and f_-. We found that we could get an excellent parametrization of the data using either a 5-parameter fit (fit #1 of Table 5.1) or a 6-parameter fit (fit #2 of Table 5.1), both of which had a $\log^2 s/s_0$ behavior as $s \to \infty$. We recall that fit #2 used an even Regge exchange term $Cs^{\mu-1}$, with $\mu = 0.5$, whereas fit #1 had $C = 0$. Both fits used $a = \epsilon = 0$.

In this section, we will use the results of fits #1 and #2 to obtain the s dependence of the nuclear slope parameters B for $p\bar{p}$ and pp elastic scattering, using experimental data in the near-forward direction (defined as the small $|t|$ region, $|t| < 0.02(\text{GeV}/c)^2$). We write the invariant hadronic elastic differential scattering cross section as

$$\frac{d\sigma_n}{dt} = \frac{\pi|f_+ g_+(t,s) \pm f_- g_-(t,s)|^2}{p^2}, \tag{6.2}$$

where p is the laboratory momentum. We have assumed real, exponential

"form factors" in Eq. (6.2), with $g_+(t,s) = \exp(B^+t/2)$ being the form factor for the even amplitude and $g_-(t,s) = \exp(B^-t/2)$ being the form factor for the odd amplitude. Since we are concerned only with very small $|t|$, the assumption of an exponential form is the practical equivalent of replacing $e^{Bt/2}$ by $1 + Bt/2$. We rewrite Eq. (6.2) as

$$\frac{d\sigma_n}{dt} = \frac{\pi}{p^2}\Big\{[Ref_+\exp(B^+t/2) \pm Ref_-\exp(B^+t/2)]^2 + [Imf_+\exp(B^+t/2) \pm Imf_-\exp(B^-t/2)]^2\Big\}, \tag{6.3}$$

with the + sign for $p\bar{p}$ and the − sign for pp. In the limit of $s \to \infty$ and $\rho \to \infty$, we can simplify Eq. (6.1), using Eq. (6.3), to become

$$B(s) = B^+(s) \pm \frac{\sigma^-}{\sigma^+}\Delta B(s), \tag{6.4}$$

with the + sign for $p\bar{p}$ and the − sign for pp, defining $\Delta B(s) = B^-(s) - B^+(s)$. We have assumed in Eq. (6.4) that the ratio of the odd to even cross sections $\sigma^-/\sigma^+ \ll 1$ (σ^- and σ^+ are defined in Eq. (5.4)).

In our analysis we will include slope data in the high energy region $5 < \sqrt{s} < 62$ GeV, and only those data measured in the very low $|t|$ region, $|t| \sim 0.02(\text{GeV}/c)^2$, so that we can reasonably approximate the definition of B made in Eq. (6.1).

In order to determine the form of the s dependence of $B^+(s)$, we observe that as $s \to \infty$, $B(p\bar{p}) = B(pp) = B^+$, since $M^-/p \to 0$. The high energy elastic scattering is known to be diffractive, with an

approximately exponential slope B. Further, at high energies, ρ is known to be small. Thus, setting $\rho = 0$, we approximate σ_{el}, the total elastic scattering cross section, as Σ_{el}, i.e.,

$$\sigma_{el} \approx \Sigma_{el} = \frac{1}{B^+}\left(\frac{d\sigma_n}{dt}\right)_{t=0} \approx \frac{\sigma_{tot}^2}{16\pi B^+}, \tag{6.5}$$

where we have used the optical theorem in Eq. (6.5) and σ_{tot} is the total cross section. We rewrite Eq. (6.5) as

$$\frac{\sigma_{el}}{\sigma_{tot}} \approx \frac{\sigma_{tot}}{16\pi B^+}. \tag{6.6a}$$

Since σ_{el}/σ_{tot} must be less than 1, we must require that B grow with s at least as rapidly as the total cross section σ_{tot}, i.e., that $B^+(s)$ must grow as $\log^2 s$, since σ_{tot} grows as $\log^2 s$ (Horn and Zachariasen, 1973). We therefore parametrize the even slope as

$$B^+(s) = C^+ + D^+\log s + E^+\log^2 s, \tag{6.6b}$$

where s is measured in GeV^2. The odd amplitude is a Regge exchange term, $Ds^{\alpha-1}$, so we choose for the odd slope the normal Regge behavior

$$B^-(s) = C^- + D^-\log s, \tag{6.7}$$

where s is in GeV^2. We emphasize the importance at high energies of the term in $\log^2 s$ in Eq. (6.6). It is essential for the slope parameter at $t = 0$ to follow the trend of the total cross section for large s. This term has not been included in a recent analysis of Burq *et al.*, and its absence has seriously distorted their slope predictions for high s. In particular, if one plots B vs. $\log s$, a positive curvature similar to that measured for σ_{tot} is expected, and not a straight line, at large s.

The measurements of B in the energy range $5 < \sqrt{s} < 62$ GeV do not form a smooth set in s, unlike the situation for ρ and σ_{tot}, where there is a good agreement between various experimental groups. Indeed, the slope situation is quite confused, and even after corrections for curvature, many groups quote inconsistent values at the same energies.

It is a Solomonic task to decide which results are correct and should be included, and which results are false and should be excluded from our analysis. We were guided in our judgment by the principle that the slope data should roughly resemble the shape of the total cross section curve as a function of s, and thus have positive curvature. Using this principle to choose between conflicting sets of data, we chose to fit the data from the sources displayed in Table 6.1. The data have been fitted in a χ^2 minimization program using the experimental data for $B(\mathrm{p\bar{p}})$, $B(\mathrm{pp})$ and ΔB, along with their associated errors. No attempt has been made to adjust the data for systematic errors between various data sets.

The results for fit #1 are, in $(\mathrm{GeV}/c)^{-2}$:

$$C^+ = 10.90 \pm 0.55,$$
$$D^+ = -0.08 \pm 0.19,$$
$$E^+ = 0.043 \pm 0.016,$$
$$C^- = 23.27 \pm 1.6,$$
$$D^- = 0.93 \pm 0.17,$$

with $\chi^2/d.f. = 1.51$ for 52 degrees of freedom.

The results for fit #2 are:

$$C^+ = 10.94 \pm 0.45,$$
$$D^+ = -0.09 \pm 0.15,$$
$$E^+ = 0.043 \pm 0.013,$$
$$C^- = 23.30 \pm 1.4,$$
$$D^- = 0.94 \pm 0.13,$$

with $\chi^2/d.f. = 1.51$ for 52 degrees of freedom. The correlated errors for fit #2 are given in Table 6.2.

The results of these fits are essentially indistinguishable. Fig. 6.1 is a plot of our fit #2 for the slopes $B(\mathrm{p\bar{p}})$ and $B(\mathrm{pp})$ vs. $\sqrt{s}$, where only data in the energy interval $5 < \sqrt{s} < 62$ GeV have been used in the fitting. We have also plotted in Fig. 6.1 the recent SPS measurement for $B(\mathrm{p\bar{p}})$ at $\sqrt{s} = 540$ GeV for comparison with our prediction. The

agreement is within errors. Our prediction at $\sqrt{s} = 540$ GeV for fit #2 is $B(\mathrm{p\bar{p}}) = 16.66 \pm 0.59\,(\mathrm{GeV}/c)^{-2}$, where the error in the prediction is due to the uncertainties in the fitting parameters.

Our prediction for $B(\mathrm{p\bar{p}})$ at the Tevatron collider ($\sqrt{s} = 2$ TeV) is $19.53 \pm 1.41\,(\mathrm{GeV}/c)^{-2}$, and at the SSC ($\sqrt{s} = 40$ TeV) is $28.34 \pm 3.81\,(\mathrm{GeV}/c)^{-2}$.

We can now determine the total elastic scattering cross sections Σ_{el} as a function of s, for both $\mathrm{p\bar{p}}$ and pp elastic scattering. If we consider a non-zero ρ value, Eq. (6.5) is modified to become

$$\Sigma_{el} = \sigma_{tot}^2(1+\rho^2)/16\pi B, \tag{6.8}$$

and

$$\Sigma_{el}/\sigma_{tot} = \sigma_{tot}(1+\rho^2)/16\pi B. \tag{6.9}$$

We plot the ratio of Σ_{el}/σ_{tot} vs. s for both the $\mathrm{p\bar{p}}$ and pp systems (for Fit #2) in Fig. 6.2. The ratio for pp at $\sqrt{s} = 3$ GeV is 0.27 ± 0.06 and is about 0.17 ± 0.003 in the ISR range. The $\mathrm{p\bar{p}}$ ratio at $\sqrt{s} = 3$ GeV is 0.24 ± 0.06, is about 0.17 ± 0.003 in the ISR range, and goes up to 0.22 ± 0.008 at the SPS collider ($\sqrt{s} = 540$ GeV). The measured ratio at the SPS is 0.21 ± 0.01, in good agreement with our prediction. It is easy to show, using Eqs. (6a) - (6d) and (6.6), that asymptotically, the ratio

$$\Sigma_{el}/\sigma_{tot} \to \beta/16\pi E^{+} \quad \text{as} \quad s \to \infty. \tag{6.10}$$

Thus, at infinite energy, (using Table 1 in Eq. (6.10)), the ratio $\Sigma_{el}/\sigma_{tot} = 0.74 \pm 0.23$. Indeed, this result is also consistent with the black disk prediction of 0.5. We remark that even at as large an energy as $\sqrt{s} = 500$ TeV, the ratio has only grown to 0.44.

VII. A REGULARITY OF THE $p\bar{p}$ AND pp SYSTEMS

We notice from Fig. 6.2 that for all s, the ratios Σ_{el}/σ_{tot} are suprisingly close to being the same for both the $p\bar{p}$ and the pp system, in spite of the fact that at the lower energies, the total cross sections, ρ values and nuclear slopes B are very different. An even more suprising regularity is seen when we examine the quantity A, defined as

$$A = \frac{\sigma_{tot}\sqrt{(1+\rho^2)}}{16\pi B} = \frac{\Sigma_{el}}{\sigma_{tot}\sqrt{(1+\rho^2)}}, \tag{7.1}$$

which is proportional to the magnitude of the impact parameter amplitude at zero impact parameter. The ratio

$$R = \frac{A(p\bar{p})}{A(pp)}, \tag{7.2}$$

is plotted vs. s in Fig. 6.3. This ratio is compatible with 1, within the errors of our fitting procedure. For example, the error in R at $\sqrt{s} =$ 3 GeV is ± 0.040, at $\sqrt{s} =$ GeV is ± 0.025, at $\sqrt{s} = 10$ GeV is ± 0.010, at $\sqrt{s} = 52.8$ GeV is ± 0.001 and essentially goes to zero for $\sqrt{s} < 62.5$ GeV. The above errors take into account the correlation errors of fit #2 for the forward scattering amplitudes, as well as the slope fit. It is of course not surprising that $R = 1$ for the high energy data, where $\Delta\sigma_{tot}$, $\Delta\rho$ and $\Delta B \to 0$ as $s \to \infty$. What is important is that at the lowest energies, ($3 < \sqrt{s} < 15$ GeV), where the total cross sections and nuclear slopes are very different (up to $\sim 35\%$), the ratio R is compatible with 1, within

fitting errors of $< 2.5\%$. This result implies that at all s, the magnitude of the impact parameter amplitude is the same for $p\bar{p}$ and pp elastic collisions at *zero* impact parameter. At large impact parameters and low energies they diverge, since the slope parameters B (which determine the shape of the impact parameter representation) are very different. It remains a fundamental problem for any model of elastic $p\bar{p}$ and pp scattering at high energies to explain this newly-observed regularity.

VIII. CONCLUSIONS

Elastic pp and $p\bar{p}$ scattering are of renewed interest since the acquisition of high quality $p\bar{p}$ data from the ISR. Those data demonstrated that the total cross section for $p\bar{p}$ scattering exhibits the same rising trend first observed for pp scattering at the ISR. Measurements at very small t have determined the ratio of the real to the imaginary part of the scattering amplitude in the same energy regime.

Just as the ISR program was concluding, a new and dramatic chapter in elastic scattering was beginning with the SPS collider. The enormous jump in energy was a great challenge to our ability to extrapolate from the ISR and lower energy data. Indeed the extrapolation indicated that the SPS total cross sections should be more than 50% higher than the minimum pp cross section of $\simeq$ 39 mb. Predictions for the slope parameter were not as easy to make since the low energy data were inconsistent.

The extrapolations of the cross section were not just curve fitting because analyticity connects the cross section with the real part of the forward amplitude. Indeed the simultaneous fitting of the σ_{tot} and ρ data with analytic functions is impressive evidence for analyticity.

Not only are the analytic fits quite successful, but their form is very provocative. The data *cannot* be fitted successfully with a $\log(s/s_0)$ rise, but are *well fitted* by a $\log^2(s/s_0)$ rise. Thus, the total cross section seems to saturate the form of the Froissart-Martin bound - $\sigma_{tot} \sim \log^2 s/s_0$ - although with a coefficient about 1% as large as that allowed in principle. If we surmise that asymptotically the elastic scattering will

be described by a black disk, we find that its radius is only about 1/7 as large as allowed by the Froissart-Martin bound. Why? If quantum chromodynamics is indeed the correct theory of hadronic interactions, it should be able to explain this fundamental result. High energy nucleon-nucleon scattering poses a long-term challenge to the theoretical community.

Does the $\log^2(s/s_0)$ growth of the total cross section persist indefinitely? Only further experimentation can tell. It is possible, however, to quantify the issue. By introducing the parameter a we have allowed for deviations from the $\log^2 s$ form. Roughly, the increasing part of the total cross section varies as

$$\frac{\log^2 s/s_0}{1 + a \log^2 s/s_0}. \tag{8.1}$$

Here a is a small positive quantity. The smaller it is, the closer the form is to the Froissart behavior. The value of a can be translated into an energy scale at which there is departure from the $\log^2 s$ form by considering the curvature of the cross section as a function of $\log s$. The curvature is positive near the minimum of the cross section, but is eventually negative as the cross section approaches its constant asymptotic value. We define s_{tr} as the value of s at the transition where the curvature is zero. It is easy to see that

$$\sqrt{s_{tr}} = \sqrt{s_0} e^{1/\sqrt{12a}} \tag{8.2}$$

The values obtained in Fit #3 give

$$\sqrt{s_{tr}} = 865 \, {}^{+4400}_{-450} \text{GeV}, \tag{8.3}$$

While from Fit #4 we find

$$\sqrt{s_{tr}} = 400 \, {}^{+500}_{-150} \text{GeV}. \tag{8.4}$$

The introduction of $\sqrt{s_{tr}}$ is analogous to the introduction of a scale parameter in QED to measure the departure from an idealized theory of point particles. The analogy here is that the idealized theory is $\sigma(s \to \infty) \sim \log^2(s/s_0)$, and $\sqrt{s_{tr}}$ gives a measure of the lowest energy needed to observe a meaningful departure from it. The numbers in Eqs. (8.4) and (8.5) indicate it may be possible at the SPS and Tevatron Colliders to see deviations from the $\log^2 s/s_0$ behavior.

The ISR data showed that the pp and $p\bar{p}$ total cross sections continue to approach each other as the energy increases, in conformity with the usual description which has the difference of the cross sections varying as $s^{-1/2}$. There is no fundamental reason for this, especially if the total cross sections increase as a power of $\log s$. To make a precise conclusion about the difference cross section, we have considered a class of odd amplitudes, odderons, which only contribute significantly at high energies. When we add odderon terms to our fits, we find that these amplitudes are typically about a 2.5 standard deviation effect from zero, and are $\simeq 1\%$ as strong as the dominant even amplitude. The behavior of odderon 2 from our Fit #9 is most intriguing. It predicts a substantial difference between ρ(pp) and $\rho(p\bar{p})$ at $\sqrt{s} > 1$TeV, with $\rho(p\bar{p}) \simeq 0.22$ and $\rho(pp) \simeq 0.10$, an easily measured effect if one had both pp and $p\bar{p}$

collisions available at these energies. At $\sqrt{s} = 40$ TeV, this fit gives $\sigma(pp) - \sigma(p\bar{p}) \simeq 5$mb. Strikingly, the pp cross section climbs above the $p\bar{p}$ cross section at $\sqrt{s} \simeq 100$GeV and remains above it. The presence of odderon terms cannot be completely ruled out at present energies and only ultra-high energy comparisons between pp and $p\bar{p}$ collisions will be able to shed any light on this interesting and mysterious possibility.

In this regard, one should note that the asymptotic theorems, such as that due to Fischer, should be applied with caution. It is always tempting to imagine that the behavior at the highest energy for which there are measurements represents the asymptotic pattern. However, we have seen that fits can be made to the present data in which at slightly higher energies the pp total cross section exceeds that of $p\bar{p}$ and in which the difference cross section does not go to zero but instead increases at higher energies. Such is the case in our Fits #7-10. These fits show that at energies as low as $\sqrt{s} = 100$GeV, surprising results might appear. To find such effects, we need direct pp *vs.* $p\bar{p}$ comparisons at the same energies.

The nuclear slope, B, is of interest in its own right. Our predictions here are less firm because of the poorer quality of the data, but we are guided by the reliable fits for the forward amplitudes and by the principle that B must grow as fast as $\log^2 s$ if the total cross section does. Failure to include such behavior must eventually be incompatible with measurement, if indeed the cross section continues to increase as $\log^2 s$. The slope measurement can be combined with the total cross section to give Σ_{el}. In all reasonable models, $\sigma_{el} \simeq \Sigma_{el}$. The energy behavior of the ratio Σ_{el}/σ_{tot} is of special interest. In many models, asymptotically the proton becomes a black disk and the ratio tends to one-half. Our fits indicate that a substantial increase from the value $\simeq 0.18$ characteristic

of the ISR energy range is to be anticipated. This is confirmed by early SPS numbers.

An examination of our 6-parameter fit to the experimental data shows that

$$R = \left[\frac{\sigma_{tot}\sqrt{1+\rho^2}}{16\pi B}\right]_{p\bar{p}} \Bigg/ \left[\frac{\sigma_{tot}\sqrt{1+\rho^2}}{16\pi B}\right]_{pp}$$

is nearly unity within the errors of the fit, for the entire energy region $3 < \sqrt{s} < 62$ GeV. This of course is not surprising in the high energy region. What is important is that at the lowest energies ($3 < \sqrt{s} < 5$ GeV), where the total cross sections and nuclear slopes are *very* different for $p\bar{p}$ and pp, the ratio R is compatible with 1, within fitting errors of less than 2.5%. This suggests that for all energies considered, $a(0)$, the impact parameter amplitude at zero separation, is the *same* for $p\bar{p}$ and pp. This new regularity remains as an important problem to be explained by models of nucleon-nucleon scattering.

The data from the SPS collider have confirmed the extrapolations from the lower energy data. The total cross section is increasing rapidly as is the slope parameter. Still much remains to be determined. More precise measurements at the SPS collider will be invaluable. Even more exciting are the prospects for measurements of the cross section and ρ at the Tevatron collider. These measurements should help enormously in deciding whether we have begun a continuing $\log^2 s$ climb which would make the total cross section at the Superconducting Super Collider (at 40 TeV) about 200 mb, or whether we are just being misled by a local tendency which will flatten out and give a cross section at the SSC which

is substantially smaller.

For a wide class of models that have total cross sections increasing with s, the nucleon-nucleon profile in impact parameter space eventually becomes that of a sharp disk. We regard the energy domain in which this happens as "asymptopia". In "asymptopia", the value of the curvature parameter, C, must be negative, since it is that of a disk. Experiment show C to be positive at the ISR and SPS Collider energies. Using our predicted σ_{tot} and ρ to fix the Chou-Yang mode, we show that the Chou-Yang and sharp disk models give elastic scattering distributions which are nearly indistinguishable at $\sqrt{s} = 40$ TeV, the SSC energy; in particular, the value of C for the Chou-Yang model has become quite negative. We have defined the onset of "asymptopia" as the energy at which $C = 0$, and have shown that this will occur near the Tevatron Collider energy, $\sqrt{s} = 2$ TeV. These forthcoming machines should finally give us our first experimental glimpse of "asymptopia".

Acknowledgments

MMB would like to thank the Aspen Center for Physics for its hospitality during the writing of this manuscript. We would like to thank Norman Amos and Shakar Shukla of Northwestern University for their assistance in preparing this report.

References

Abramowitz, M. and I. A. Stegun, eds., 1964, *Handbook of Mathematical Functions* , National Bureau of Standards.

Amaldi, U., *et al.*1971, *Phys. Lett.* **36B**, 504.

Amaldi, U., *et al.*1973a, *Phys. Lett.* **43B**, 231.

Amaldi, U., *et al.*1973b, *Phys. Lett.* **44B**, 112.

Amaldi, U., M. Jacob, and G. Matthiae, 1976, *Ann. Rev. Nuc. Sci.* **26**, 385.

Amaldi, U. *et al.*, 1976, *Phys. Lett.* **62B**, 460.

Amaldi, U. *et al.*, 1978, *Nucl. Phys.* **B145**, 367.

Amaldi, U. *et al.*, 1977, *Phys. Lett.* **66B**, 390.

Amaldi, U., and K. R. Schubert, 1980, *Nucl. Phys.* **B166**, 301.

Amendolia, S. R., *et al.*, 1973a, *Phys. Lett.* **44B**, 119.

Amendolia, S. R., *et al.*, 1973b, *Nuov. Cim.* **174**, 735.

Amos, N., *et al.*, 1983a, *Phys. Lett.* **120B**, 460.

Amos, N., *et al.*, 1983b, *Phys. Lett.* **128B**, 343.

Antipov, Yu. M.,*et al.*, 1973, *Nucl. Phys.* **B57**, 333.

Auberson, F., T. Kinoshita, and A. Martin, 1971 , *Phys. Rev.* **D3**, 3185.

Ayres, D. S. *et al.*, 1977, *Phys. Rev.* **D15**, 3105.

Baksay, L. *et al.*, 1978, *Nucl. Phys.* **B141**, 1.

Ball, J. S. and F. Zachariasen, 1972, *Phys. Lett.* **40B**, 411.

Barbiellini, G., *et al.*, 1972, *Phys. Lett.* **39B**, 663.

Bartenev, V., *et al.*, 1972a, *Phys. Rev. Lett.* **29**, 1755.

Bartenev, V., *et al.*, 1973a, *Phys. Rev. Lett.* **31**, 1088.

Bartenev, V., *et al.*, 1973b, *Phys. Rev. Lett.* **31**, 1367.

Bethe, H. A., 1958 , *Ann. Phys.* **3**, 190.

Belletini, G., *et al.*, 1965, *Phys. Lett.* **14**, 164.

Bjorken, J. D., 1979, in *Proceedings of Summer Institute on Particle Physics, Quantum Chromodynamics.*

Block, M. M., and R. N. Cahn, 1982a, *Phys. Lett.* **120B**, 224.

Block, M. M., and R. N. Cahn, 1982b, *Phys. Lett.* **120B**, 229.

Block, M. M. and R. N. Cahn, 1983a, in *Proceedings of the 18th Rencontre de Moriond on Elementary Particle Physics, vol.III,* Editions Frontières

Block, M. M., 1983b, private communication.

Block, M. M., and R. N. Cahn, 1984, to be published.

Bourrely, C. and J. Fischer, 1973, *Nucl. Phys.* **B61**, 513.

Bourrely, J. Soffer, and T. T. Wu, 1983, *Phys. Lett.* **121B**, 284.

Bronzan, J., 1973 *in Argonne Symposium on the Pomeron, Argonne National Laboratory, ANL/HEP 7327,* p.33

Bronzan, J., G. L. Kane, and U. P. Sukhatme, 1974, *Phys. Lett.* **49B**, 272.

Burq *et al.*, 1982, *Phys. Lett.* **39B??**, 124.

Cahn, R. N.,1982a, in *Proceedings of the 17th Rencontre de Moriond on Elementary Particle Physics, vol.II* Editions Frontières

Cahn, R. N., 1982b, *Zeit. Phys.* **C15**, 253.

Cahn, R. N., 1982c, in *Proceedings of the 10th SLAC Summer Institute on Particle Physics,* Stanford

Carboni, G., *et al.*, 1982a, *Phys. Lett.* **108B**, 145.

Carboni, G., *et al.*, 1982b, *Phys. Lett.* **113B**, 87.

Carroll, A. S., *et al.*, 1974, *Phys. Rev. Lett.* **33**, 928.

Cheng, H., J. K. Walker, and T. T. Wu, 1973, *Phys. Lett.* **44B**, 97.

Chernev, Kh. M. *et al.*, 1971, *Phys. Lett.* **36B**, 266.

Chou, T. T. and C. N. Yang, 1968, *Phys. Rev.* **170**, 1591.

Chou, T. T. and C. N. Yang, 1983, *Phys. Lett.* **128B**, 457.

Cornille, H. and A. Martin, 1972a, *Phys. Lett.* **40B**, 671.

Cornille, H. and A. Martin, 1972b, *Nucl. Phys.* **B48**, 104.

Cornille, H. and A. Martin, 1972c, *Nucl. Phys.* **B49**, 413.

Cornille, H. and A. Martin, 1974, *Nucl. Phys.* **B77**, 141.

Del Prete, T., 1983, in *Proceedings of the 18th Rencontre de Moriond on Elementary Particle Physics, vol.III* Editions Frontières

Denisov, S. P., *et al.*, 1971a, *Phys. Lett.* **36B**, 415.

Denisov, S. P., *et al.*, 1971b, *Phys. Lett.* **36B**, 528.

Durand., L. and R. Lipes, 1968, *Phys. Rev. Lett.* **20**, 637.

Eden, R. J., 1966, *Phys. Rev. Lett.* **16**, 39.

Eden, R. J., 1967, *High Energy Collisions of Elementary Particles*, Cambridge Univ. Press, 1967.

Erdély, A., 1953, *Higher Transcendental Functions, v. II*, McGraw-Hill, p.58.

Fajardo, L. A., *et al.*, 1981, *Phys. Rev.* **D24**, 46.

Favart, D., *et al.*, 1981, *Phys. Rev. Lett.* **47**, 1191.

Fischer, J., 1981, *Physics Reports* **76**, 157.

Fischer, J. *et al.*, 1978, *Phys. Rev.* **D18**, 4271.

Foley, K. J. *et al.*, 1967, *Phys. Rev. Lett.* **19**, 857.

Froissart, M., 1961, *Phys. Rev.* **123**, 1053.

Gauron, P. and B. Nicolescu, 1984, , to be published..

Giacomelli, G. and M. Jacob, 1979, *Physics Reports* **55**, 1.

Gilbert, W., 1957, *Phys. Rev.* **108**, 1078.

Gradshteyn, I. S. and I. M. Ryzhik, 1965 *Table of Integrals , Series, and Products,* Academic Press, New York

Holder, M., *et al.*, 1971, *Phys. Lett.* **36B**, 400.

Horn, D. and F. Zachariasen, 1973 *Hadron Physics at Very High Energies* Benjamin/Cummings, Reading, Mass.

Jackson, J. D., 1960, in *Dispersion Relations, Scottish Universities' Summer School, 1960,* Ed. G. R. Screaton, Interscience Pub., Edinburgh

Jackson, J. D.,1973, in the *Proceedings of the Fourteenth Scottish Universities*

Summer School in Physics, 1973, R. L. Crawford and R. Jennings, eds., Academic Press, London, 1974.

Joynson, D., *et al.*1975, *Nuovo Cimento* **30A**, 345.

Kang, K., and B. Nicolescu, 1975, *Phys. Rev.* **D11**, 2461.

Lukaszuk, L. and B. Nicolescu, 1973, *Nuovo Cim. Lett.* **8**, 405.

Kinoshita, T.,1966, in *Perspectives in Modern Physics,* R. E. Marshak Ed., Wiley and Sons, New York, 1966, p.211

MacDowell, S. W. and A. Martin, 1964, *Phys. Rev.* **135B**, 960.

Martin, A.,1966, *Nuovo Cimento* **42**, 930.

Martin, A. and F. Cheung, 1970, *Analytic Properties and Bounds of the Scattering Amplitudes* , Gordon and Breach.

Martin, A., 1973, *Let. al Nuovo Cim.* **7**, 811.

Martin, A.,1982a, *Zeit. Phys.* **C15**, 185.

Pomeranchuk,I. Ya., 1958, *Soviet Physics JETP* **7**, 499.

Söding, P., 1964, *Phys. Lett.* **8**, 285.

Titchmarsh, E. C., 1939, *The Theory of Functions* , Oxford University Press.

UA1 Collaboration, 1983, *Phys. Lett.* **128B**, 336.

UA4 Collaboration, 1982a, *Phys. Lett.* **115B**, 333.

UA4 Collaboration, 1982b, *Phys. Lett.* **117B**, 126.

Van der Meer, S., 1968 *CERN report ISR-PO/68-31, unpublished.*

West, G. B., and D. Yennie, 1968 , *Phys. Rev* **172**, 1413.

Table 3.1. Values of t_{min} and θ_{min} for the Coulomb interference region for $p\bar{p}$ elastic scattering. See Eq. (3.13) and (3.14).

$\sqrt{s}$ (GeV)	Accelerator	$\|t\|_{min}$ $(GeV/c)^2$	θ_{min} (mrad)
23.5	ISR	0.0017	3.6
30.7	ISR	0.0017	2.7
52.8	ISR	0.0016	1.5
62.5	ISR	0.0016	1.3
540	SPS	0.0010	0.12
2000	Tevatron	0.00073	0.027
40000	SSC	0.00037	0.00097

Table 5.1 Sources for the data used in the fits for σ and ρ for pp and $p\bar{p}$.

Reference	Data	Accelerator
Foley et al., 1967	$\sigma(pp), \rho(pp)$	AGS
Denisov et al., 1971a,b	$\sigma(p\bar{p}), \sigma(pp)$	Serpukhov
Bartenev et al., 1973b	$\rho(pp)$	FNAL
Carroll et al., 1974	$\sigma(pp), \sigma(p\bar{p})$	FNAL
Fajardo et al., 1981	$\rho(p\bar{p})$	FNAL
Amaldi and Schubert, 1980	$\sigma(pp), \rho(pp)$	ISR
Amos et al., 1983a,b	$\Delta\sigma, \Delta\rho, \rho_{av}$	ISR

Table 5.2. Results of fits to total cross sections and ρ values. See Eqs. (5.1) - (5.6). The parameters A, β, and ϵ are in mb, s_0 is in GeV^2, α, μ and a are dimensionless, C is in mb $GeV^{2(1-\mu)}$ and D is in mb $GeV^{2(1-\alpha)}$.

Fit	#1	#2	#3	#4
A	41.74 $\pm$0.04	41.30 $\pm$0.28	41.70 $\pm$0.04	41.11 $\pm$0.23
β	0.66 $\pm$0.01	0.62 $\pm$0.03	0.64 $\pm$0.02	0.59 $\pm$0.02
s_0	338.5 $\pm$7.7	293.6 $\pm$28	332.7 $\pm$7.9	275.1 $\pm$22
C		8.4 $\pm$5.1		10.9 $\pm$4.1
μ		0.5		0.5
D	-39.37 $\pm$1.6	-40.51 $\pm$1.8	-39.20 $\pm$1.5	-41.32 $\pm$1.9
α	0.48 $\pm$0.01	0.47 $\pm$0.01	0.48 $\pm$0.01	0.46 $\pm$0.01
a			0.0056 $\pm$0.003	0.0082 $\pm$0.003
$\chi^2/d.f$	1.165	1.146	1.127	1.058
$d.f$	76	75	75	74

Table 5.3. Results of fits to total cross sections and ρ values including odderons.. See Eqs. (5.1) - (5.6). The parameters A, β, and ϵ are in mb, s_0 is in GeV^2, α, μ and a are dimensionless, C is in mb $GeV^{2(1-\mu)}$ and D is in mb $GeV^{2(1-\alpha)}$. Fits #5 and #6 correspond to odderon 0, fits #7 and #8 to odderon 1 and fits #9 and #10 to odderon 2.

Fit	#5	#6	#7	#8	#9	#10
A	41.73	41.51	41.70	41.61	41.66	41.36
	$\pm$0.04	$\pm$0.30	$\pm$0.04	$\pm$0.29	$\pm$0.05	$\pm$0.26
β	0.68	0.65	0.67	0.66	0.65	0.62
	$\pm$0.02	$\pm$0.03	$\pm$0.01	$\pm$0.04	$\pm$0.01	$\pm$0.03
s_0	340.4	317.4	345.8	336.0	350.3	316.1
	$\pm$0.5	$\pm$31	$\pm$8.1	$\pm$33	$\pm$9.6	$\pm$30
C		4.3		1.7		6.0
		$\pm$5.6		$\pm$5.7		5.0
μ		0.5		0.5		0.5
D	$-$42.07	$-$42.31	$-$41.35	$-$41.47	$-$35.34	$-$36.70
	$\pm$2.2	$\pm$2.2	$\pm$1.7	$\pm$1.8	$\pm$2.1	$\pm$2.4
α	0.46	0.45	0.48	0.48	0.50	0.49
	$\pm$0.02	$\pm$0.02	$\pm$0.01	$\pm$0.01	$\pm$0.02	$\pm$0.02
ϵ	$-$0.29	$-$0.25	$-$0.12	$-$0.11	$-$0.04	$-$0.04
	$\pm$0.12	$\pm$0.13	$\pm$0.04	$\pm$0.04	$\pm$0.02	$\pm$0.02
$\chi^2/d.f$	1.105	1.112	1.059	1.072	1.089	1.084
$d.f.$	75	74	75	74	75	74

Table 6.1 Sources for the data used in the fits for the slope parameter.

Reference	Data Used	Accelerator
Foley et al., 1963	B(pp)	AGS
Belletini et al., 1965	B(pp)	CERN-PS
Amaldi et al., 1971	B(pp)	ISR
Chernev et al., 1971	B(pp)	Serpukhov
Holder et al., 1971	B(pp)	ISR
Barbiellini et al., 1972	B(pp)	ISR
Bartenev et al., 1972a,b	B(pp)	FNAL
Antipov et al., 1973	B($p\bar{p}$)	Serpukhov
Ayres et al., 1977	B(pp)	FNAL
Baksay et al., 1978	B(pp)	ISR
Fajardo et al., 1981	Δ B	FNAL
Northwestern-Louvain Coll., 1982	B(pp), B($p\bar{p}$)	ISR

Table 6.2 The error squared matrix for slope Fit #2.

	C^+	D^+	E^+	C^-	D^-
C^+	$1.9 \cdot 10^{-1}$	$-6.7 \cdot 10^{-2}$	$5.5 \cdot 10^{-3}$	$-1.1 \cdot 10^{-1}$	$4.8 \cdot 10^{-2}$
D^+		$2.3 \cdot 10^{-2}$	$-1.9 \cdot 10^{-3}$	$5.7 \cdot 10^{-2}$	$-1.8 \cdot 10^{-2}$
E^+			$1.7 \cdot 10^{-4}$	$-5.5 \cdot 10^{-3}$	$1.5 \cdot 10^{-3}$
C^-				$1.9 \cdot 10^{-0}$	$-1.3 \cdot 10^{-1}$
D^-					$1.7 \cdot 10^{-2}$

Table 7.1. Predictions for σ_{tot}, ρ, and B at high energies. The predictions are the same for pp and $p\bar{p}$ since, no odderons are included. Both fit #1 and #2 have cross sections growing as $\log^2 s$.

Fit	$\sqrt{s}$ (TeV)	σ (mb)	ρ	B $(GeV/c)^{-2}$	Σ_{el}/σ
#1	.540 (SPS)	70.37±0.62	0.200±0.002	16.65±0.74	0.227
#2	.540 (SPS)	69.32±0.89	0.194±0.005	16.66±0.59	0.223
#1	2.00(Tevatron)	98.30±1.17	0.198±0.002	19.53±1.41	0.270
#2	2.00(Tevatron)	95.93±1.87	0.193±0.004	19.57±1.12	0.263
#1	20.0	169.46±2.57	0.172±0.001	26.03±3.15	0.347
#2	20.0	163.39±4.55	0.168±0.002	26.13±2.50	0.332
#1	40.0 (SSC)	196.38±3.10	0.163±0.001	28.34±3.81	0.368
#2	40.0 (SSC)	188.84±5.60	0.160±0.002	28.47±3.03	0.352
#1	100.0	235.87±3.88	0.152±0.001	31.64±4.78	0.394
#2	100.0	226.15±7.15	0.149±0.002	31.81±3.79	0.376
#1	500.0	316.00±5.46	0.134±0.000	38.14±6.75	0.436
#2	500.0	301.75±10.4	0.133±0.001	38.39±5.35	0.413

FIGURE CAPTIONS

Chapter III

Fig. 3.1 An experimental plot of $d\sigma_{tot}/dt$ vs. $|t|$ for pp elastic scattering at $\sqrt{s} = 23.5$ GeV. The fitted curve used the parametrization of Eq. (3.10). The data were taken at the ISR by the Northwestern-Louvain (R211) group.

Fig. 3.2 An experimental plot of $d\sigma_{tot}/dt$ vs. $|t|$ for $p\bar{p}$ elastic scattering at $\sqrt{s} = 52.8$ GeV. The fitted curve used the parametrization of Eq. (3.10). The data were taken at the ISR by the Northwestern-Louvain (R211) group.

Fig. 3.3 Survey of experimental data for total cross sections σ_{tot}, in mb, for both $p\bar{p}$ and pp interactions in the energy interval $5 < \sqrt{s} < 62$ GeV. The $p\bar{p}$ points are indicated with an "x" and the pp points with an "o".

Fig. 3.4 Survey of experimental data for $\rho = Ref_n(0)/Imf_n(0)$ for both $p\bar{p}$ and pp interactions in the energy interval $5 < \sqrt{s} < 62$ GeV. The $p\bar{p}$ points are indicated with an "x" and the pp points with an "o".

Fig. 3.5 Survey of experimental data for B, the nuclear slope parameter, in $(\text{GeV}/c)^{-2}$, for both $p\bar{p}$ and pp elastic scattering, in the t region $|t| < 0.02(\text{GeV}/c)^2$ and in the energy interval $5 < \sqrt{s} < 62$ GeV. The $p\bar{p}$ points are indicated with an "x" and the pp points with an "o".

Chapter IV

Fig. 4.1 The Argand circle. The partial wave amplitude, a_l, or the impact parameter amplitude, $a(b)$, must lie on or insider the circle of radius 1/2. If $Re\delta = \delta_R$ and $Im\delta = \delta_I$, the central angle is $2\delta_R$ and the length from the center of the circle to the amplitude point is $(1/2)\exp(-2\delta_I)$.

Fig. 4.2 A semi-log plot of various profiles, $Ima(b)$, each of which gives $\sigma_{tot} = 43$ mb and $B = 13$ $(\text{GeV}/c)^2$. The gray disc is shown as dot-dash. The parabolic form, Eq. (4.39), is shown as the dotted curve. The Gaussian shape gives the solid curve. The dashed line is the Chou-Yang model.

Fig. 4.3 A semi-log plot of the differential elastic cross cross sections for the shapes shown in Fig. 4.2. The dot-dash curve is for the gray disc, the dotted for the parabolic shape, the solid for the Gaussian and the dashed for the Chou-Yang model.

Fig. 4.4 The functions $X = \sigma_{el}/\sigma_{tot}$ (solid curve) and $Y = \Sigma_{el}/\sigma_{tot}$ (dashed curve) in the Chou-Yang model, as a function of σ_{tot}.

Fig. 4.5 The quadratic slope parameter, C, in the Chou-Yang model, as a function of σ_{tot}.

Fig. 4.6 A plot of the impact parameter amplitude $a(b)$ vs. b, in fermis, for the Chou-Yang model (solid curve) and the sharp disk (dashed curve), for energy $\sqrt{s} = 540$ GeV in (a), $\sqrt{s} = 2$ TeV in (b) and $\sqrt{s} = 40$ TeV in (c).

Fig. 4.7 A plot of $d\sigma_n/dt$, the elastic differential scattering cross section, for both the Chou-Yang model and the sharp disk,

using the impact parameter amplitudes show in Fig. 4.6.. The dotted curves (for $\rho = 0$) and the dash-dotted curves (for non-zero ρ) are the Chou-Yang predictions, whereas the dashed curves (for $\rho = 0$) and the solid curves (for non-zero ρ) are the predictions for the sharp disk. The energies are (a) $\sqrt{s} = 540$ GeV, (b) $\sqrt{s} = 2$ TeV, (c) $\sqrt{s} = 40$ TeV.

Fig. 4.8 The complex E plane. The physical pp amplitude is obtained as the limit of the analytic function $\mathcal{F}$ approaching the right hand cut from above. The physical $p\bar{p}$ amplitude is obtained by approaching the left hand cut from below. The unphysical cut is not shown. The integral dispersion relations are obtaned by integrating along the indicated contour (if one ignores the unphysical cut and pole). The contours are really closed by infinite semi-circles above and below the real axis.

Fig. 4.9 Definition of the cut structure for $\mathcal{G}_-$ of Eq. (4.64). $\mathcal{G}_-$ is made well-defined by specifying that $\mathcal{G}_- = |m - E|^\alpha e^{i\eta\alpha} - |m + E|^\alpha e^{-i\phi\alpha}$. See Eqs. (4.67) - (4.71). For the pp amplitude, $\eta \to 0, \phi \to \pi$.

Chapter V

Fig. 5.1(a) The total cross sections σ_{tot}, in mb, for $p\bar{p}$ and pp, as a function of $\sqrt{s}$, in GeV. Below $\sqrt{s} = 100$ GeV, the upper curve corresponds to pp and the lower to $p\bar{p}$, using the fit #1 ($C, a = 0$). Above this energy, the difference in cross sections is too small to be visible. The upper curve above this energy corresponds to the Froissart bound form, with

$a = 0$ ($C = 0$, fit #1), while the lower curve is the best fit for $a \neq 0$ ($C = 0$, fit #3). The experimental data used in the fit were in the energy interval $5 < \sqrt{s} < 62$ GeV. The experimental SPS $p\bar{p}$ cross section at $\sqrt{s} = 540$ GeV is appended for comparison, as is the cosmic ray lower limit for the pp cross section. To guide the reader, the energies of the Tevatron collider and the SSC are shown.

Fig. 5.1(b) The ρ values for $p\bar{p}$ and pp. Below $\sqrt{s} = 40$ GeV, the upper curve is for $p\bar{p}$ and the lower for pp, using fit #1 ($a, C, \epsilon = 0$). Above this energy, the curves split, with the lower of each pair corresponding to $a \neq 0$ ($C = 0$, from fit #3) and the upper to $a = 0$ ($C = 0$, from fit #1). At very high energies, the differences between $p\bar{p}$ and pp disappear and the two $a = 0$ curves (fit #1) coalesce, as do the two $a \neq 0$ curves (fit #3).

Fig. 5.2(a) Total cross sections σ_{tot} for $p\bar{p}$ and pp, as a function of $\sqrt{s}$. The legend is the same as for Fig. 5.1(a), except that the even Regge coefficient C ($C \neq 0$) is fitted. The fit used for $a = 0$ is fit #2 and the fit used for $a \neq 0$ is fit #4.

Fig. 5.2(b) The ρ values for $p\bar{p}$ and pp, as a function of $\sqrt{s}$. The legend is the same as for Fig. 5.1(b), except that the even Regge coefficient C is fitted. The fit used for $a = 0$ is fit #2 and the fit used for $a \neq 0$ is fit #4.

Fig. 5.3(a) The total cross sections σ_{tot}, in mb, for $p\bar{p}$ and pp, as a function of $\sqrt{s}$, in GeV. The solid curve is for pp and the dased curve is for $p\bar{p}$. The fit utilizes odderon 2 ($C = 0$,

from fit #9). The data utilized in the fit are in the energy interval $5 < \sqrt{s} < 62$ GeV. The SPS experimental cross section at $\sqrt{s} = 540$ GeV is appended for comparison.

Fig. 5.3(b) The ρ values for $p\bar{p}$ and pp, as a function of $\sqrt{s}$. The legend is the same as that for Fig. 5.3(a).

Fig. 5.4(a) Total cross sections for σ_{tot} for $p\bar{p}$ and pp, as a function of $\sqrt{s}$. The legend is the same as that for Fig. 5.3(a), except that the odderon 0 was used ($C = 0$, from fit #5).

Fig. 5.4(b) The ρ values for $p\bar{p}$ and pp, as a function of $\sqrt{s}$. The legend is the same as that for Fig. 5.3(b), except that odderon 0 was used ($C = 0$, from fit #5).

Fig. 5.5(a) Total cross sections σ_{tot} for $p\bar{p}$ and pp, as a function of $\sqrt{s}$. The legend is the same as that for Fig. 5.3(a), except that odderon 1 was used ($C = 0$, from fit #7).

Fig. 5.5(b) The ρ values for $p\bar{p}$ and pp, as a function of $\sqrt{s}$. The legend is the same as that for Fig. 5.3(b), except that odderon 1 was used ($C = 0$, from fit #7).

Chapter VI

Fig. 6.1 Nuclear slope parameters B for $p\bar{p}$ and pp elastic scattering, evaluated at $|t| = 0.02(\text{ GeV}/c)^2$. The solid curve is for pp and the dashed curve for $p\bar{p}$. The data used in the fit were in the energy interval $5 < \sqrt{s} < 62$ GeV. The four ΔB values of Ref. 3 were used in the fit, but are not shown in the figure. The experimental SPS $p\bar{p}$ slope value at $\sqrt{s} = 540$ GeV is

appended for comparison. To guide the reader, the energies of the Tevatron collider and the SSC are shown.

Fig. 6.2 The ratio of Σ_{el}/σ_{tot}, for $p\bar{p}$ and pp, as a function of $\sqrt{s}$. The solid curve is for pp and the dashed curve for $p\bar{p}$. The curve was computed using fit #2 (a, $\epsilon = 0$, $C \neq 0$).

Fig. 6.3 The ratio $R = A(p\bar{p})/A(pp)$, as a function of $\sqrt{s}$, where $A = \sigma_{tot}\sqrt{(1+\rho^2)}/16\pi B$.

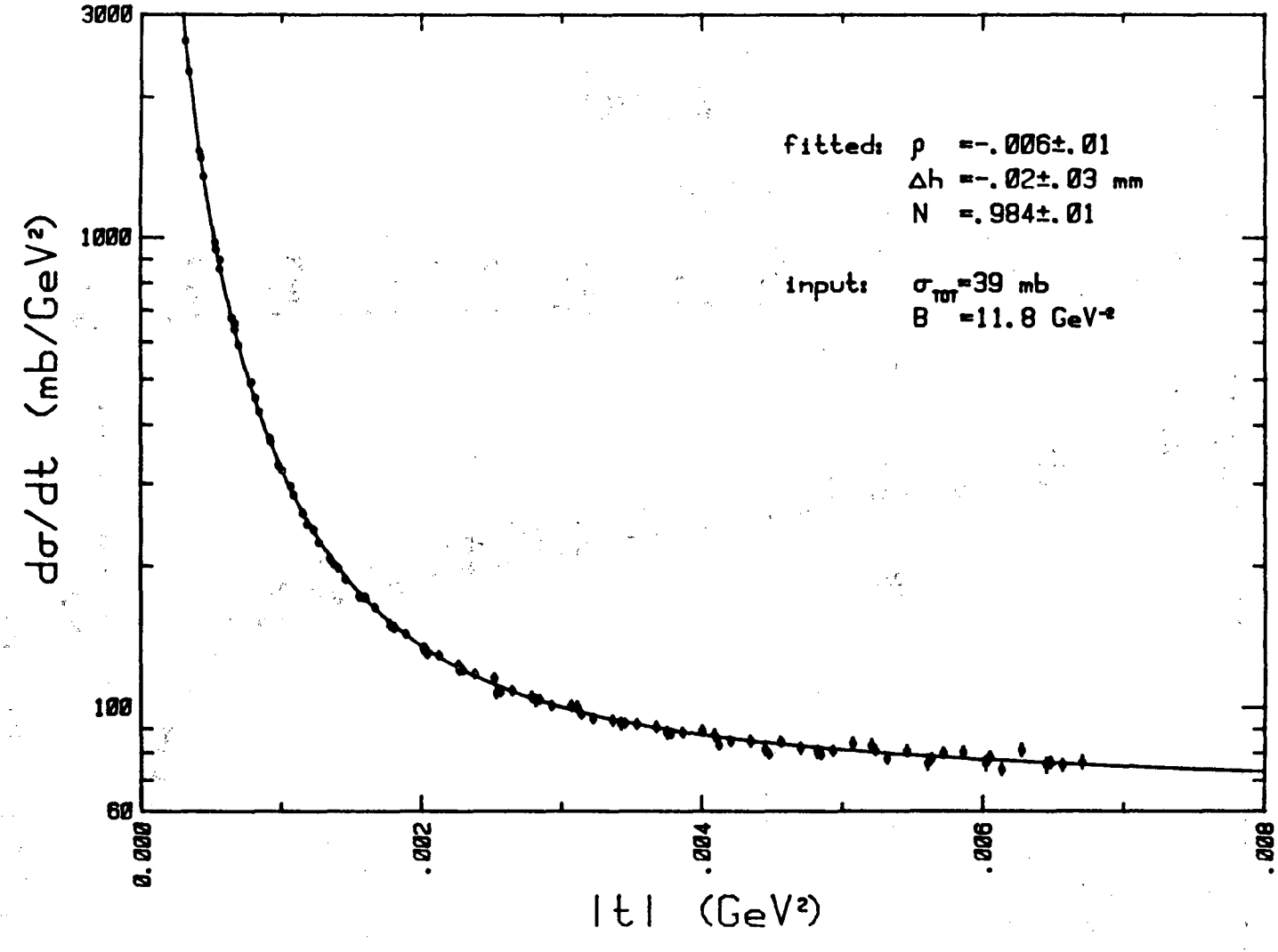
3000
1000
100
60
dσ/dt (mb/GeV²)
fitted: ρ =-.006±.01
Δh =-.02±.03 mm
N =.984±.01
input: σTOT=39 mb
B =11.8 GeV⁻²
0.000
.002
.004
.006
.008
|t| (GeV²)

Fig. 3.1

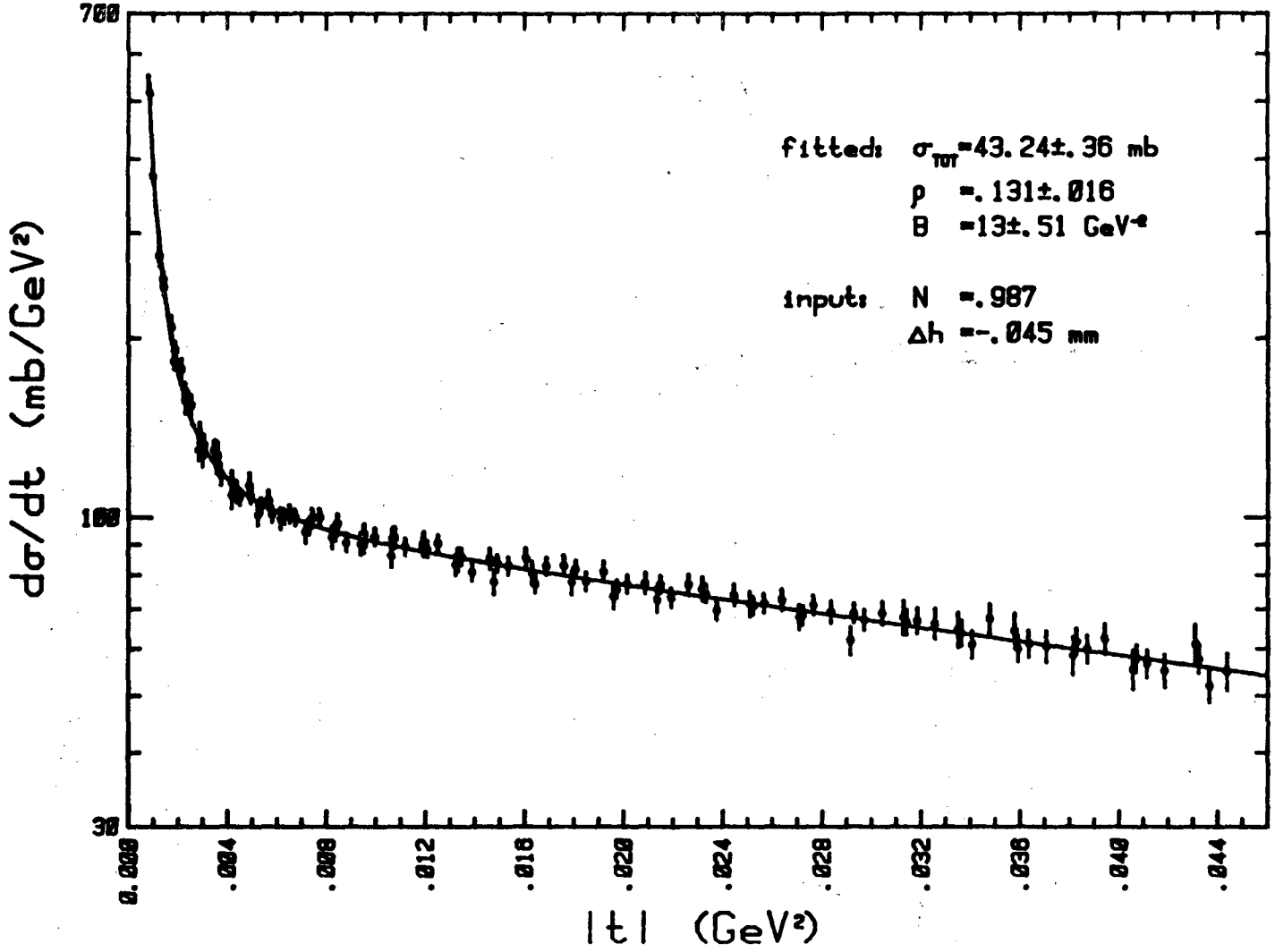
700
100
30
dσ/dt (mb/GeV²)
fitted: σ_TOT=43.24±.36 mb
ρ =.131±.016
B =13±.51 GeV⁻²
input: N =.987
Δh =-.045 mm
0.000
.004
.008
.012
.016
.020
.024
.028
.032
.036
.040
.044
|t| (GeV²)

Fig. 3.2

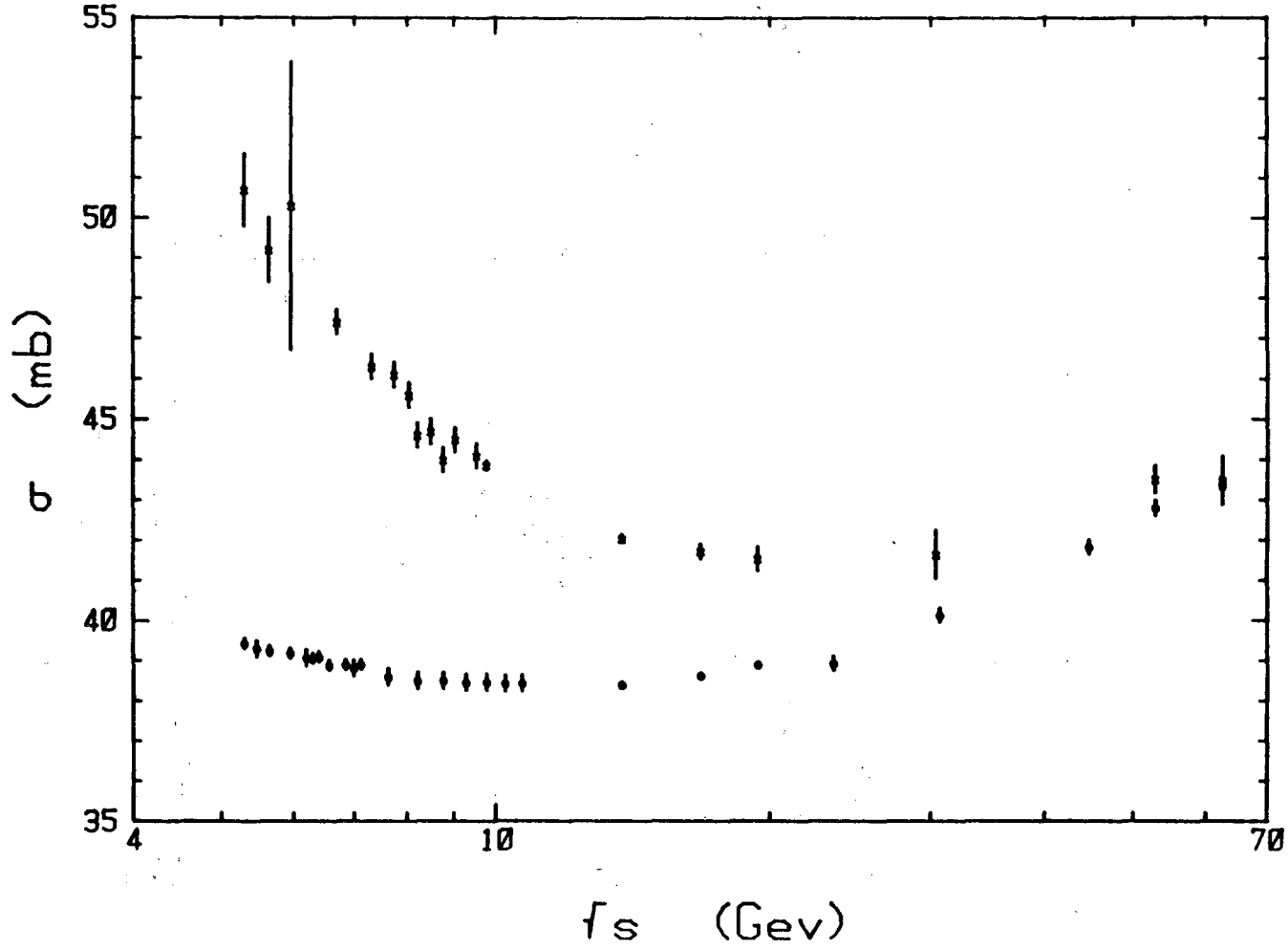

Fig. 3.3

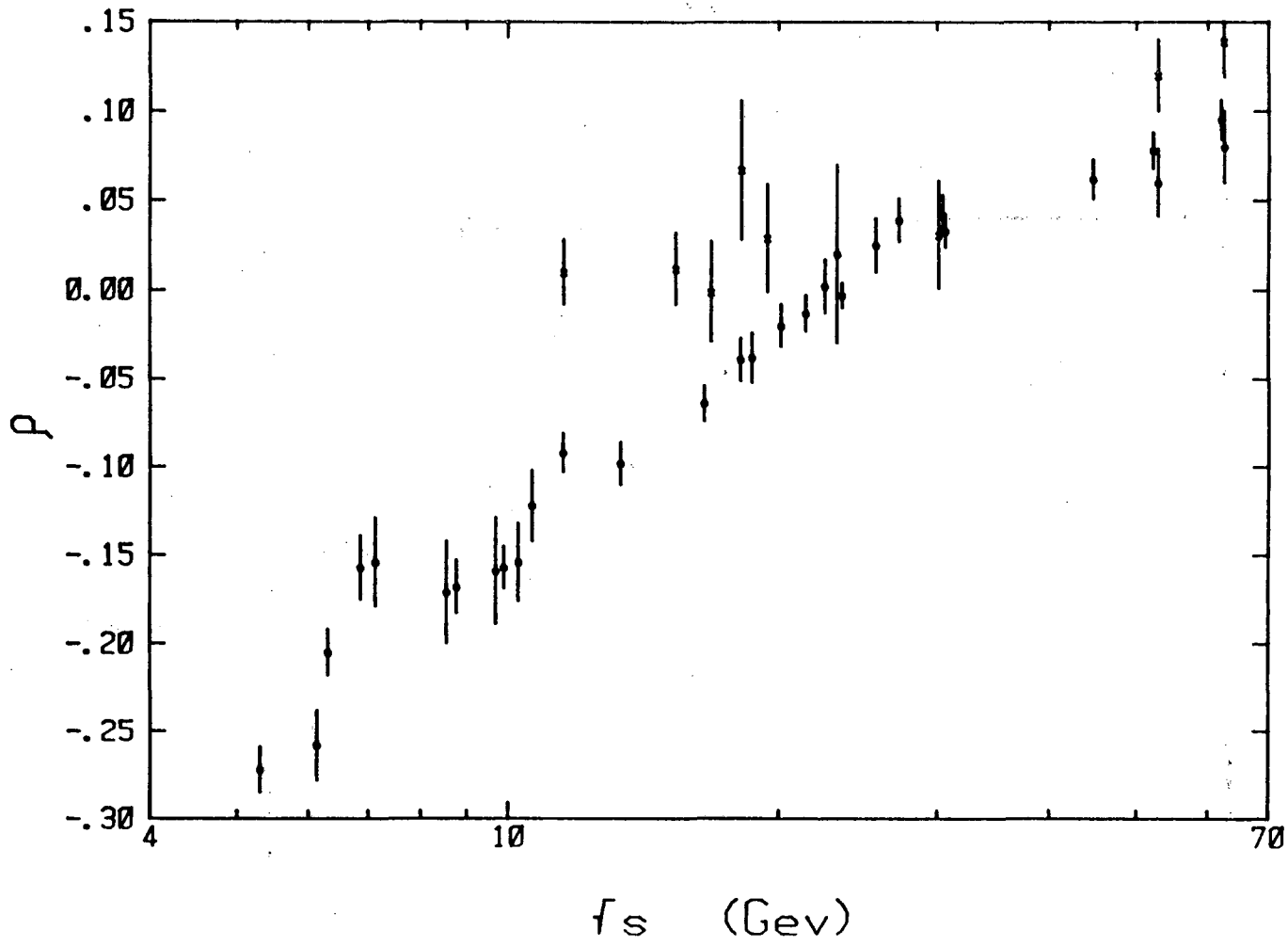

Fig. 3.4

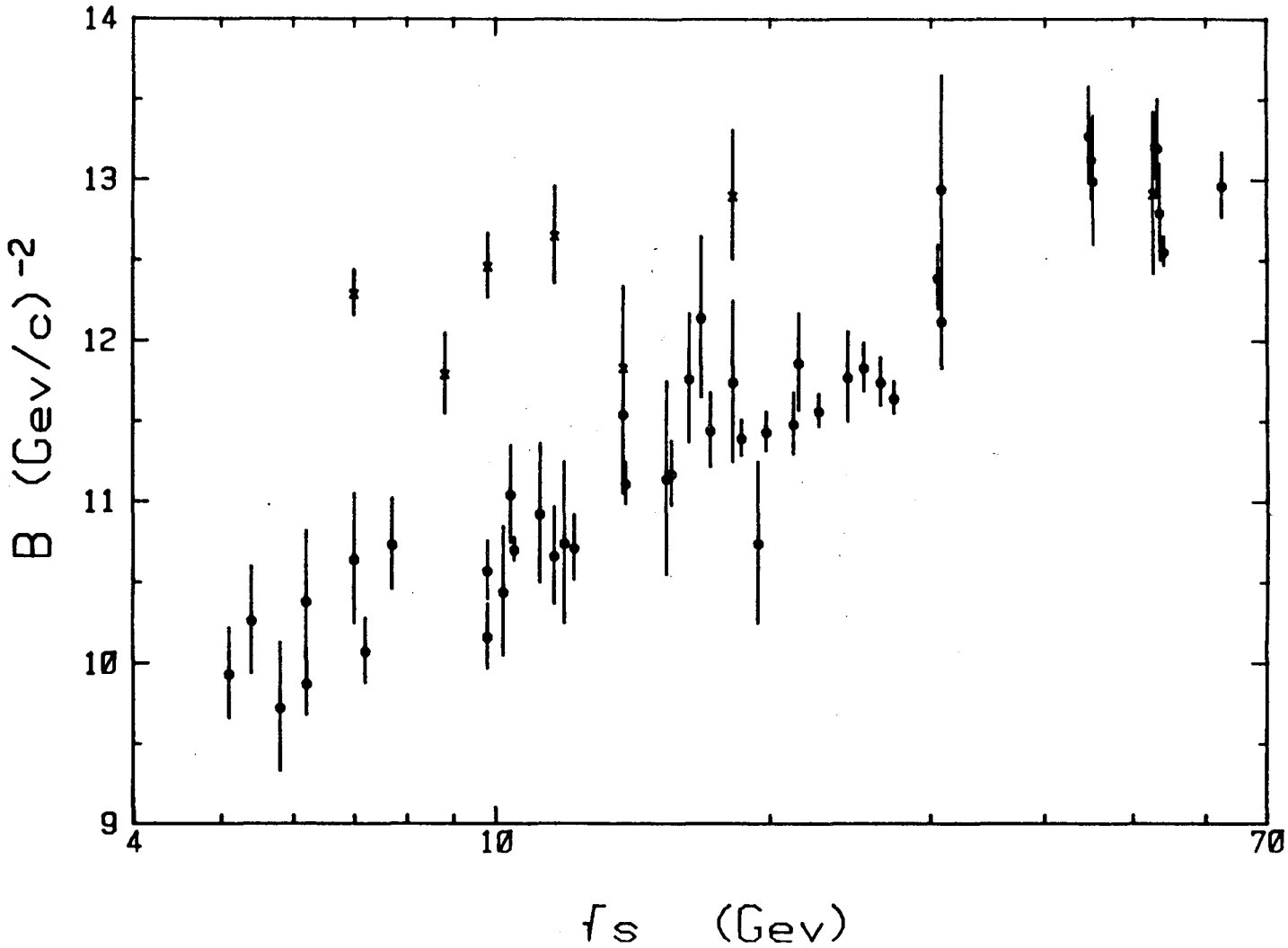

Fig. 3.5

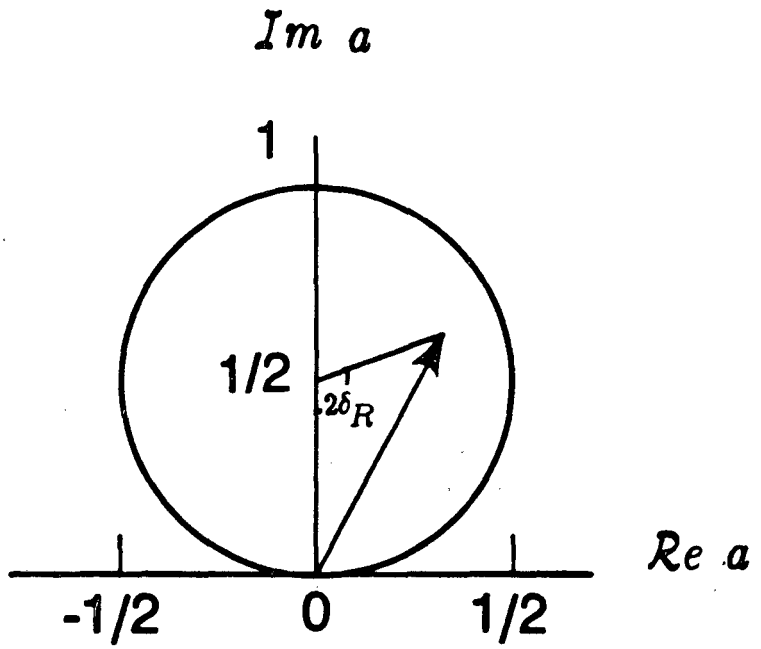

Fig. 4.1

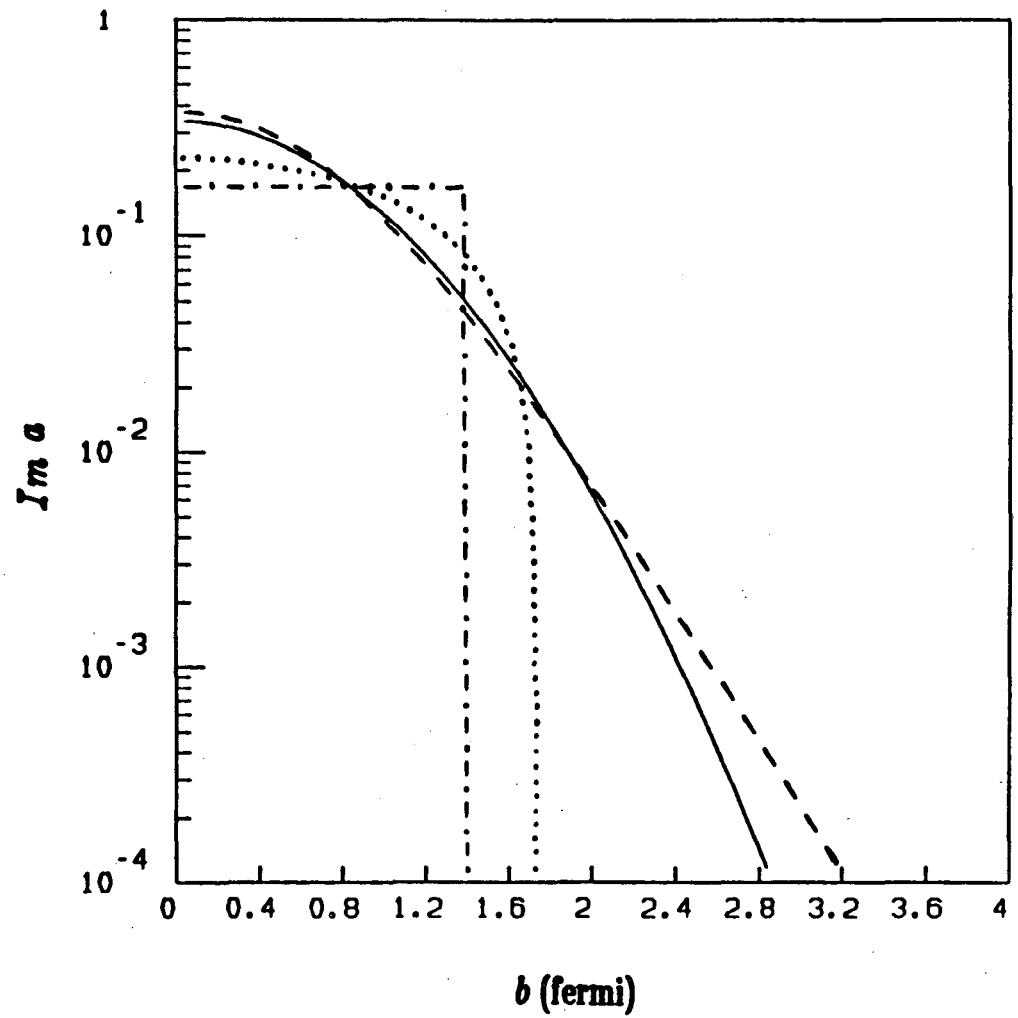

Fig. 4.2

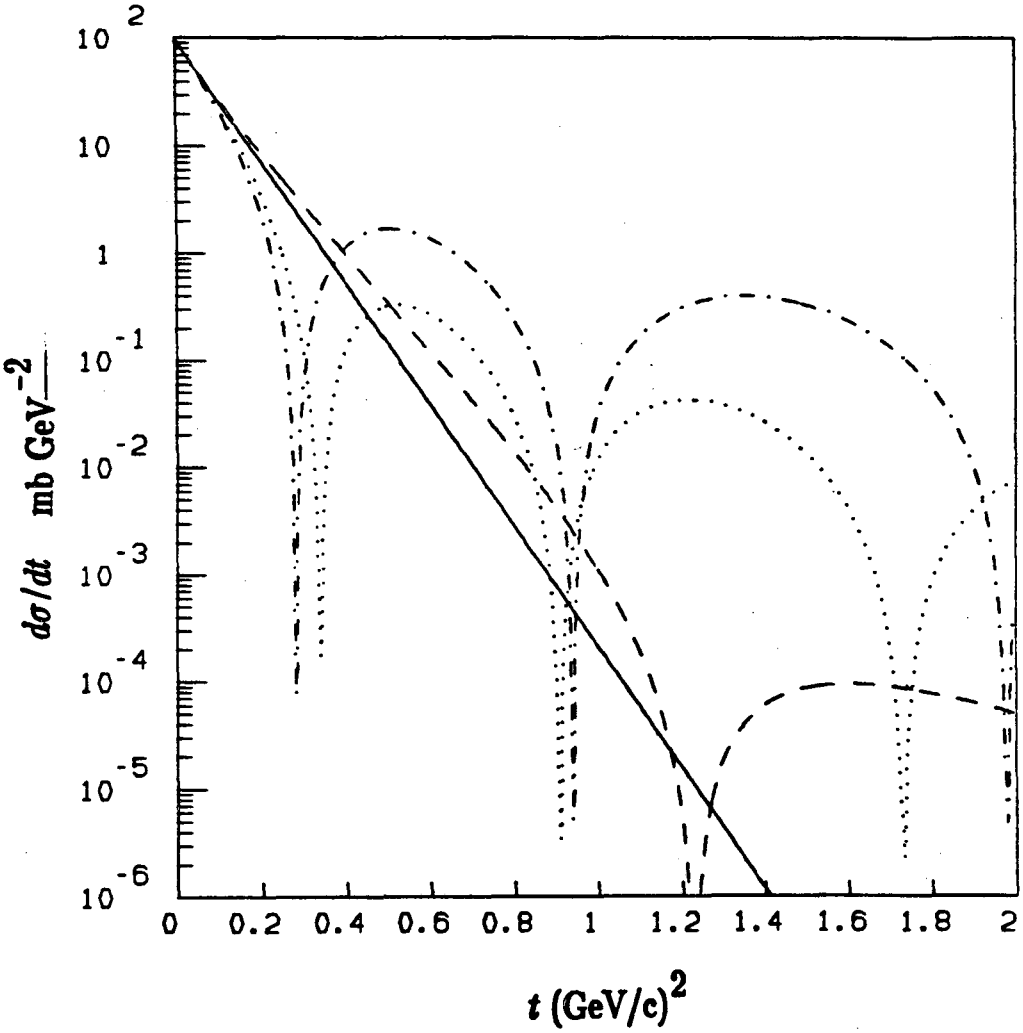
10^2
10
1
10^{-1}
10^{-2}
10^{-3}
10^{-4}
10^{-5}
10^{-6}
$d\sigma/dt$ mb GeV^{-2}
0
0.2
0.4
0.6
0.8
1
1.2
1.4
1.6
1.8
2
t (GeV/c)^2

Fig. 4.3

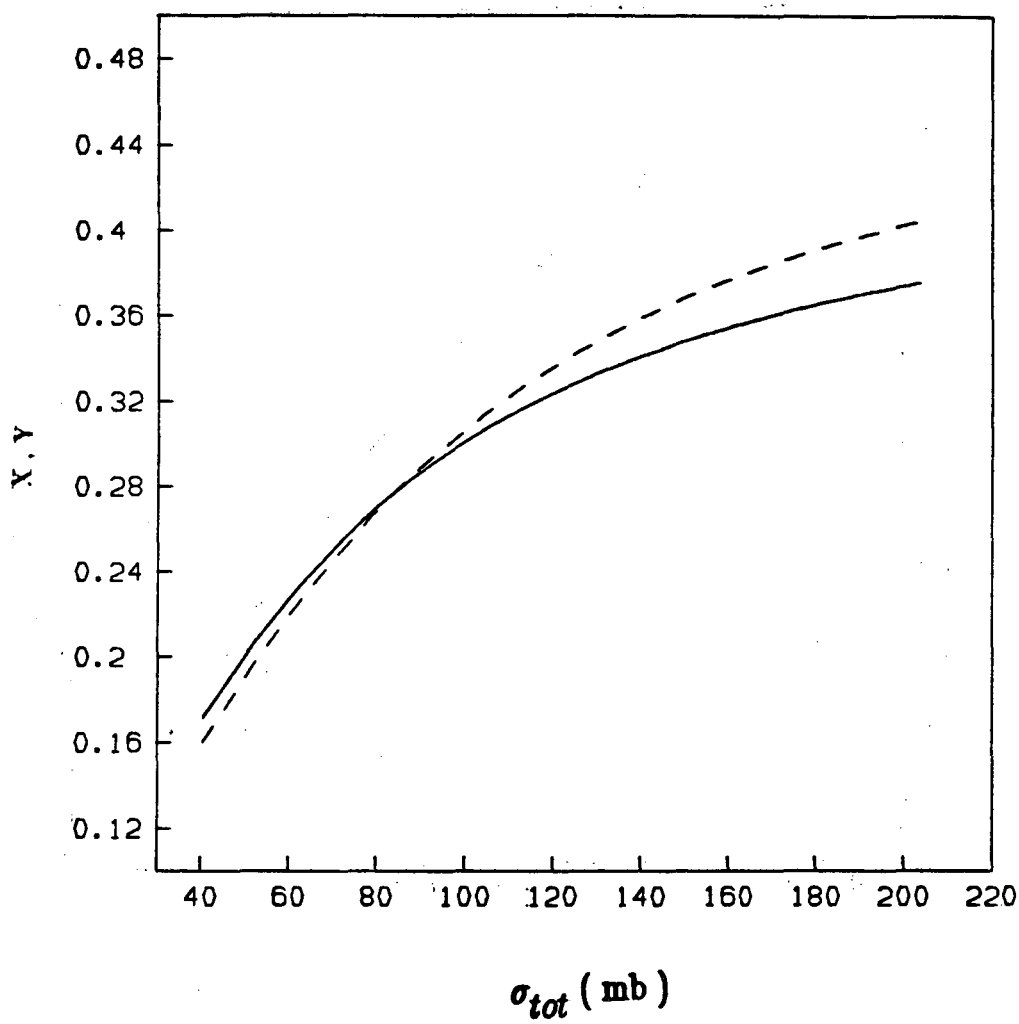
0.48
0.44
0.4
0.36
0.32
0.28
0.24
0.2
0.16
0.12
X, Y
40
60
80
100
120
140
160
180
200
220
σ_{tot} (mb)

Fig. 4.4

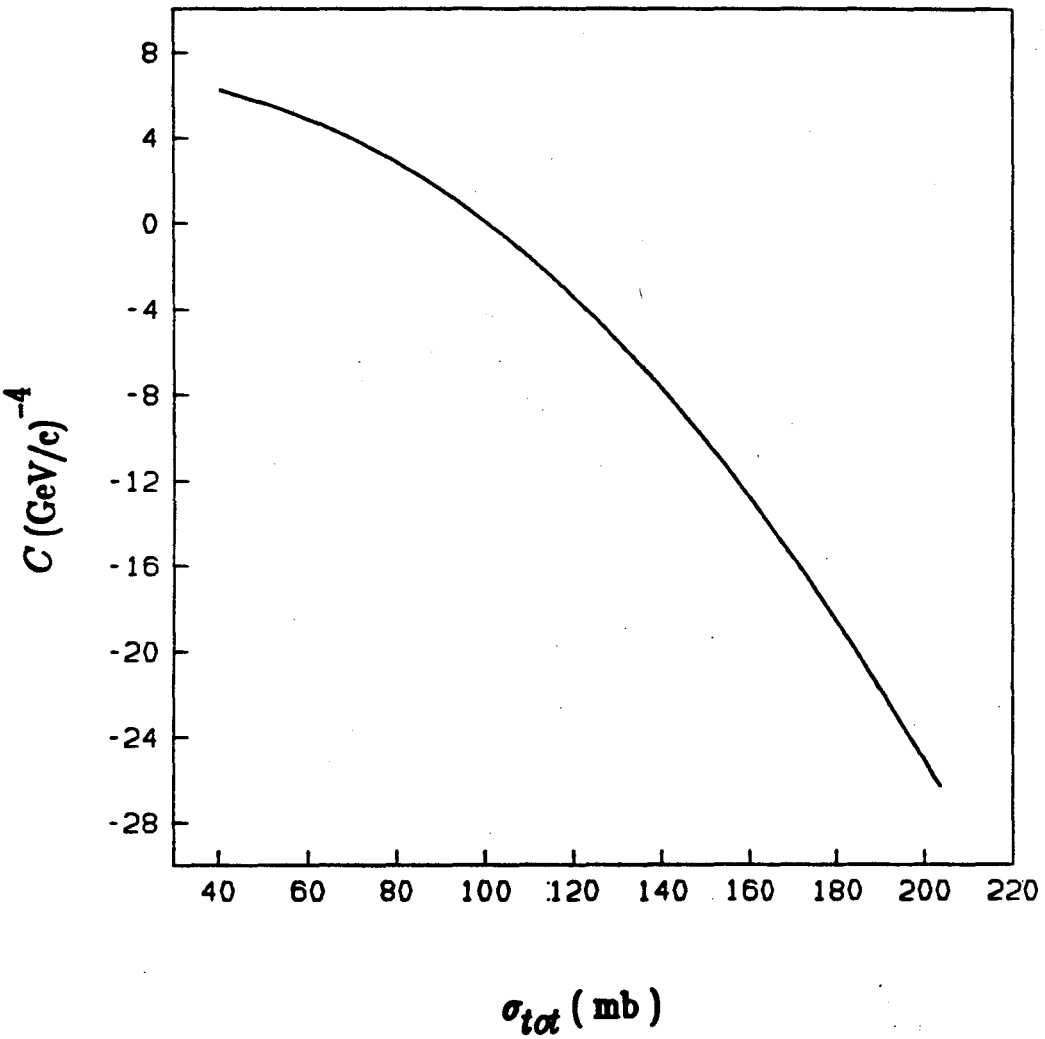
8
4
0
-4
-8
-12
-16
-20
-24
-28
C (GeV/c)^-4
40
60
80
100
120
140
160
180
200
220
σtot (mb)

Fig. 4.5

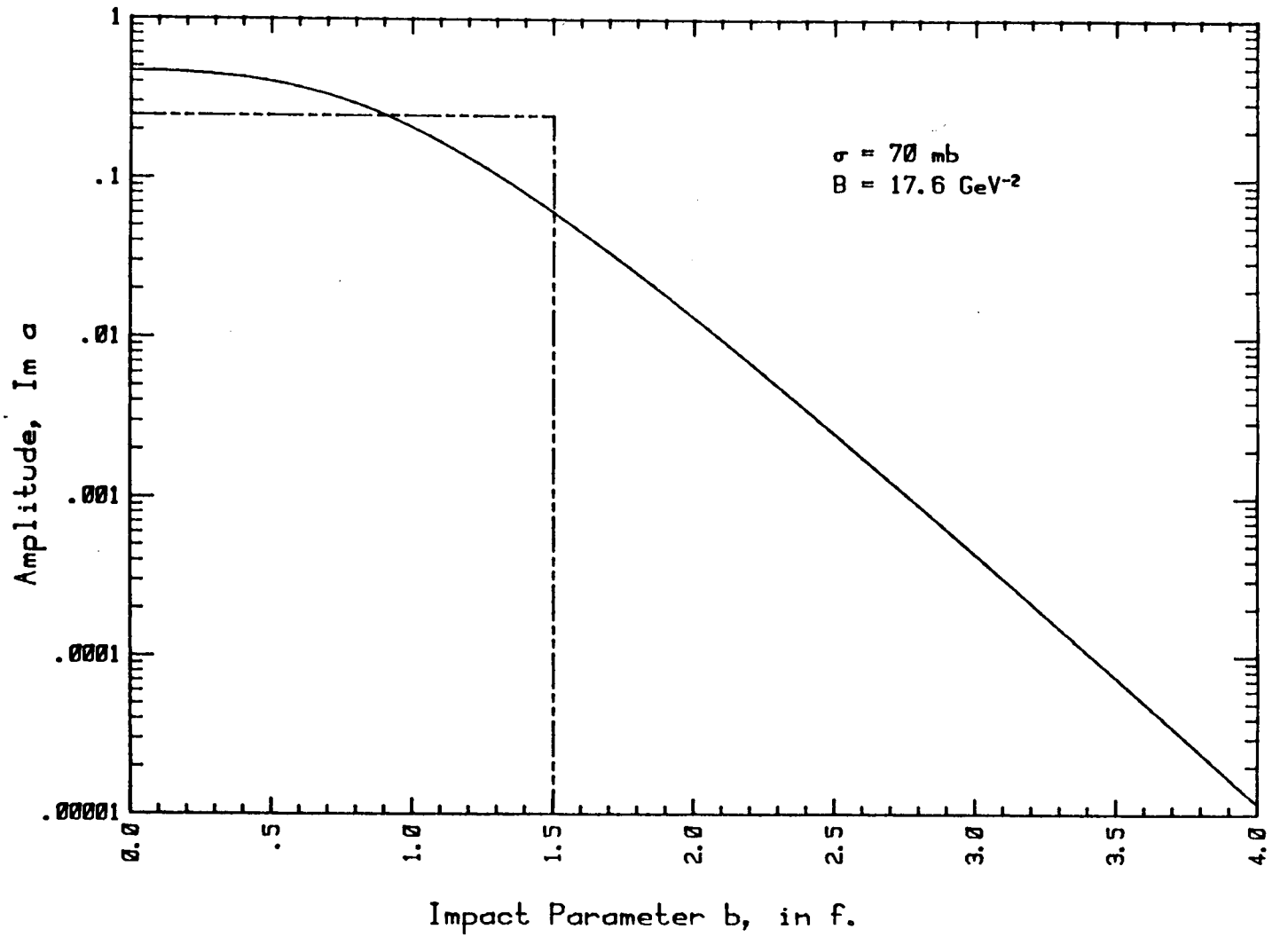
σ = 70 mb
B = 17.6 GeV⁻²
Amplitude, Im a
1
.1
.01
.001
.0001
.00001
0.0
.5
1.0
1.5
2.0
2.5
3.0
3.5
4.0
Impact Parameter b, in f.

Fig. 4.6(a)

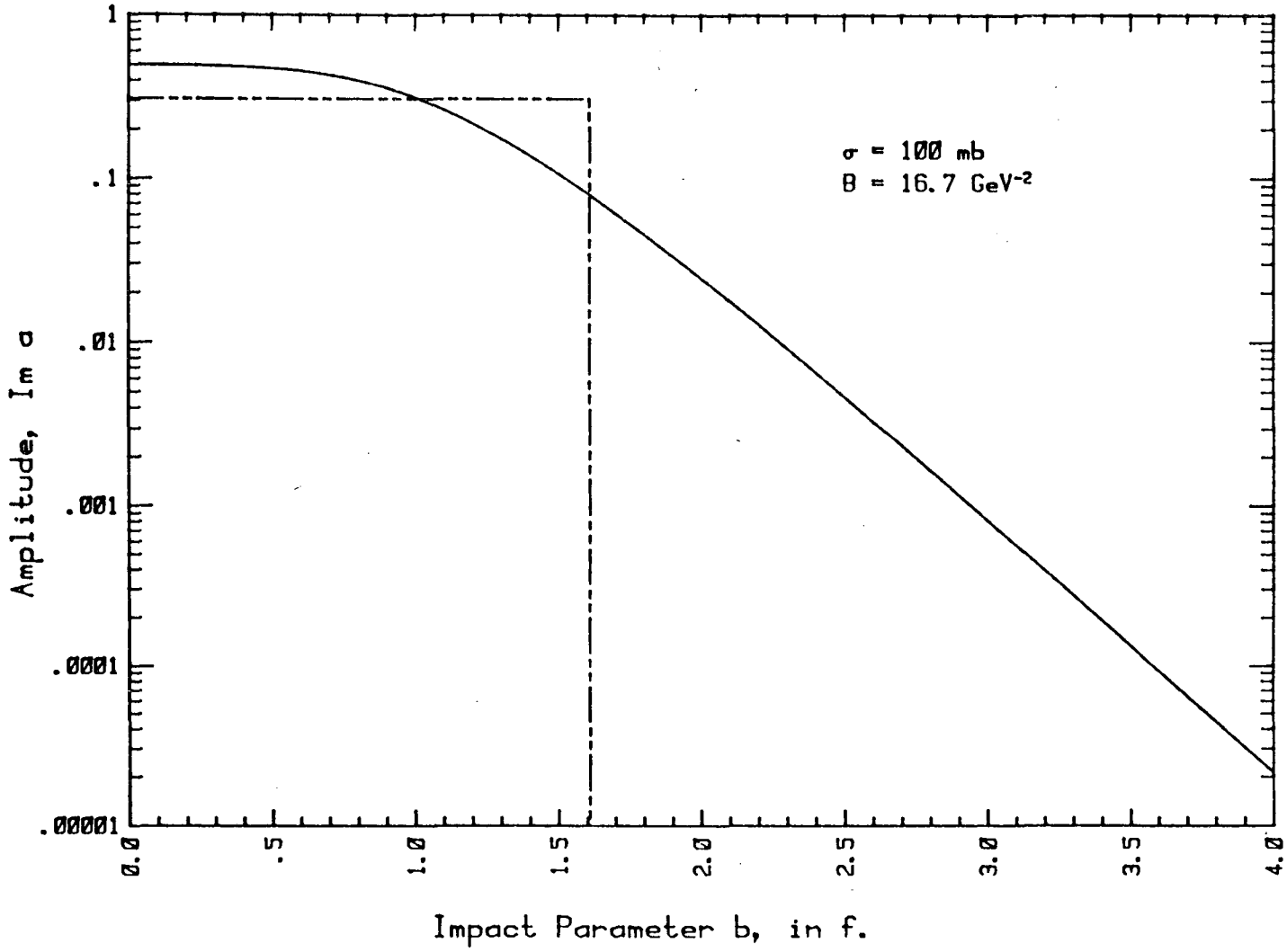
σ = 100 mb
B = 16.7 GeV⁻²
Amplitude, Im a
1
.1
.01
.001
.0001
.00001
0.0
.5
1.0
1.5
2.0
2.5
3.0
3.5
4.0
Impact Parameter b, in f.

Fig. 4.6(b)

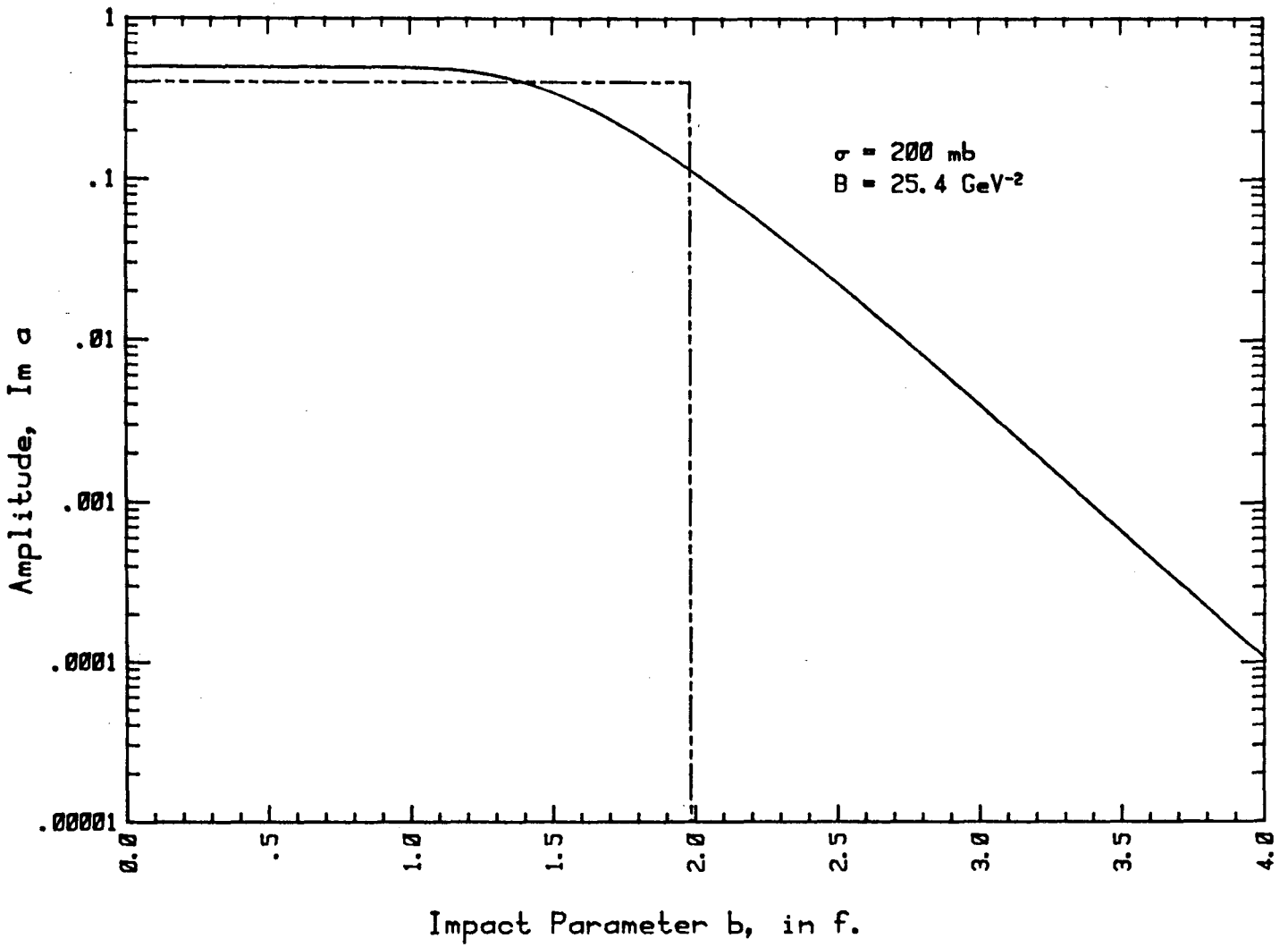
σ = 200 mb
B = 25.4 GeV⁻²
Amplitude, Im a
1
.1
.01
.001
.0001
.00001
0.0
.5
1.0
1.5
2.0
2.5
3.0
3.5
4.0
Impact Parameter b, in f.

Fig. 4.6(c)

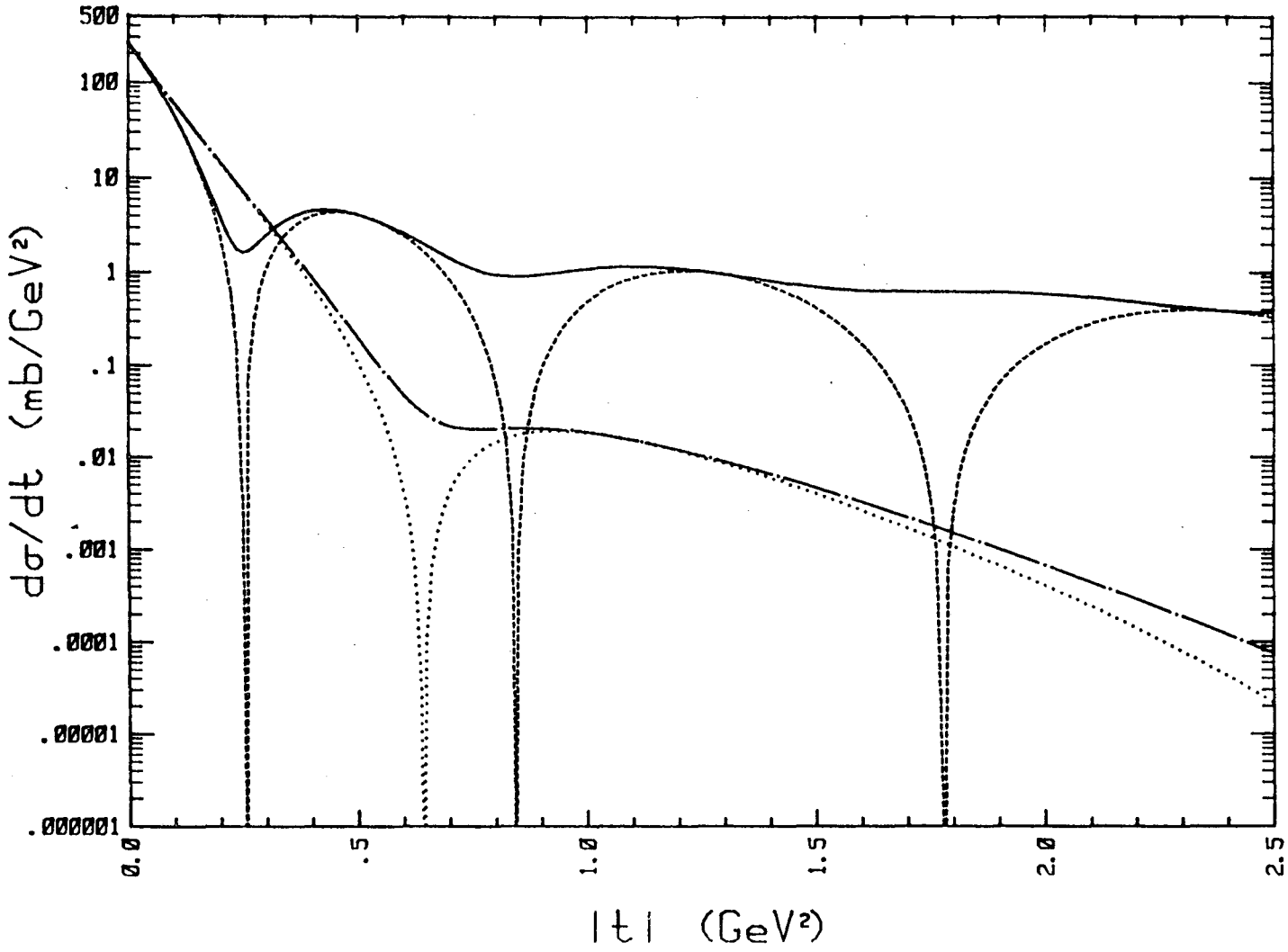
500
100
10
1
.1
.01
.001
.0001
.00001
.000001
dσ/dt (mb/GeV²)
0.0
.5
1.0
1.5
2.0
2.5
|t| (GeV²)

Fig. 4.7(a)

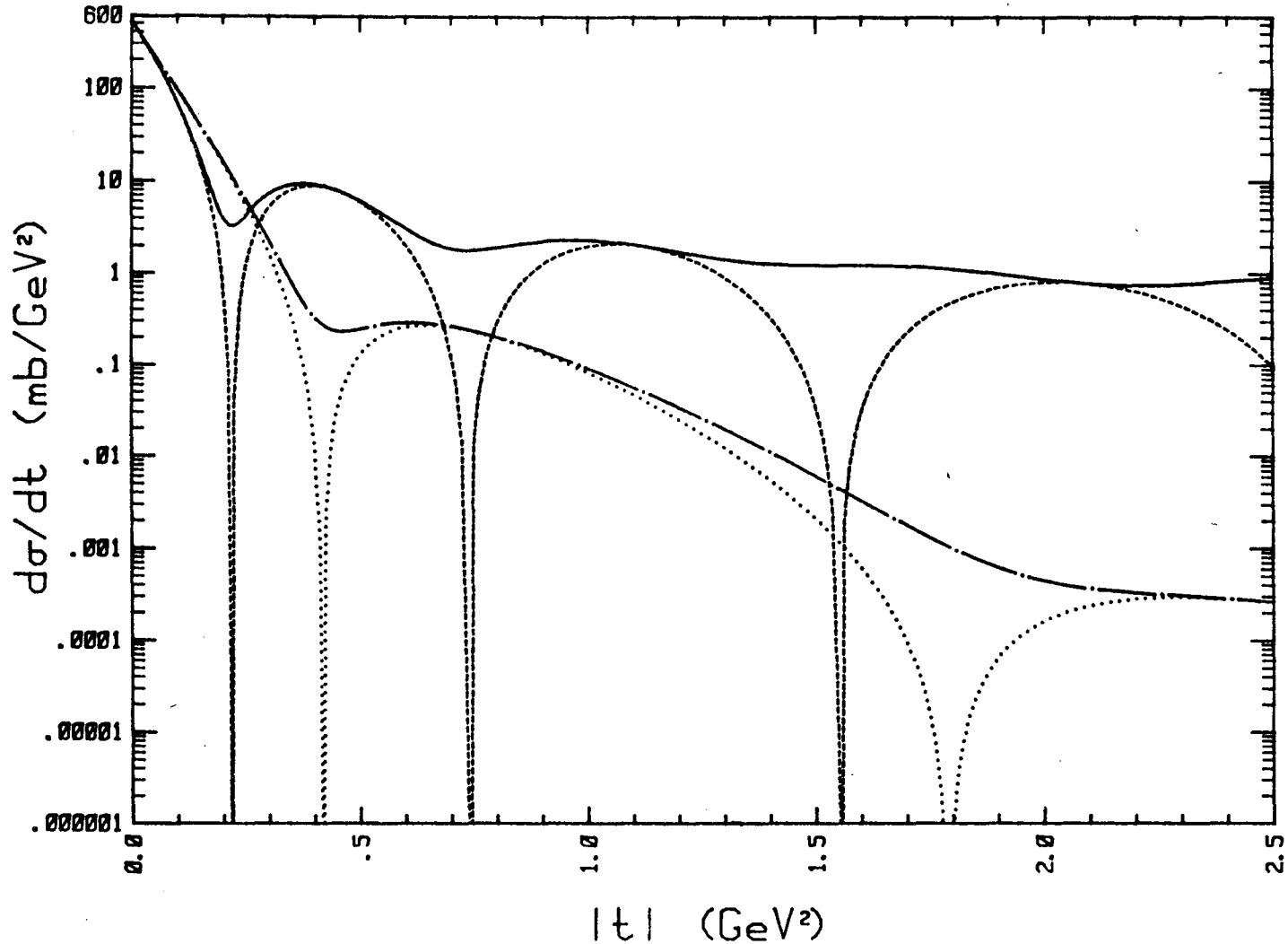
600
100
10
1
.1
.01
.001
.0001
.00001
.000001
0.0
.5
1.0
1.5
2.0
2.5
dσ/dt (mb/GeV²)
|t| (GeV²)

Fig. 4.7(b)

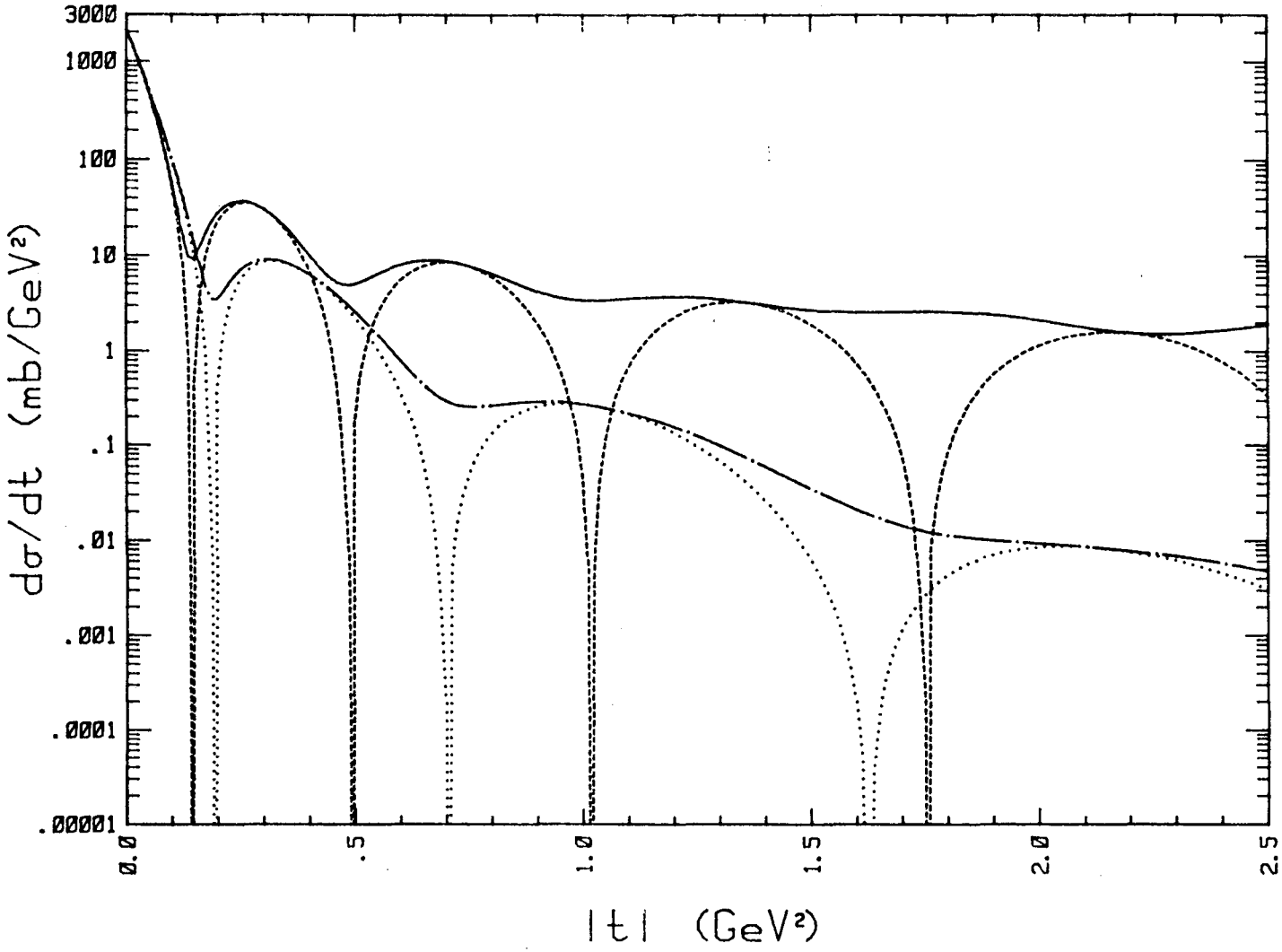
3000
1000
100
10
1
.1
.01
.001
.0001
.00001
dσ/dt (mb/GeV²)
0.0
.5
1.0
1.5
2.0
2.5
|t| (GeV²)

Fig. 4.7(c)

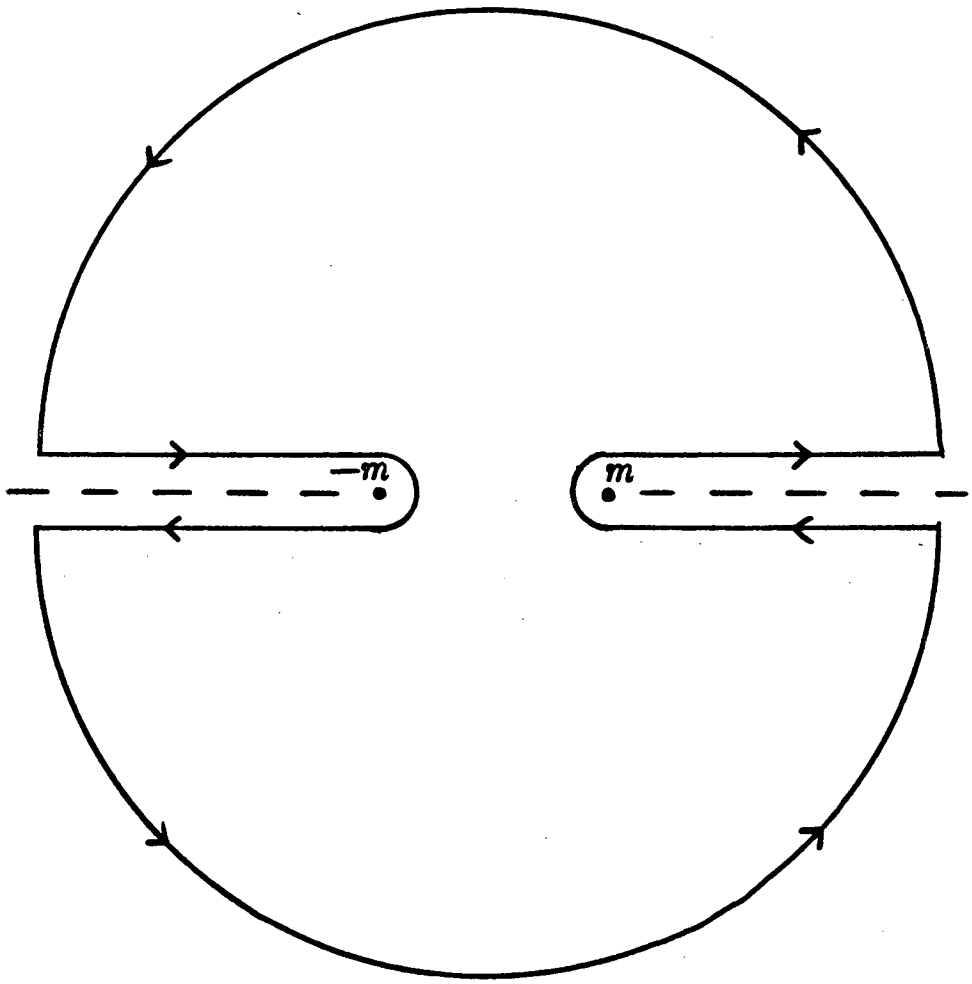

Fig. 4.8

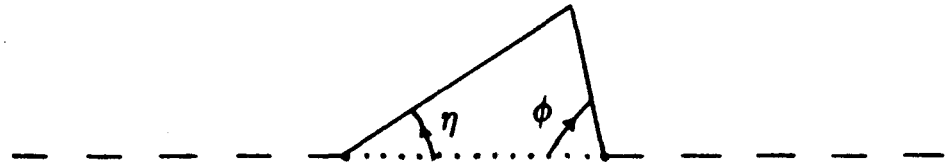

Fig. 4.9

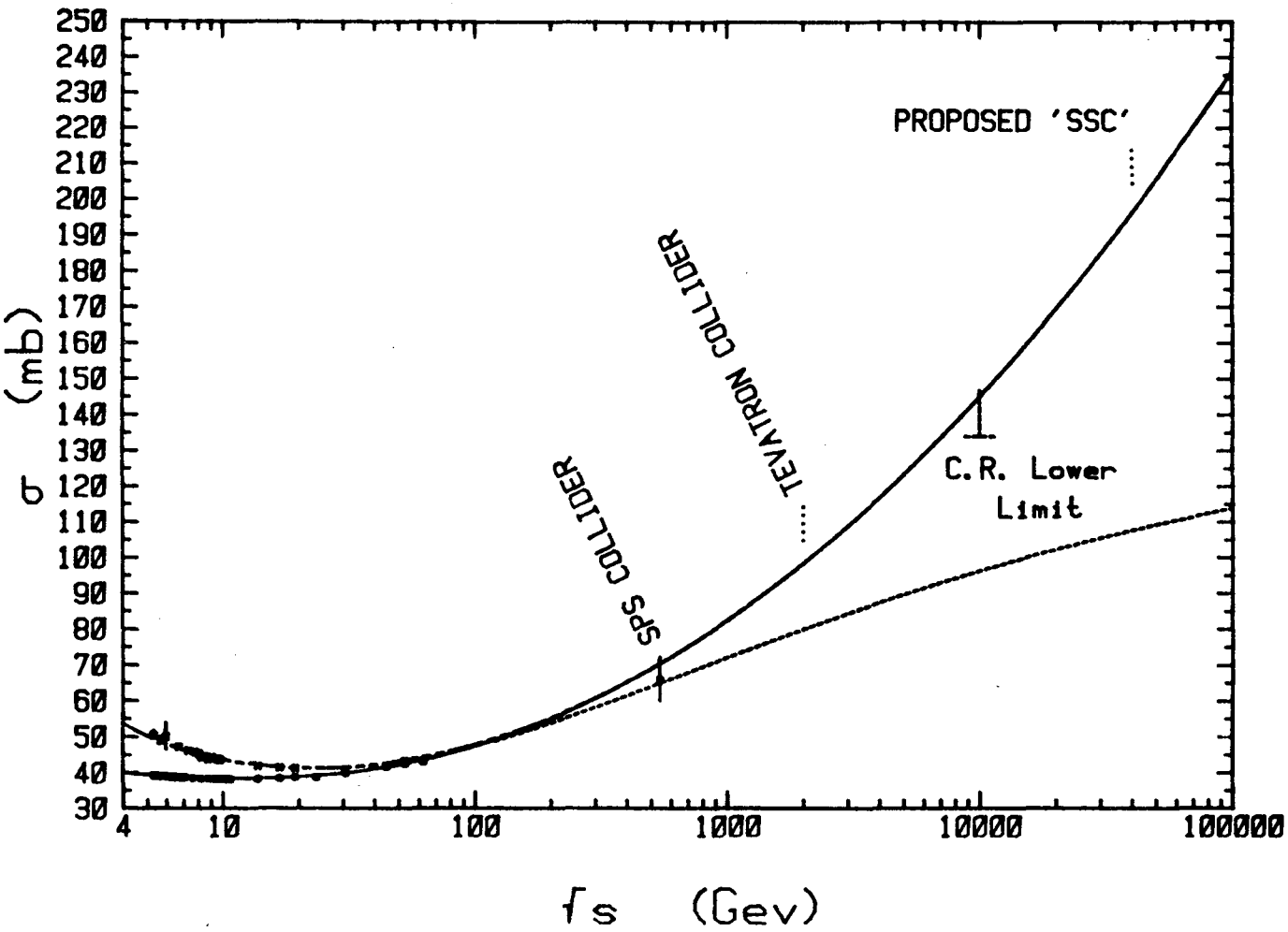
PROPOSED 'SSC'
TEVATRON COLLIDER
SPS COLLIDER
C.R. Lower Limit
σ (mb)
√s (Gev)
250
240
230
220
210
200
190
180
170
160
150
140
130
120
110
100
90
80
70
60
50
40
30
4
10
100
1000
10000
100000

Fig. 5.1(a)

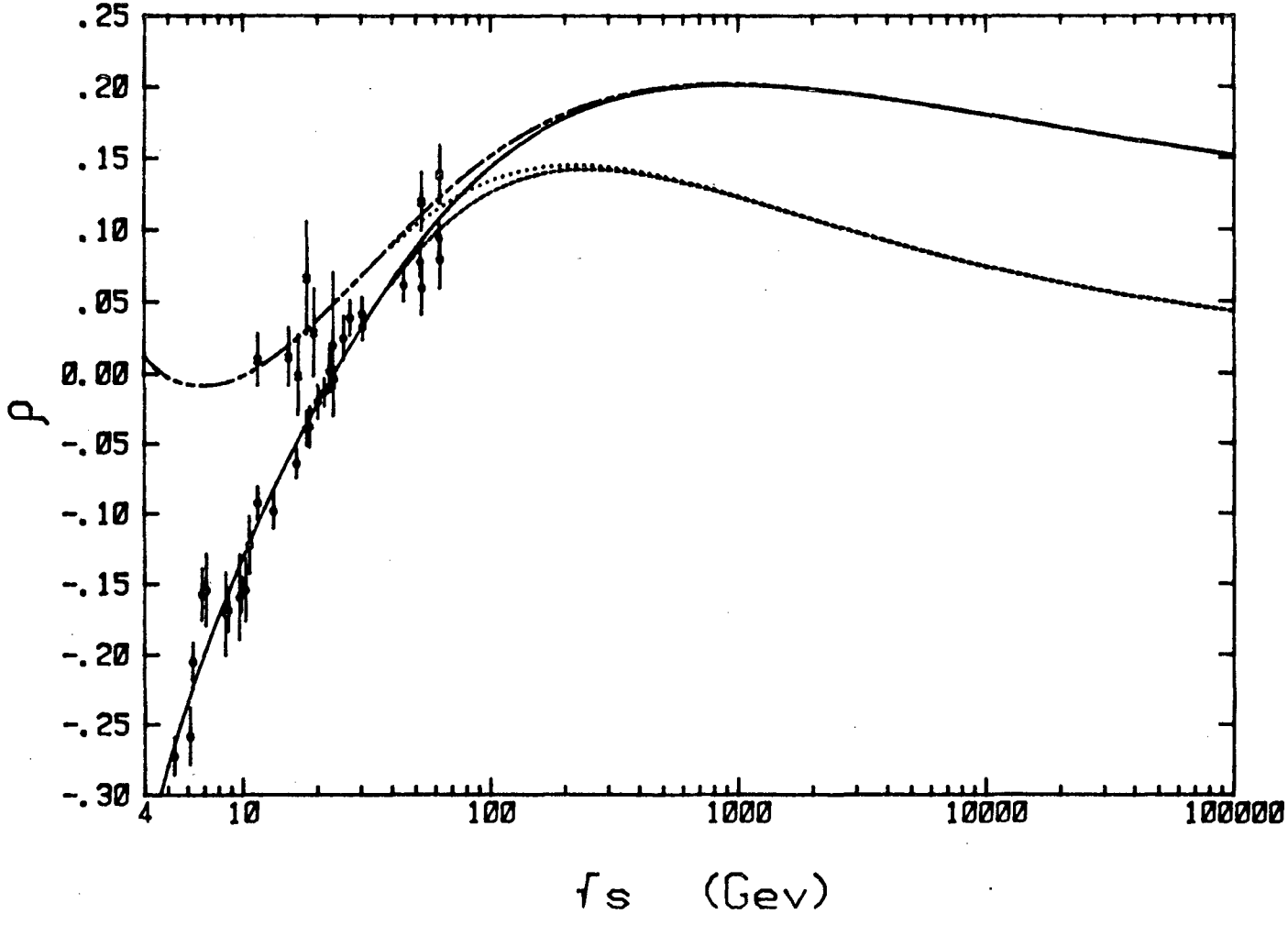
.25
.20
.15
.10
.05
0.00
-.05
-.10
-.15
-.20
-.25
-.30
ρ
4
10
100
1000
10000
100000
√s (Gev)

Fig. 5.1(b)

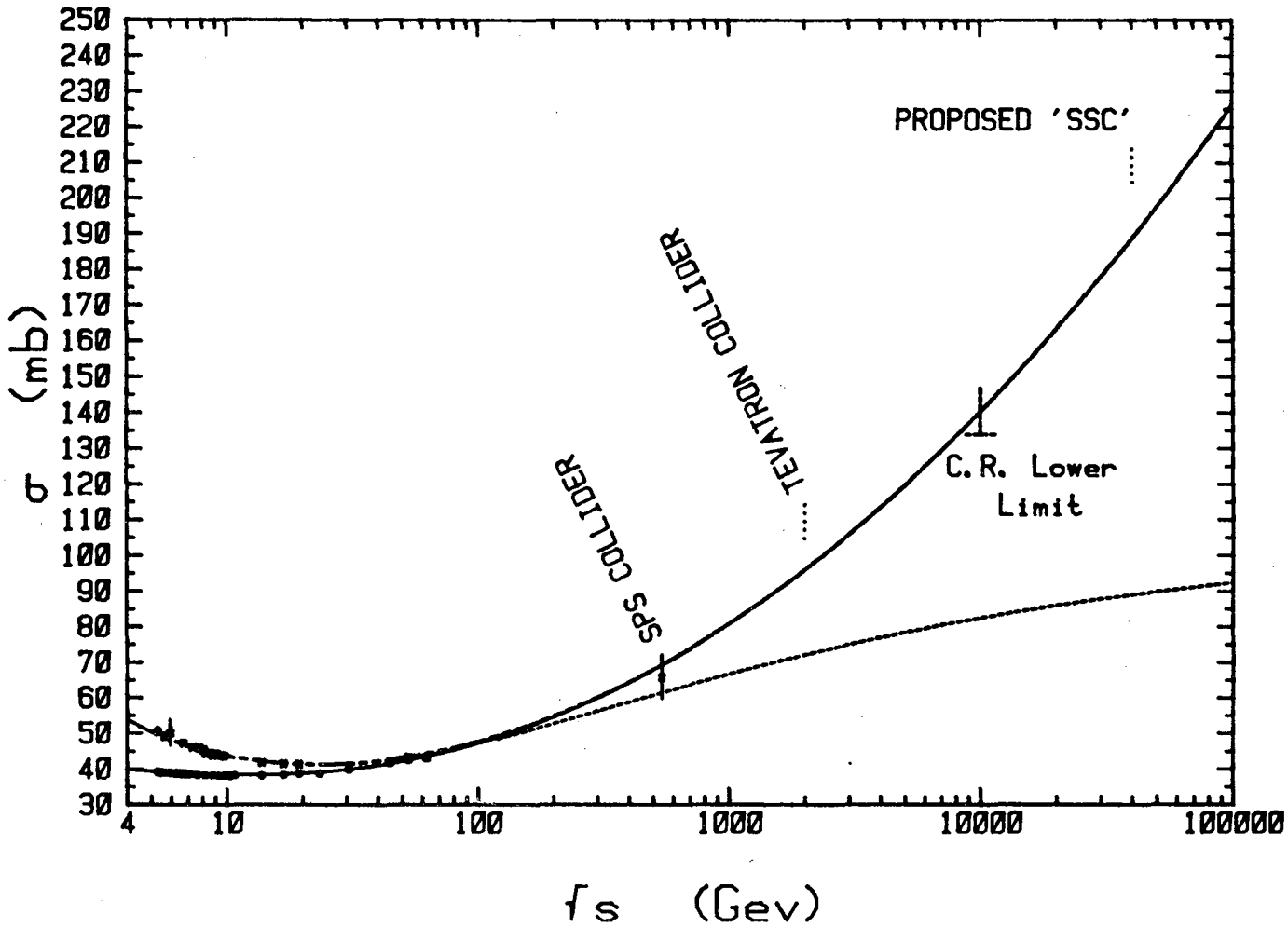
250
240
230
220
210
200
190
180
170
160
150
140
130
120
110
100
90
80
70
60
50
40
30
σ (mb)
4
10
100
1000
10000
100000
√s (Gev)
PROPOSED 'SSC'
TEVATRON COLLIDER
SPS COLLIDER
C.R. Lower
Limit

Fig. 5.2(a)

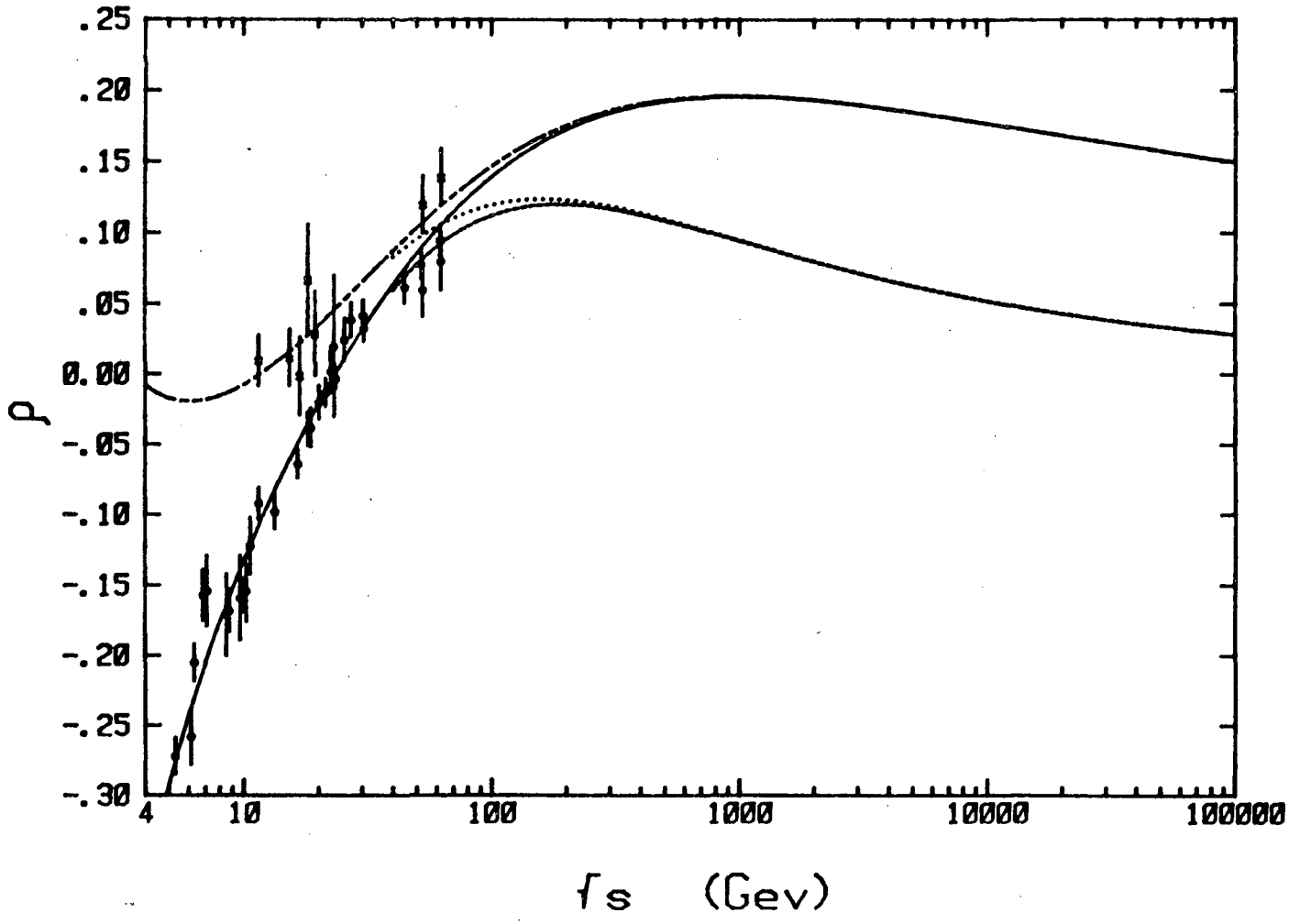
.25
.20
.15
.10
.05
0.00
-.05
-.10
-.15
-.20
-.25
-.30
ρ
4
10
100
1000
10000
100000
√s (Gev)

Fig. 5.2(b)

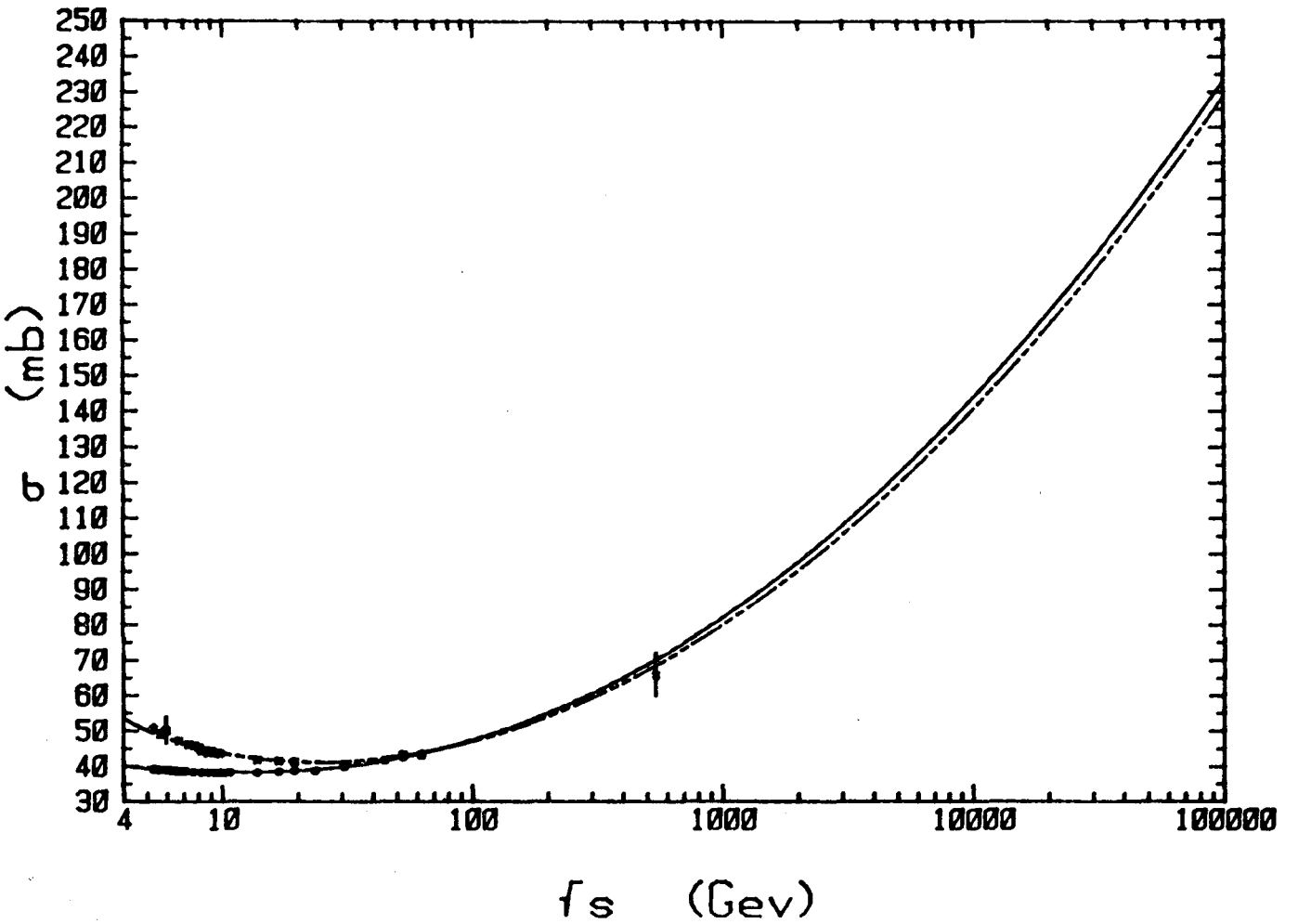
250
240
230
220
210
200
190
180
170
160
150
140
130
120
110
100
90
80
70
60
50
40
30
σ (mb)
4
10
100
1000
10000
100000
√s (Gev)

Fig. 5.3(a)

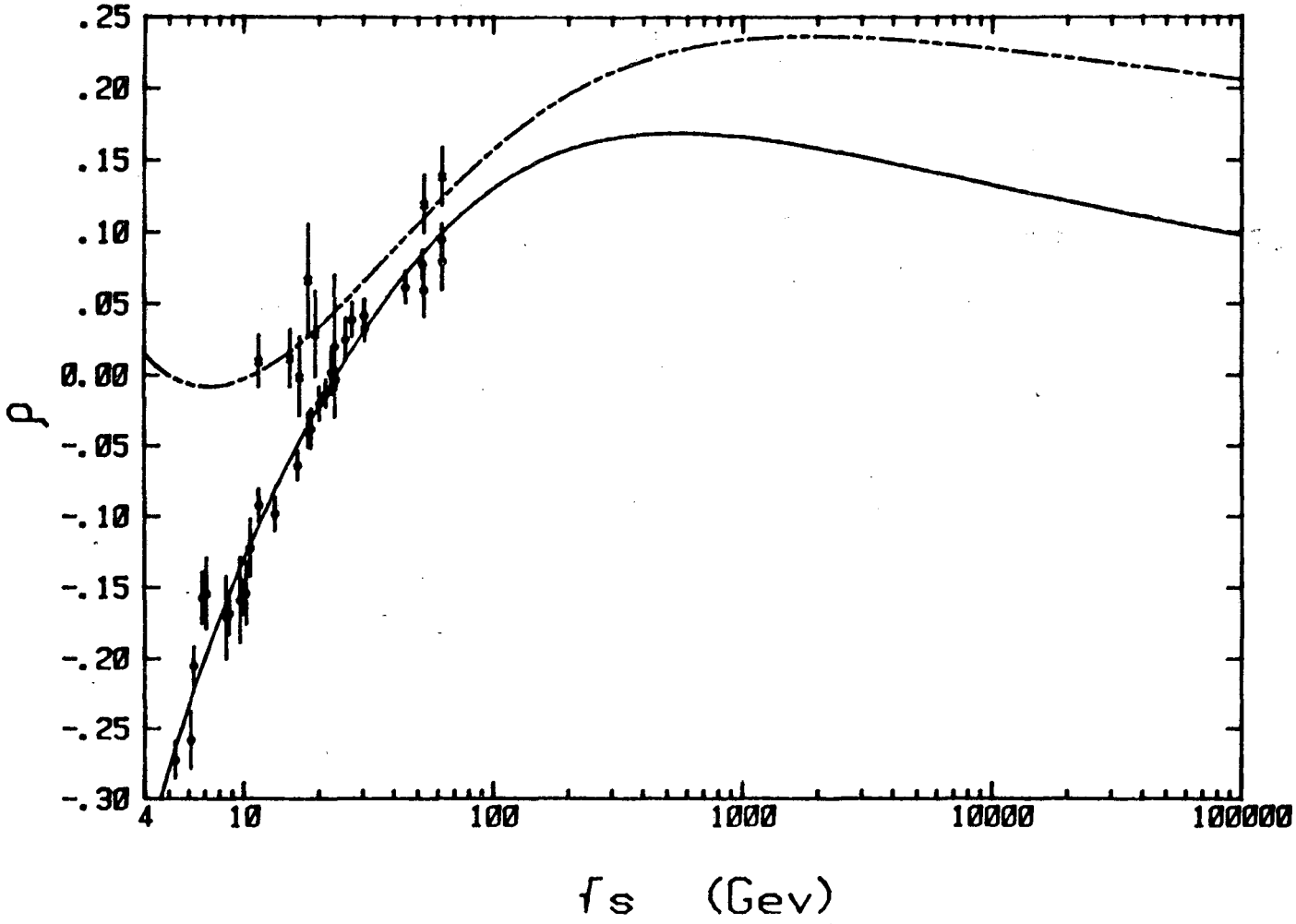
.25
.20
.15
.10
.05
0.00
-.05
-.10
-.15
-.20
-.25
-.30
ρ
4
10
100
1000
10000
100000
√s (Gev)

Fig. 5.3(b)

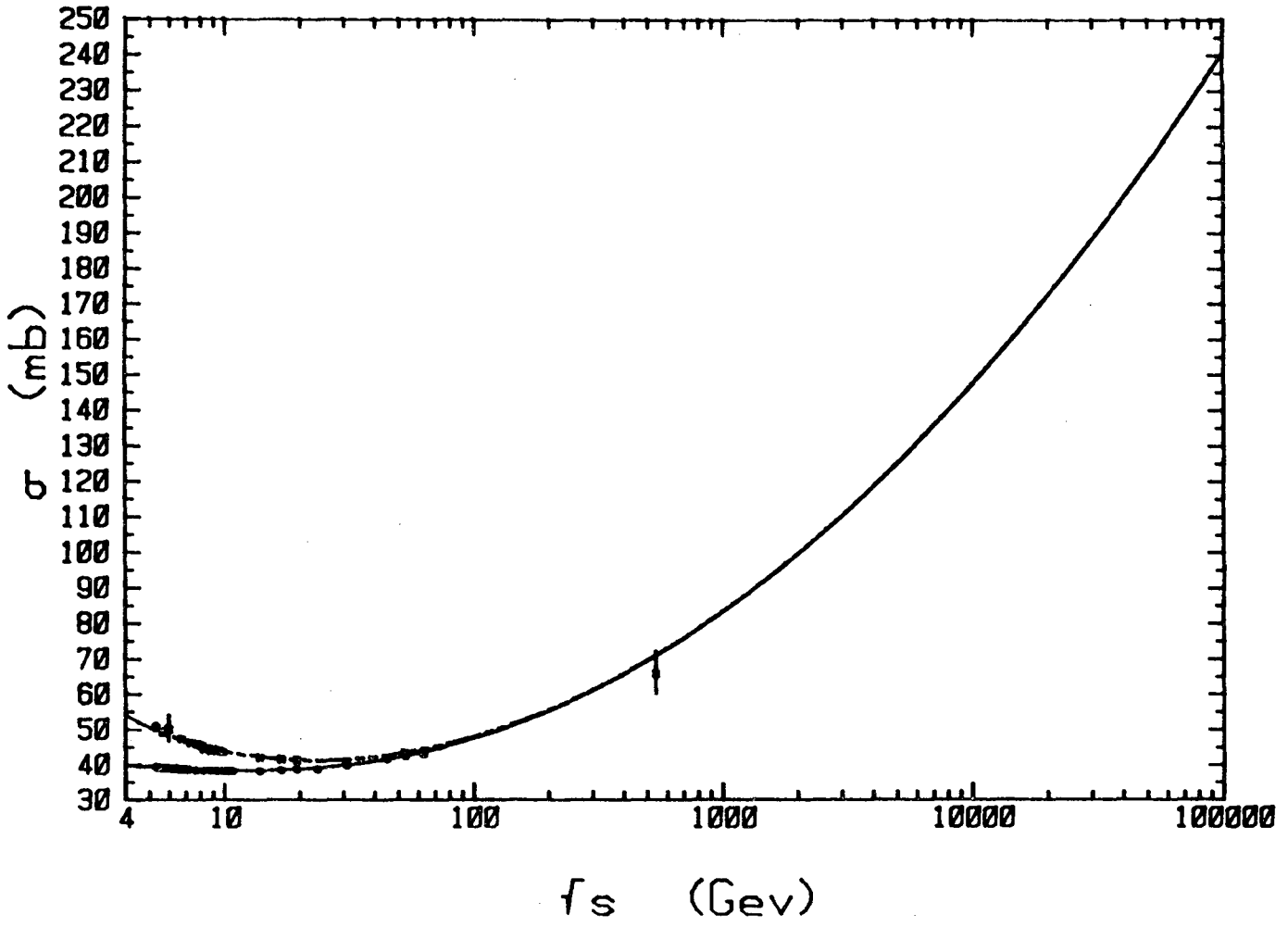
250
240
230
220
210
200
190
180
170
160
150
140
130
120
110
100
90
80
70
60
50
40
30
σ (mb)
4
10
100
1000
10000
100000
√s (Gev)

Fig. 5.4(a)

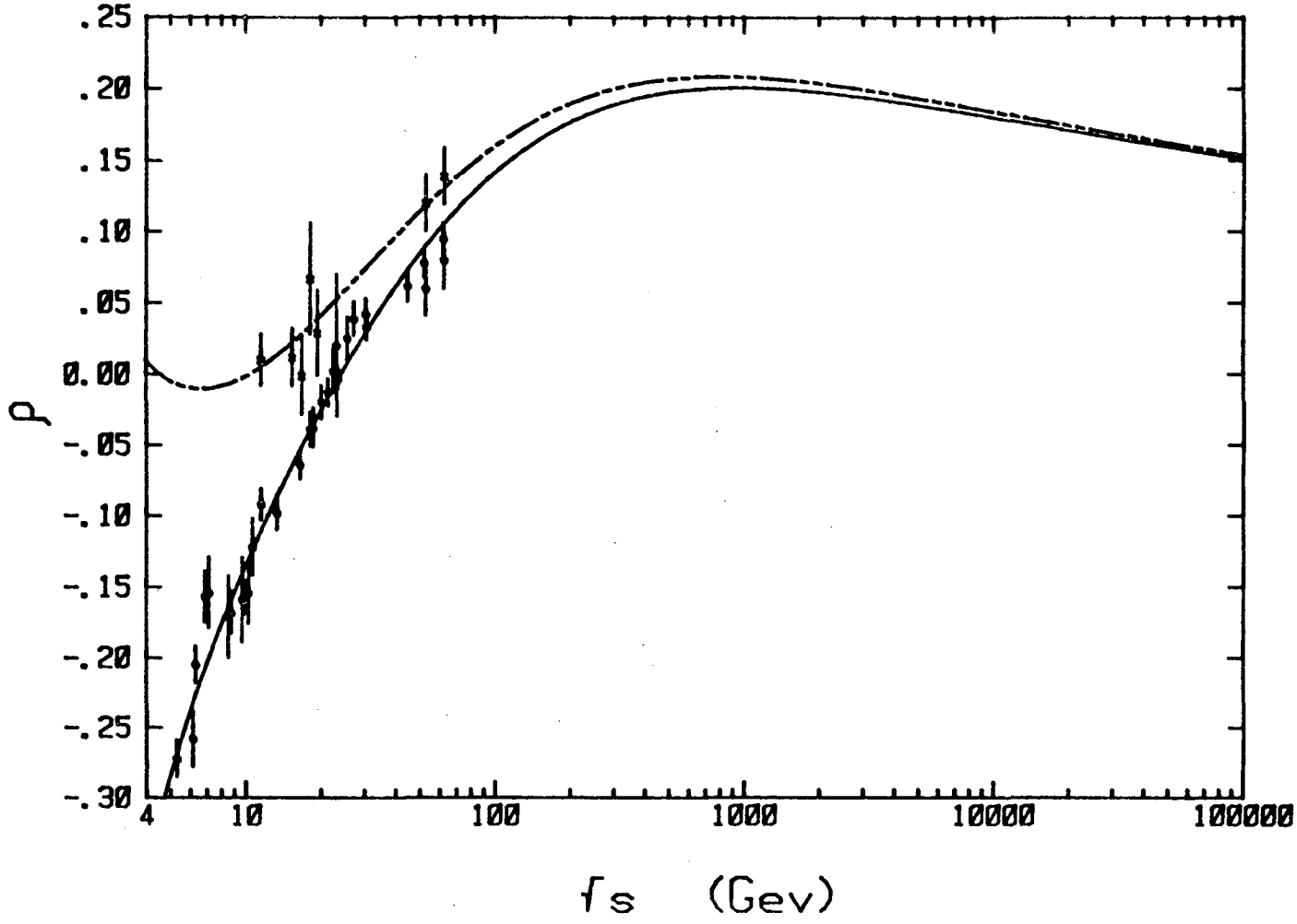
.25
.20
.15
.10
.05
0.00
-.05
-.10
-.15
-.20
-.25
-.30
ρ
4
10
100
1000
10000
100000
√s (Gev)

Fig. 5.4(b)

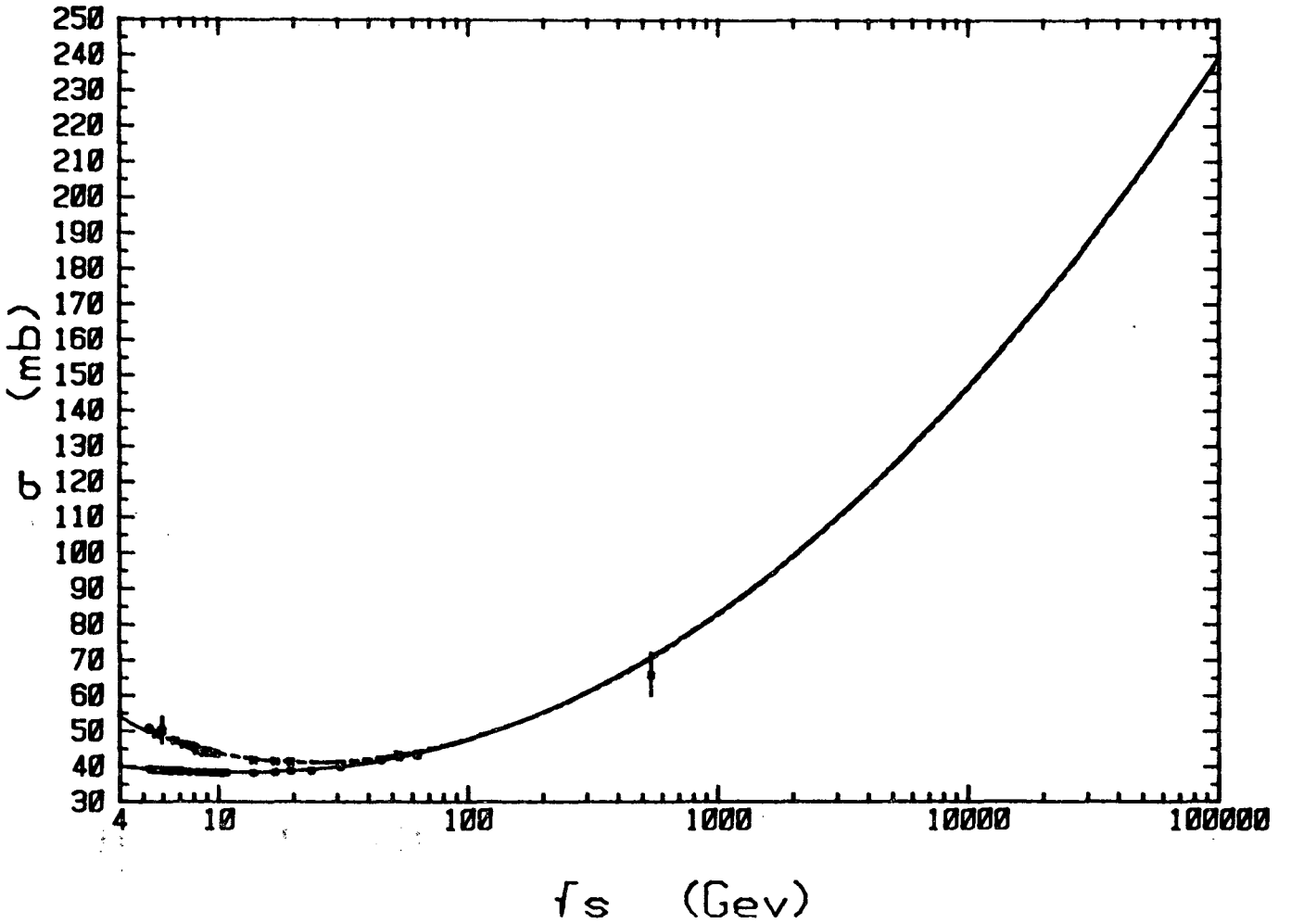
250
240
230
220
210
200
190
180
170
160
150
140
130
120
110
100
90
80
70
60
50
40
30
σ (mb)
4
10
100
1000
10000
100000
√s (Gev)

Fig. 5.5(a)

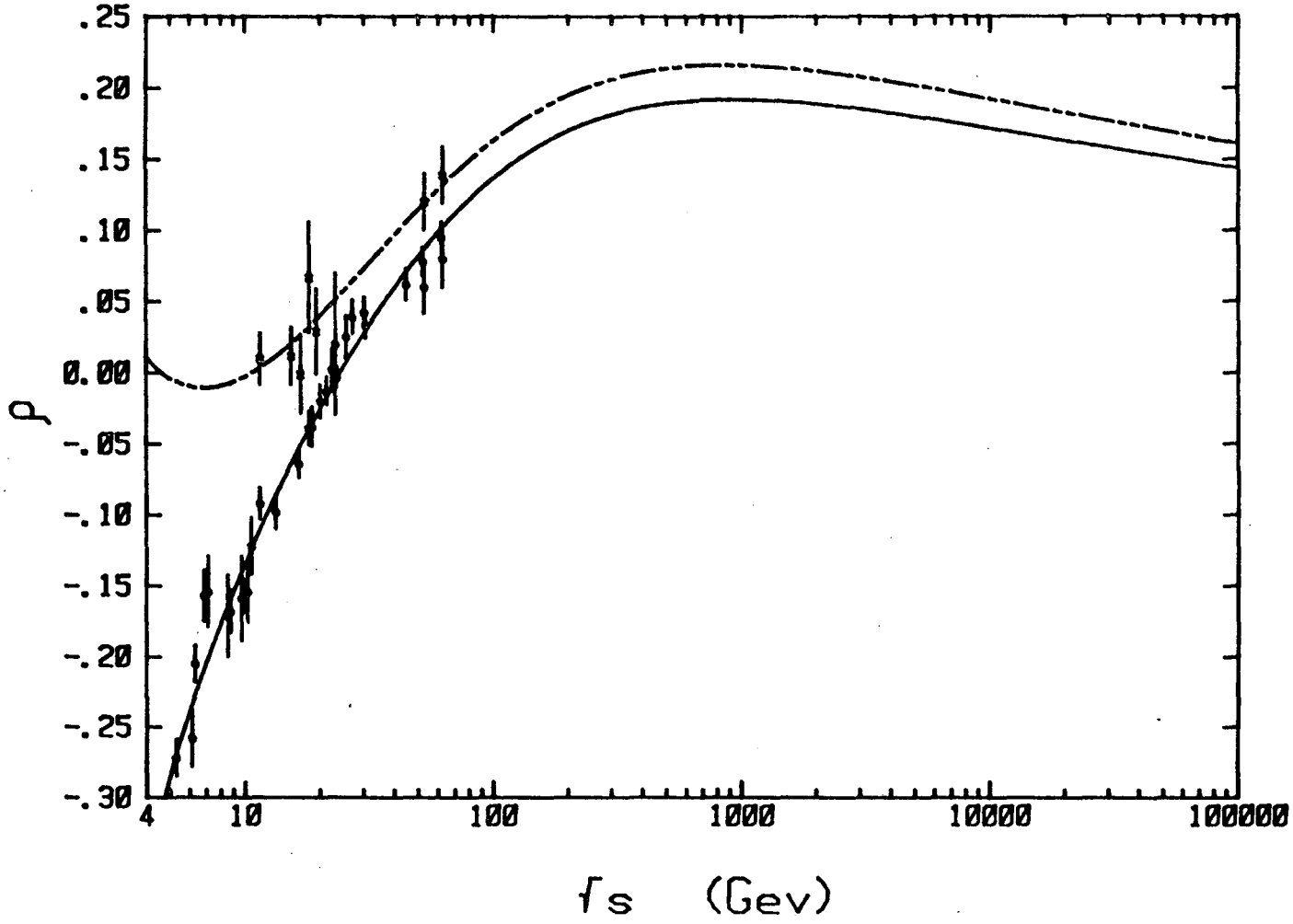
.25
.20
.15
.10
.05
0.00
-.05
-.10
-.15
-.20
-.25
-.30
ρ
4
10
100
1000
10000
100000
√s (Gev)

Fig. 5.5(b)

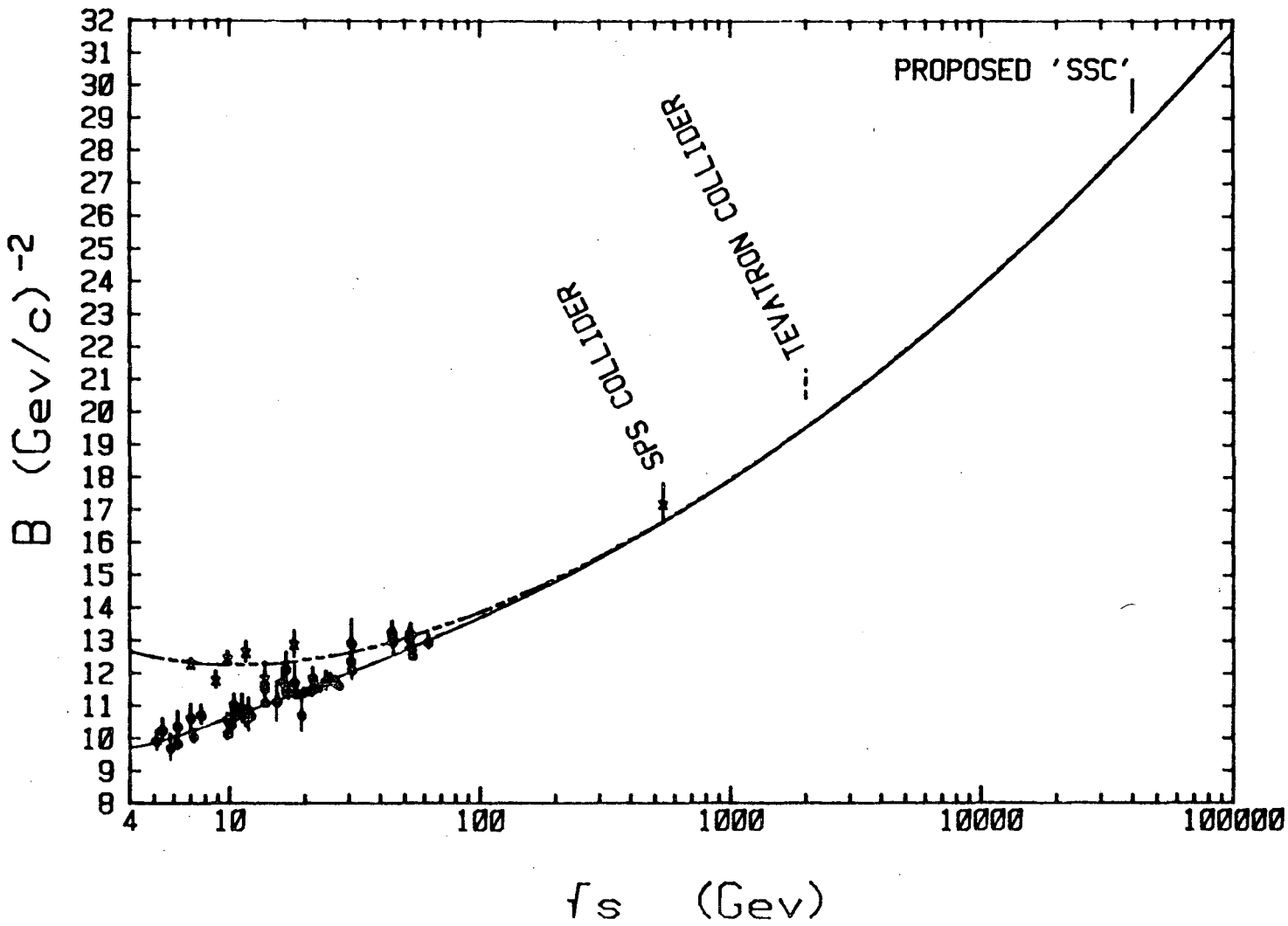
B (Gev/c)$^{-2}$
32
31
30
29
28
27
26
25
24
23
22
21
20
19
18
17
16
15
14
13
12
11
10
9
8
4
10
100
1000
10000
100000
$\sqrt{s}$ (Gev)
PROPOSED 'SSC'
TEVATRON COLLIDER
SPS COLLIDER

Fig. 6.1

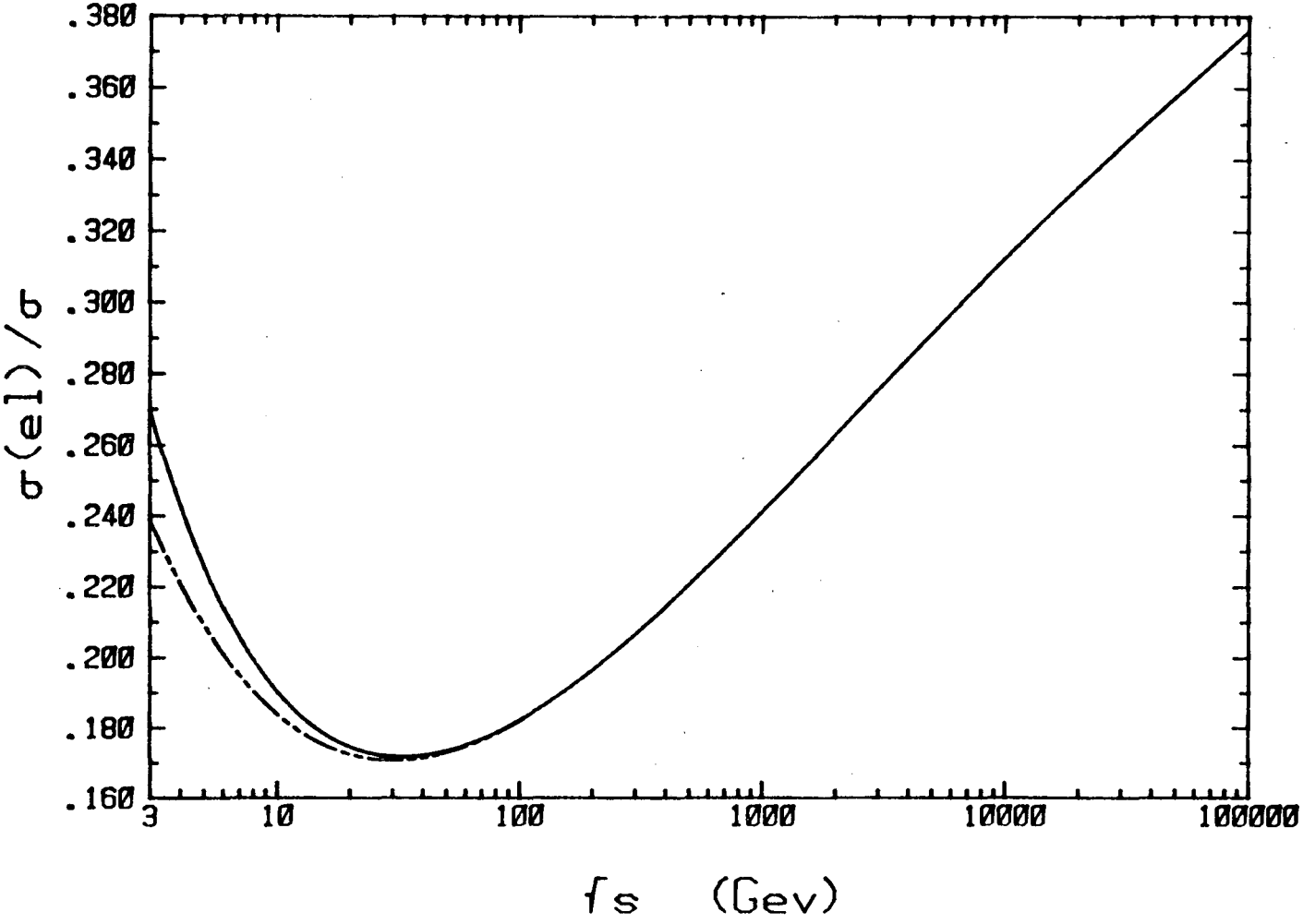
.380
.360
.340
.320
.300
.280
.260
.240
.220
.200
.180
.160
σ(el)/σ
3
10
100
1000
10000
100000
√s (Gev)

Fig. 6.2

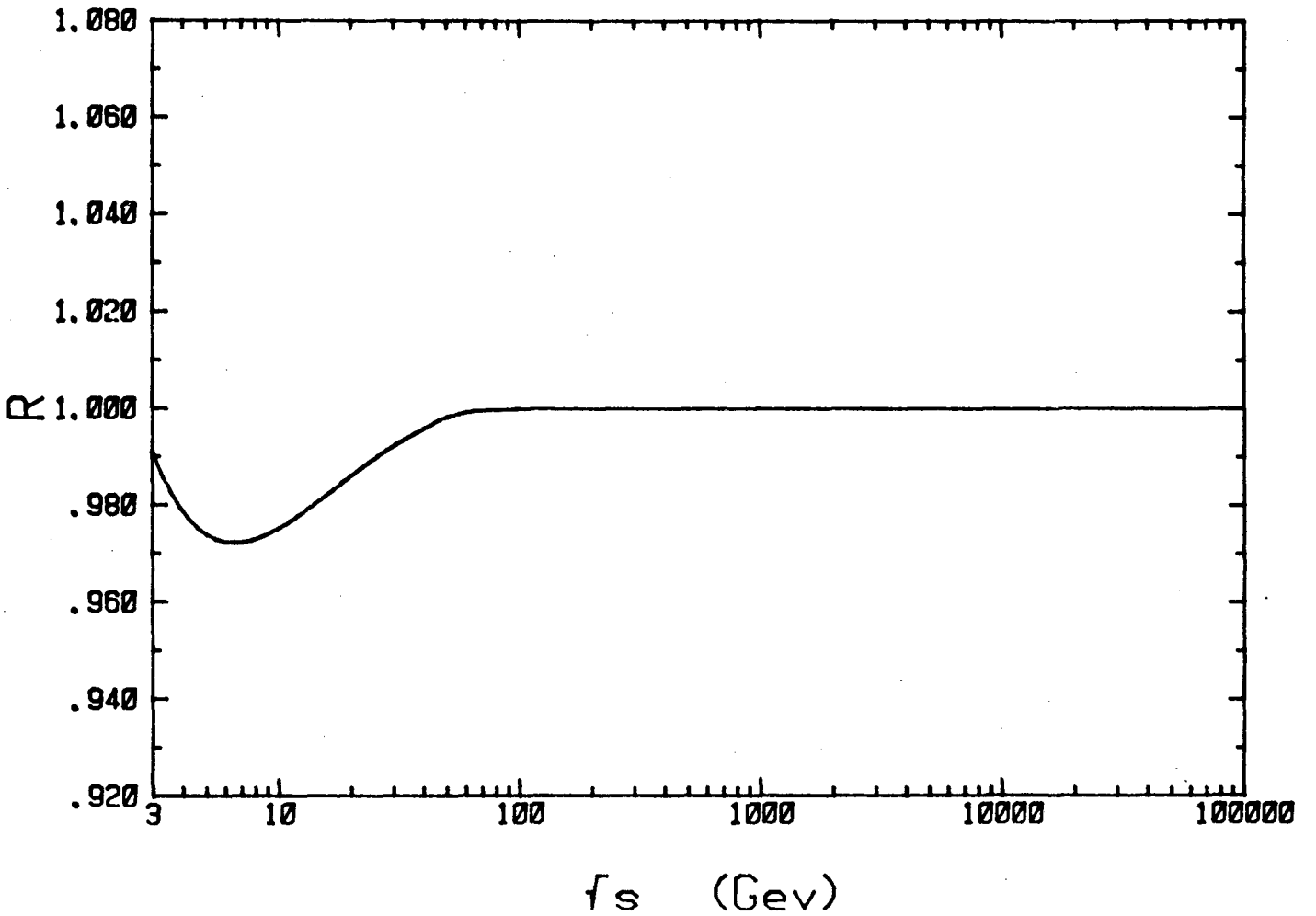
1.080
1.060
1.040
1.020
R 1.000
.980
.960
.940
.920
3
10
100
1000
10000
100000
√s (Gev)

Fig. 6.3

This report was done with support from the Department of Energy. Any conclusions or opinions expressed in this report represent solely those of the author(s) and not necessarily those of The Regents of the University of California, the Lawrence Berkeley Laboratory or the Department of Energy.

Reference to a company or product name does not imply approval or recommendation of the product by the University of California or the U.S. Department of Energy to the exclusion of others that may be suitable.

TECHNICAL INFORMATION DEPARTMENT
LAWRENCE BERKELEY LABORATORY
UNIVERSITY OF CALIFORNIA
BERKELEY, CALIFORNIA 94720